Winter 2001

Coastal Ocean Morphodynamics and the Resulting Erosion and Deposition: An Analytical Approach

Shejun Fan
Old Dominion University

COASTAL OCEAN MORPHODYNAMICS AND THE RESULTING EROSION AND DEPOSITION: AN ANALYTICAL APPROACH

by

Shejun Fan
B.A. July 1987, Peking University, China
M.S. October 1990, Shanghai Jiao Tong University, China

A Dissertation Submitted to the Faculty of
Old Dominion University in Partial Fulfillment of the
Requirement for the Degree of

DOCTOR OF PHILOSOPHY

OCEANOGRAPHY

OLD DOMINION UNIVERSITY
December 2001

Approved by:

Donald J.P. Swift (Director)

David R. Basco (Member)

Ronald E. Johnson (Member)

Christopher W. Reed (Member)

ABSTRACT

COASTAL OCEAN MORPHODYNAMICS AND THE RESULTING EROSION AND DEPOSITION: AN ANALYTICAL APPROACH

Shejun Fan
Old Dominion University, 2001
Director: Dr. Donald J. P. Swift

Coastal ocean morphodynamics is the study of the morphological change of the coastal ocean system. Environmental conditions, such as climatic and geological controls, are exogenous inputs of the system, which are responsible for geographic variation among coastal oceans. In the coastal ocean system, coastal morphological changes are the results of a series of morphodynamical processes. In this treatise, quantitative, dynamical sedimentary models are developed to provide an analytical understanding of morphodynamical processes in coastal ocean environments. These dynamical sedimentary models numerically simulate the sedimentary processes over a range of time scales from an event time scale, based on the fundamental physics of sediment dynamics in coastal ocean environment, to a longer, facies time scale. The abandoned Yellow River delta of China and the Eel River continental shelf of northern California are chosen as study areas. These model simulated geologic processes serve to test the hypotheses concerning the processes that are responsible for the coastal stability of abandoned Yellow River underwater delta and event stratigraphy formation on the northern California continental shelf.

This dissertation is dedicated to my wife Dun Tan,
my fountain of support and encouragement.

ACKNOWLEDGMENTS

I would like to deeply thank my advisor, Dr. Donald J.P Swift, for his continuous support, guidance and encouragement on my research presented in this dissertation. I also appreciate the assistance and guidance of my committee members, Drs. Christopher W. Reed, David R. Basco, and Ronald E. Johnson.

The abandoned Yellow River delta study has been funded by National Science Foundation of China. The northern California continental shelf research has been funded by the U.S. Office of Naval Research through the STRATAFORM project, under the guidance of Dr. Joseph Kravitz. I thank these several agencies for their financial support.

I would also like to thank all the STRATFORM-ERs who have been supportive of my work, including Dr. Alan Wm. Niedoroda, Dr. Charles Nittrouer, Dr. Michael Steckler, Dr. John A. Goff, Dr. David E. Drake, Dr. Peter Traykovski, Dr. Samuel Bentley and Dr. Courtney K Harris, and many others. Rodney L. Clayton provided assistance in the sediment analysis. I benefit a lot from the discussion with Stephen B. Parsons. Special thanks should go to Cathy McConaugha for her long time logistics, fiscal, graphics and editing supports.

I especially would like to express my most sincere thanks to Dr. Yong Zhang, my wonderful long time friend and colleague, for all the moments we worked together, for all the ideas we discussed.

TABLE OF CONTENTS

LIST OF TABLES

LIST OF FIGURES

CHAPTER I

INTRODUCTION

GEOLOGIC PERSPECTIVE

This thesis consists of three papers, submitted for peer-reviewed publication, that examine related problems of coastal ocean morphodynamics. The morphology evolution of coastal oceans is the consequence of morphodynamic processes that occur in response to changes in external conditions (Wright and Thom, 1977). Coastal morphodynamics is defined as the 'mutual adjustment of topography and fluid dynamics involving sediment transport' (Wright and Thom, 1977). The environmental conditions, such as climatic and geological, are exogenous inputs of the coastal ocean system, which are responsible for the geographic variation among coastal ocean. In the coastal ocean system, the coastal morphological changes are the results of a series of fluid dynamic and morphodynamic processes at different temporal and spatial scales. At short time scales (seconds to days), the coastal flows (waves, currents and winds) drive boundary layer flows; the near-bed boundary layer flows entrain and carry the sediments. If we know the sediment budgets during the time period of interest, we can determine the erosion and deposition of the coastal zone and the resulting topography and event stratigraphy. The changes of

---

The model journal for this dissertation is Marine Geology

topography will in turn affect the coastal flows and the near-bed boundary layer flows. Identification of which environment conditions and morphodynamic processes are important, and how they might be modeled best, has been the subject of most of the efforts of coastal process studies over the past two decades (e.g., Wright, 1987, 1993; Cowell and Thom, 1994) and is by no means complete.

Dynamical sedimentary processes need to be extended over longer time scales (decades to thousands years) in order to study the morphologic responses and facies formation of coastal ocean. A sedimentary facies is defined as a body of sediments or sedimentary rocks with specified characteristics (Reading, 1986). Sedimentary lithofacies (hereafter called facies) are characterized by their distinctive sedimentary textures and structures, which reflect the relevant depositional environments. Although the construction and use of facies models for the interpretation of sedimentary environments have been adopted by stratigraphers in recent years (Walker and James, 1992; Reading, 1986), these existing facies models are descriptive. The test for processes that control facies successions and geometries by comparing modern and ancient depositional environments, and by interpreting strata formation through analog and pattern-matching techniques. Only recently, has a quantitative dynamical facies model, based on fundamental physics of sediment dynamics, been proposed and applied on the northern California continental shelf (Zhang et al., 1997). In order to extend on this pioneering approach, the abandoned Yellow River delta of China and the Eel River continental shelf of northern California have been chosen as sites in which to study how coastal ocean topography and sedimentary facies change as the results of the most important

environmental and morphodynamic processes. By demonstrating the sedimentation processes through successive temporal and spatial scales, quantitative dynamical models for nearshore processes on the abandoned Yellow River delta, and models of storm driven sediment sedimentation and event stratigraphy formation on northern California continental shelf have been developed. These models will be used to test hypotheses concerning the processes that are responsible for the coastal stability of abandoned and subsided Yellow River delta and for event stratigraphy and facies formation on the northern California continental shelf. These dynamical sedimentary models lead to significant geologic insights and dynamical understandings of the coastal ocean sedimentary processes that traditional, descriptive sedimentology and stratigraphy cannot easily provide or prove.

PROBLEMS EXAMINED

The Stability and Profile Evolution on Muddy Coast

How do coastal line and profile response to waves and currents? What is the fate of sediment? How may the evolution of coastline and coastal profile be predicted? As a consequence of the development of coastal zone, the assessment of coastal change is becoming more and more important for purposes of coastal management. It also is a phenomenon of fundamental interest to geologists and oceanographers. In the past, the prediction of coastal change and profile evolution was mainly conducted by relying on experience and on the results of hydraulic model tests. In more recent years, however,

numerical models have gradually been developed and are increasingly applied for this purpose (Schoonees, 1995; Nairn and Southgate, 1993; Brϕker Hedegaard et al., 1992). But most of these researches were conducted on sandy coasts. Few have been conducted on muddy, or cohesive, coast. It has been recognized that muddy, or cohesive, coasts are fundamentally different from sandy coasts in their morphodynamical processes (Fan et al, 1997a, 1997b; Zhang et al., 1998; Nairn and Southgate, 1993). On open cohesive coasts, the cohesive sediments of the sea floor are resuspended into the water column by nearshore waves. The reworked cohesive sediments are dispersed over great distances by tidal currents in a suspensive mode owing to their very low settling velocity, and are rarely redeposited in their original locations (Yu et al., 1987). In this study, the abandoned, submerged Yellow River delta is chosen as a site in which to study coastal stability and profile evolution in a muddy coastal setting.

Storm Driven Sediment Sedimentation on the Storm-Dominated Continental Shelf

On storm and river flooding dominated continental shelves, storm waves, storm currents and river flooding are major processes driving sedimentation, and result in patchy event beds and a central or outer shelf mud-belt beyond a nearshore zone of wave-winnowed sands. This pattern has been observed in the Celtic Sea and the Gulf of Gascony (McCave 1972), the shelf of Western South Africa (Birch, 1977), the Southeastern Australia shelf (Davies 1979; Roy and Thom 1981), the Nayarit shelf of

western Mexico (Curray 1969), the Gironde shelf of France (Lesueur et al. 1996) and Northern California continental shelf, USA (Nittrouer et al. 1979; Nittrouer and Sternberg 1981, Borgeld 1985; Bouchard and Borgeld 1988; Wheatcroft 1996). In all these cases, the geometry and radiogeochemistry of the offshore deposit shows that much or most of the fine-grained sediments of the central and outer shelf are derived from the river, especially during river floods, and that a smaller part of silty fine sand is derived from in the sandy covering of the inner shelf, during high-energy (i.e. storm) events (Sommerfield and Nittrouer, 1999). But the mechanisms of cross-shelf dispersal and deposition, i.e., how does sediment rain out from the inshore flood plume and get to the central and outer shelf, how the patchy event beds are formed and how they undergo modification during burial processes are not well understood, nor is the nature of the resulting event stratigraphy. We address these questions by examining the dynamics of the Eel River sector of the northern California shelf.

Transgressive Stratigraphy on the Storm-Dominated Continental Shelf

Stratigraphy is the study of sedimentary deposits at all spatial scales. At the small-scale end, stratigraphy is defined by sedimentological concepts, such as beds, bed sets, and bed cosets (Swift and Parsons, 2000; McKee and Weir, 1953; Campbell, 1967). At the larger-scale end, Stratal termination patterns, systems tracts and relative sea level changes are used to described stratigraphy (Vail et al., 1977 and many later papers).

Between these two end members is an intermediate region called "facies" (Swift and Parsons, 2000). Traditionally sequence stratigraphy is studied by mapping geometry of stratal terminations, distribution of unconformities, and facies stacking patterns. Recently stratigraphic numerical models are increasingly used as analytical tools for purposes as diverse as petroleum exploration, naval warfare, and coastal engineering (Bagirov and Lerche, 1999, Syvitski, et al., 1997; Niedoroda et al., 1995). Stratigraphic sections in sedimentary basins are self-similar across a range of time and space scales. Therefore, process-based forward numerical modeling of stratigraphic sections is faced with a significant problem of upscaling, in moving from the process of event bed formation (times scales of seconds to days), to the evolution of depositional sequences (time scales of thousands to millions of years). The problem is compounded by the differing backgrounds of persons modeling at the extremes of this range; physical and geological oceanographers model storm beds (Niedoroda et al., 1989; Zhang et a., 1999; Harris and Wiberg 2001), while students of lithospheric mechanics model depositional sequences (Steckler, 1999). There is often little connection between the two approaches. In this thesis, a numerical model is presented for simulating stratigraphic sections at intermediate temporal scales (decades to thousands of years) that has been developed as part of ONR's STRATAFORM program. We show how this model (FACIES) is related to models of short-term boundary layer behavior, and suggest ways that it can be embedded in models of sediment accumulation at longer time scales.

APPROACH

In order to study the problems described above, the abandoned Yellow River delta of China and the Eel River continental shelf of northern California are chosen as case study areas. The abandoned Yellow River delta has been an erosional coastal zone since the Yellow River changed its course in 1855. The Eel River continental shelf is dominated by winter floodings and storms. By demonstrating the sedimentation processes through successive temporal and spatial scales, quantitative dynamical models of nearshore processes on the abandoned Yellow River delta, and of storm driven sediment sedimentation and resulted transgressive stratigraphy on northern California continental shelf have been developed. These model simulated geologic processes serves to test the hypotheses concerning the processes that are responsible for the coastal stability of abandoned Yellow River underwater delta and event stratigraphy formation on the northern California continental shelf.

Chapter II studies the stability and profile evolution of the abandoned submerged Yellow River delta. The old Yellow River delta in Jiangsu province, China, has been abandoned since 1985, when the Yellow River changed its course to Shandong Province. With the ending of river-supplied sediment, the abandoned delta-top platform has subsided below sea level, while the delta front has been eroded by waves and tidal currents, resulting in its large-scale truncation, and the removal of the eroded sediment.

As a result, three different types of morphological features have formed. A pro-delta shelf extends from 10 m to 15 m water depth with a slope of less than 1/500. A delta front extends from 5 m to 10 m water depth with a slope of less than 1/100. A subsided delta platform lies landward of the 5 m isobath with a slope of less than 1/500. The pro-delta shelf seaward of the 10 m isobath has remained relatively stable since the delta was abandoned. However, the former delta front, between 5 m and 10 m isobath, has gradually rotated into parallelism with the longitudinal axis of the tidal ellipse, and its slope has been modified by tidal current action. On the subsided delta-front platform shallower than 5 m, the formerly severe recession of the coastline has been checked by coastal defense structures. As a result, wave-induced erosion is confined to the seabed of the delta-top platform itself. Continuing adjustment can be detected by examination of time series of profiles, which reveal recession of the point of maximum curvature and downcutting.

While the rate of morphodynamic change of the subsided delta is waning, adjustments (as indicated by continued deepening) are still incomplete. As a consequences, the present intense, along-shore flux of silt-sized material can be expected to continue into the foreseeable future. This factor will effect the local harbor construction and maintenance, and its control must enter into engineering plans for harbor construction.

Chapter III studies storm driven sediment sedimentation on the northern

California shelf, on which high and low concentration regimes play different roles. Successions of very thin-bedded to thin-bedded, sandy silt and clayey silt beds on the northern California shelf appear to be records of storm resuspension. Thicker, muddier beds are deposited during periods of river flooding. Because the turbid, brackish water, surface plumes associated with river floods do not seem to commonly reach the central shelf, the relative roles of floods and storm currents in forming shelf beds are at issue. In this chapter, after wave, current, and sediment concentration data are analyzed, a two-dimensional, across-shelf sediment transport model is presented and is used to simulate sediment re-suspension, deposition and bed evolution during a six weeks period of winter storms in 1996, in order to resolve the dilemma. The observations and simulations show that rather than dividing beds into "flood" and "storm" beds, it is more meaningful to divide the event beds into the deposits of high concentration regimes and low concentration regimes. Coast-hugging surface flood plumes occur on the inner shelf during the winter season. The plumes generate dense, near-bottom suspensions, which may attain fluid mud concentrations (> 5 g/l) as particles settle. The period of storm-heightened waves may continue into the flood period, leading to gravity-driven seaward displacment of the bottom suspension, or the wave regime may ameliorate, leaving the suspension to consolidate as a short-lived inner-shelf flood bed. Such beds tend to be resuspended within days or weeks by subsequent storm events that may recreate the original high concentrations. The sediment is dispersed seaward, by either gravity or

wind-driven flows to be deposited as a muddy "flood bed" on the central shelf. In contrast, low concentration regimes occur during storm periods when there has been no recent flood deposition on the inner shelf. The shelf floor is better consolidated than in the previous case, and the resulting suspended sediment concentrations are lower. As a consequence, beds deposited are thinner and sandier. In multi-year event bed successions, flood beds stand out, not only because more and finer material has been supplied to them, but because the change in the rate and character of supply has itself altered the dynamics and shifted the regime toward accumulation.

Chapter IV studies transgressive stratigraphy on the northern California shelf by developing a quantitative and statistical process-based facies model. Process-based forward numerical modeling of stratigraphic sections leads to a significant problem of upscaling, in moving from event bed formation (times scales of seconds to days), to the evolution of depositional sequences (time scales of thousands to millions of years.) FACIES is a model that serves to bridge this gap by simulating stratigraphic sections at intermediate time scales (decades to thousands of years FACIES employs subroutines describing short-term boundary layer processes and can be embedded in models of sediment accumulation at longer time scales. A preliminary investigation of transgressive stratal architecture on the tectonically active northern California margin has been undertaken with FACIES. Wind and wave-generated currents during winter storms resuspend sediments of the Eel sector of the Northern California Shelf, and the same winter storms may also flood the Eel and Mad rivers. Turbid, coast-hugging low-salinity plumes generated by these floods give rise to fluid muds on the inner shelf floor, which

may slide seaward under the impetus of gravity onto the central shelf or over the shelf edge. Beds deposited by this high-concentration regime are poorly sorted, mud rich, and contain pebble or sand-sized wood fragments. Low-concentration resuspension events, which are not associated with floods and lack fluid mud, create thinner, sandier beds than do the fluid mud flows. A simulation of a 400 year sequence of beds deposited by winter storms and floods suggests that on the Eel shelf, the Holocene transgressive systems tract consists of back-stepping, seaward-fining event beds, whose timelines (bedding planes) dip more gently than do their gradational facies boundaries.

CHAPTER II

STABILITY ANALYSIS AND PROFILE EVOLUTION, ABANDONED AND SUBMERGED YELLOW RIVER DELTA

INTRODUCTION

The Yellow River discharges an average of 1.1×10^9 tons of sediment into the sea annually (Qian and Dai, 1980), accounting for almost 10% of the fluvial sediments reaching oceans in the world. During AD 1128-1855, the Yellow River flowed partly or exclusively into the Yellow Sea, forming a major delta in Jiangsu (Fig. 1). The old Yellow River delta reached as far north as Lianyungang, and as far south as the Sheyang River, a distance of more than 100 km. The pro-delta front extended to –20 m and the delta as a whole occupied a area of 7,000 km^2. In 1855, the Yellow River avulsed and shifted to the north side of the Shandong Peninsula where it flowed into the Gulf of Bohai. As a consequence, the balance between fluvial and the marine process was modified significantly due to the sudden loss of the Yellow River sediment discharge. Since then the abandoned delta, composed mainly of silt and clay, has been undergoing severe erosion (Wan, 1989).

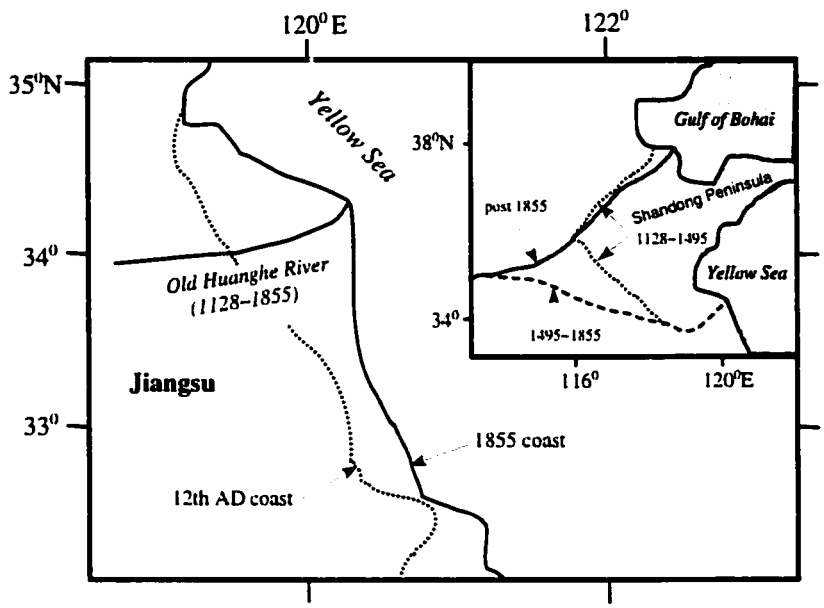

Fig. 1. Location of the abandoned Yellow River Delta.

With the ending of river-supplied sediment, the abandoned delta top platform has subsided below sea level, while the delta front has been eroded by waves and tidal currents, resulting in its large-scale truncation, and the removal of the eroded sediment. As a result, the –5, –10 and –15m isobaths have shifted rapidly toward shore and now occur at distance of 1.13 km, 2.25 km and 4.75 km from the coast line, respectively. This area has become the only hope for location for deep-water harbor along the 1000 km coastline of Jiangshu province. In order to build a deep-water harbor on muddy coast, the stability of the underwater delta and the evolution of the coastline and profile must be studied (Yu et al., 1998).

CHARACTERISTICS OF COASTAL AND UNDERWATER DELTA EVOLUTION

When the Yellow River changed its course in 1855, the erosion of the abandoned Yellow River delta began at the delta front. The recession of the underwater delta is characterized by the landward movement of –10 m isobath, subsidence and erosion of the delta platform (Yu, 1986; Wan, 1989). A map published in 1904 shows the situation of the delta after half-century erosion (Panel 1 of Fig. 2). The subsided delta has retained the characteristic deltaic shape. The -10 m isobath on the southeast end of the delta has been straightened, but the tidal sand ridge patterns on the northwest and southeast flanks of the

delta are still there. By 1935 (Panel 2 of Fig. 2), the sand ridges have been totally erased. On the south side of Tiaoziko, the –10 m isobath has moved 40 to 50 km landward, and has rotated into parallelism with the main current direction. By 1960, the southern part of –10 m isobath had further moved landward, and had cut into the north delta platform, which shows marked erosion by a coast-parallel current. By 1980, the –10 m isobath had cut through the north delta platform and had formed a deep-water channel that splits the north delta platform. Although the recession rate of –10 m isobath was slowing at this time, the –15 m isobath was shifting more rapidly toward shore. After more than one century of erosion since the river shifted its course in 1855, three different types of morphological features have emerged, which are pro-delta shelf (the zone between the 10 m and 15 m isobaths with slope of < 1/1000), delta-front slope (the zone between the 5 m and 10 m isobaths with slope about 1/100) and subsided delta platform (zone shoreward of the 5 m isobath with slope < 1/500; table 1). Recession of delta front slope and pro-delta shelf is waning (Table 2).

During the erosion of underwater delta, the coastline has also experienced severe recession. Waves, especially breaking waves, are responsible for mud flat erosion while currents carried sediment alongshore and offshore. Because the deep water of the southern part is closer to the coastal line than the northern part, waves are higher and the rate of coastal line recession is greater on the southern side. Table 3 shows the yearly average recession rate at several locations based on maps of 1923, 1956 and 1982. The

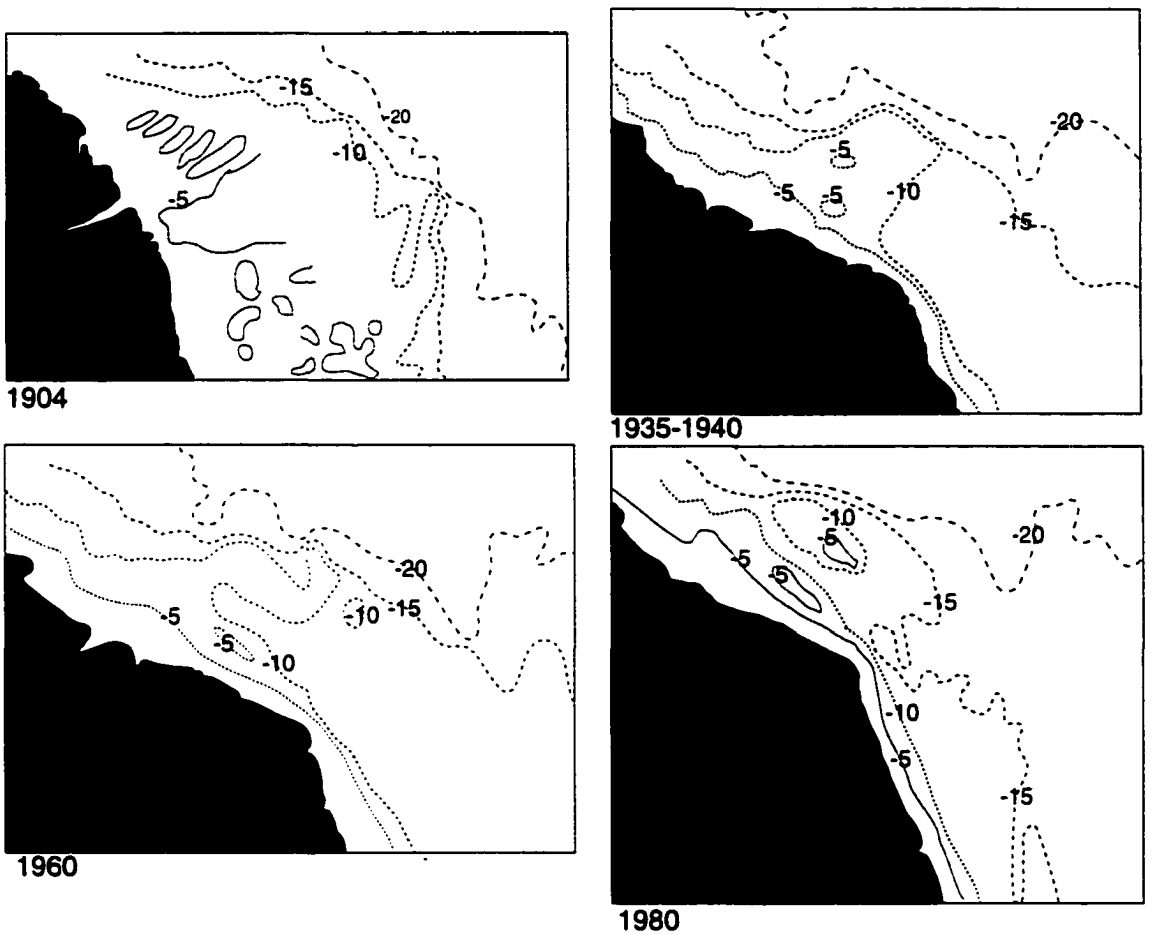

Fig. 2. Evolution of the abandoned Yellow River delta from 1904 until 1980.

Table 1

Profile characteristics of abandoned Yellow River underwater delta (based on map of 1980). The profile can be divided into three morphological zones: pro-delta shelf (10 m to 15 m isobath with slope of < 1/1000), delta front slope (5 m to 10 m isobath with slope about 1/100) and subsided delta platform (coastward of the 5 m isobath with slope < 1/500).

Cross-Shore Profiles	Subsided-delta platform (-1m ~ -5m)		Delta front slope (-5m ~ -10m)		Pro-delta shelf (-10m~ -15m)
	Width (m)	Slope	Width (m)	Slope	Slope
Mouth of New Huaihe River	5200	1/1300	700	1/120	1/1000
Mouth of Fanshenhe River	2000	1/500	1125	1/225	1/1000
Mouth of Yuhuanghe River	3500	1/700	500	1/100	1/1200

Table 2

Recession rates of –5 m and –10 m isobath (unit: meter/year)

Year	-5 m isobath	-10 m isobath
1940 ~ 1980	150	160
1980 ~ 1993	60	115
1993 ~ 1995	40	80

Table 3

Yearly average recession rates of coastal line based on maps of 1923, 1956 and 1982 (unit: meter/year)

Location	1923 ~ 1956	1956 ~ 1982
Xinhuanyanchang	70	26
Liuhezhuang	106	60 (stable by sea wall since 1968)
Zhendongza	83	50

data indicate that the erosion is slowing. To our surprise, the coastline at Liuhezhang, which used to be the most rapidly eroding part of the coastline, has been stabilized by a rather sub-standard sea wall since 1968.

NEAR SHORE HYDRODYNAMIC CHARACTERISTICS AND SEDIMENT TRANSPORT

Tides and Tidal Currents

The tides in this region are controlled by the south Yellow Sea standing wave system, and the dominant tidal constituent is M_2. The zero tide node of M_2 tide is located at $34^0 30' N.121^0 10' E$, at the far front of the underwater delta at a depth of 20 m. The tidal range is less than 2 m near shore (Yu, 1993).

In May 1993, eight small ships were employed to do current measurement and water sampling under neap, spring, and median tide periods (Fig. 3). At every site, 6 points (bottom, 0.2, 0.4, 0.6, 0.8 of water depth and surface) were measured and sampled. In January 1994, tidal currents were measured again at station 1, 2, and 3. The currents rotate anti-clockwise, the degree of ellipticity decreases shoreward. Close to shore, the ellipticity is near zero. Here the major axes are oriented between $160^0 \sim 170^0$ and $340^0 \sim 350^0$, parallel to the coast line.

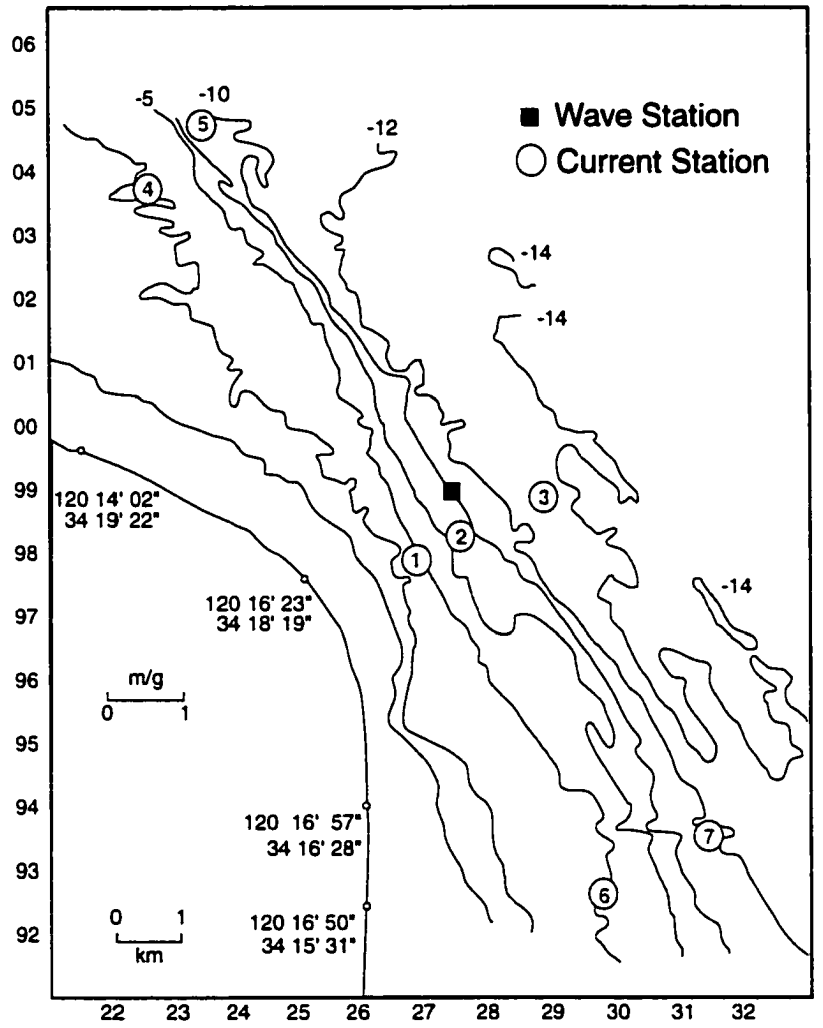

Fig. 3. Locations of wave and current measurement stations.

Table 4 presents the characteristic values of current of three different cross-shore profiles. The data show that the current is very strong when water depths exceed 5 m, here, the maximum bottom velocities of 0.6 ~ 0.7 m/s create a very strong sediment transport potential. On subsided delta platform, because of the effects of shallow water and bottom shear, the tidal current decreases. The maximum bottom velocity is 0.49 m/s, and the main role of the current is transporting eroded sediment eroded by breaking waves.

The current-induced bed shear stress, $\tau_{0c} = \rho u_{*c}^2$ where ρ is water density and u_{*c} is a characteristic shear velocity, is the parameter for describing the erosion capability of current. In the case of neutrally stratified flows with bottom velocity (50 cm above the bottom) larger than 50 cm/s, u_{*c} can be estimated from the log-layer velocity profile by the von Karman-Prantdl equation (Gross et al., 1992):

$$|u| = \frac{u_{*c}}{\kappa} \ln \frac{z}{z_{0c}} \qquad (1)$$

in which u is mean current at height z, κ is von Karman's constant (~0.4), and z_{0c} is the intercept expressing apparent roughness. In classic laboratory analyses of fully rough turbulent flow, the log-profile zero intercept, z_0, is related to the height, k_r, of the effective roughness elements by $z_0 = k_r/30$. However the apparent roughness, z_{0c}, as determined from the best fit of equation 1 to velocity profiles, is typically much greater

than $k_r/30$ because of the presence of wave and, potentially, because of sediment-induced stratification effects during high-energy events.

Figure 4 presents current shear velocities, u_{*_c}, during neap, spring, and median tide periods at different current station 1, 2, and 3. It shows that current shear velocities are almost the same at different stations when water depth larger than 5 m. It also shows that the maximum can reach 9 cm/s during flood period of spring tides, and 5 cm/s during ebb of median and neap tides. Considering the critical erosion shear stress of the sediment on the delta front slope (-8 m isobath) is about 3.5 cm/s (Huhe et al., 1996), the tidal currents can not only transport sediment, but also can erode the submerged delta.

Sediment Concentration and Sediment Flux

Figure 5 presents vertically averaged sediment concentrations during neap, spring, and median tides periods at current station 1, 2 and 3. Although the shear velocities at the different stations are almost the same, the vertically averaged sediment concentration at station 1 is much larger than that at station 2 and 3. That means that the resuspended sediments on the subsided delta platform (shallower than 5 m) were transported diffusely to the upper part of the delta-front slope and that wave orbital motions enhanced the erosion and resuspension of the local sediment. The calculation of sediment flux along an unit width (1 m, for example) at the eight stations shows that the net sediment flux is

Table 4

Maximum vertical average velocities ($\bar{u}_{flood}$ and $\bar{u}_{ebb}$) and near bottom current velocities ($\bar{u}_{bflood}$ and $\bar{u}_{bebb}$) obtained from field station measurements (unit: meter/second (degree))

Profile	Profile 1 (North of turn point)			Profile 2 (at turn point)		Profile 3 (South of turn point)	
Station	#4 (-2.0 m)	#5 (-10.0 m)	#1 (-5.0 m)	#2 (-9.0 m)	#3 (-13.0 m)	#6 (-5.0 m)	#7 (-12.0 m)
$\bar{u}_{flood}$	0.93(164)	1.01(126)	0.57(63)	0.99(116)	0.87(161)	1.10(154)	1.28(164)
$\bar{u}_{ebb}$	0.88(342)	0.96(335)	0.31(331)	0.90(325)	0.76(345)	0.88(345)	1.07(348)
$\bar{u}_{bflood}$	0.75(167)	0.67(131)	0.49(72)	0.61(116)	0.56(169)	0.76(150)	1.11(172)
$\bar{u}_{bebb}$	0.57(341)	0.66(337)		0.67(330)	0.59(351)	0.61(350)	0.73(350)

Table 5

Wave height $H_{1/10}$ distribution at 10 m isobath (July, 1993 ~ June, 1994).

$H_{1/10}$ (m)	0.0 ~ 0.5	0.5 ~ 1.0	1.0 ~ 1.5	1.5 ~ 2.0	2.0 ~ 2.5	2.5 ~ 3.0	>3.0
Frequency (%)	24.67	39.22	17.31	9.73	4.00	2.86	2.19

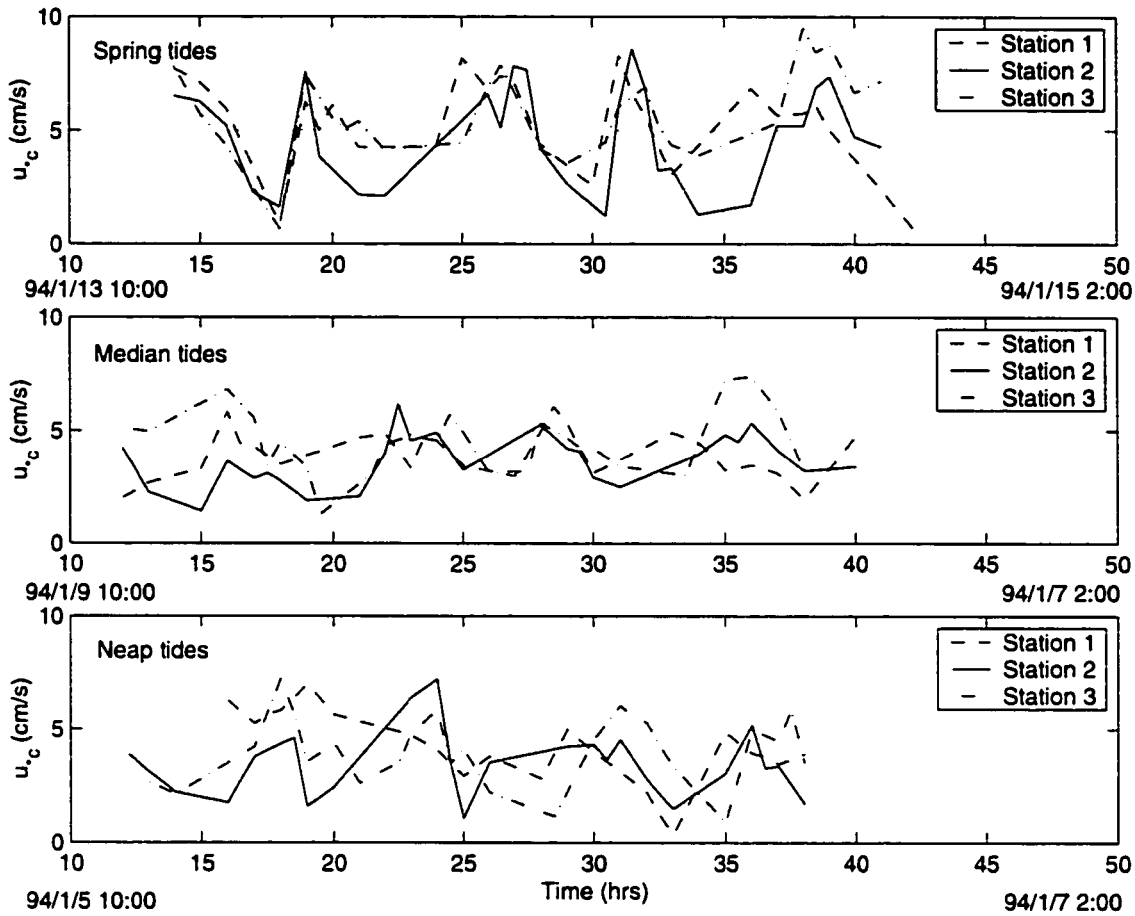

Fig. 4. Current shear velocities, u_{*_c}, during neap, spring, and median tide periods at current station 1, 2 and 3.

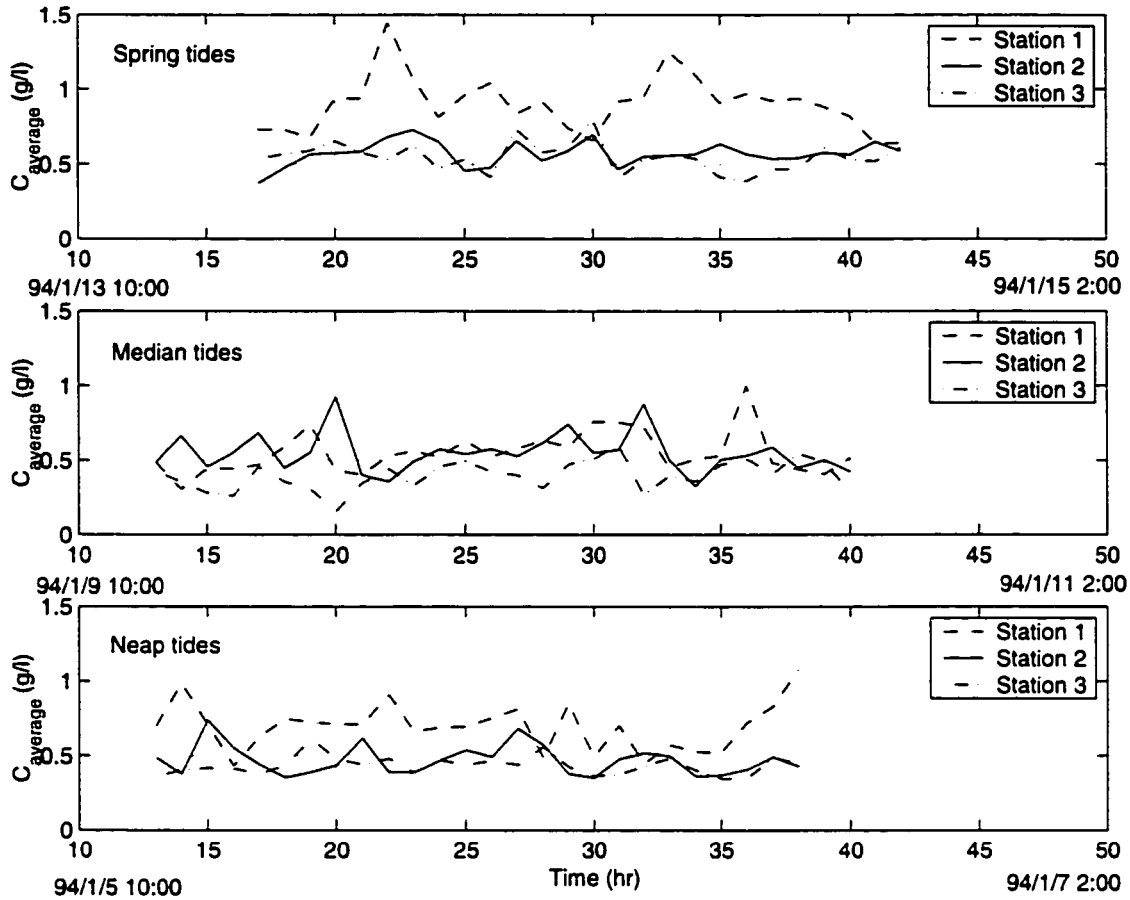

Fig. 5. Vertically averaged sediment concentrations during neap, spring, and median tide periods at current station 1, 2 and 3.

divergent around the turn of the coastline with net sediment movement to the northwest at north part, and to the southeast at south part. The eroded sediments are transported by the strong currents and cannot redeposit locally. The dominant erosion process is irreversible erosion of the cohesive material. The fine, cohesive material is eroded and winnowed offshore, and is permanently lost to the nearshore system, as occurs on the cohesive coasts of the Great Lakes (Skafel, 1995).

Waves

The center part of the coastline of the abandoned Yellow River delta is a headland with a convergence of wave energy. Since there is no shield, waves can propagate toward shore directly, and play a very important role for the stability and evolution of the coastline and submerged delta. The wave data from the wave station at the 10 m isobath shows that the most frequent wave directions are northeast and southeast, and that the strongest wave directions are north, and northeast. The distribution of 1/10 wave height, $H_{1/10}$, is presented in table 5 and the significant wave height and wave period has the relationship (Gong et al., 1994):

$$T = 5.10 H_{1/10}^{0.31} \qquad (2)$$

As surface gravity waves approaching a coast propagate into intermediate depths of the shelf, wave energy flux is approximately conserved. However, as waves move into

shallow water, shoaling, refraction, and bottom friction become important. The shoaling increases the surface wave height and reduces its stability while bottom friction attenuates the wave energy. When waves move into very shallow water, they become unstable and break, and organized wave energy is converted to turbulent water motion and dissipated. Wave orbital velocities and turbulence generated by wave breaking are the main initiators of sediment erosion in the surf zone. In order to understand the role waves played for the stability and evolution of the abandoned and submerged Yellow River delta, we need to determine the wave transformation from deep water through surf zone. Because the strongest wave direction is almost perpendicular to the isobaths and coastline and the sea-bed is open and gentle with very small slope, we use a one-dimensional cross-shelf model to study the wave transformation without considering the effects of wave refraction.

The wave transformation cross shelf can be predicted by solving the wave energy balance equation:

$$\frac{d\left(EC_g\right)}{dx} = -D_b - D_f \tag{3}$$

where $E = \frac{1}{2}\rho g H^2$ is the energy density, ρ is the density of the water, g is the gravitational acceleration, H is wave height, C_g is the group velocity, D_b and D_f are the

loss in wave energy per unit area per unit time due to wave breaking and bottom friction, separately, and x is the distance along the wave path.

Much work has been done on wave energy dissipation due to wave breaking. Two approaches are commonly used to evaluate the wave properties in the surf zone. The first approach predicts the variation of the wave properties within a wave cycle. The Boussinesq model is an example of such a detailed model (e.g. Schaffer, et al., 1993). The second approach calculates for wave properties averaged over a wave period. In most applications, such a model is sufficient. Here we relate the wave-energy-dissipation rate to the excess energy contained in a wave above some stable limit proposed by Dally, Dean and Dalrymple (1985):

$$D_b = \frac{K}{d}\left[\left(E - E_{st}\right)C_g\right] \qquad \text{for } E > E_{st} \tag{4}$$

where E_{st} is stable limit of wave energy, which is the following function of depth:

$$E_{st} = \frac{\rho g}{8}(\Gamma d)^2 \tag{5}$$

where d is water depth. The usual values for the constants, derived from the work of Horkawa and Kuo (1966) with regular waves, are:

$$K = 0.15 \text{ and } \Gamma = 0.4 \tag{6}$$

Seaward of surf zone, the bed friction is the dominant factor of wave energy attenuation. In the surf zone, bed friction damping is not significant on relatively steep bed slopes comparing with that of wave breaking, but will play a very important role

where extensive mild offshore slopes exit, such as on most cohesive coasts. Tidal flats usually have bed slopes less than 1/500 and the surf zone is much wider than in the case of a sandy beach. The estimation of the wave energy dissipation factor (f_w) is crucial to the study of bed friction damping. This factor is defined by Jonsson (1966) is:

$$\tau = \frac{1}{2}\rho f_w u^2 \tag{7}$$

where τ is the instantaneous bed shear stress at any given time and u is the instantaneous bed velocity at the same time.

The value of f_w is assumed to remain constant with respect to time at a given location so that the average rate of energy loss per unit surface area is (Nielson, 1995),

$$D_f = [\tau u]_{mean} = \frac{2}{3\pi}\rho f_w u_{b\max} \tag{8}$$

where $u_{b\max}$ is the maximum water particle velocity at the bed. For this area, $f_w = 0.015$ (Jin, 1978).

Since the nearshore slopes vary from 0.001 to 0.01, spilling is the dominant breaking wave type in this area (Battjes, 1974, Gaughan and Komar, 1975). The turbulence of spilling is mainly caused by a surface roller vortex (Peregrine and Svendsen, 1978; Basco, 1985; Deigaard *et al.*, 1986). As spilling propagates toward shore, the turbulence extends down to sea floor. The fluid field caused by spilling exhibits a quasi-stable state (Peregrine and Svendsen, 1978). Linear wave theory has been

widely used in the surf zone hydrodynamics, for example, for the wave energy transformation, under spilling conditions (Battjes and Janssen, 1978; Thornton and Guza, 1983; Lippmann *et al.*, 1996). The bottom shear stress caused by spilling can be fairly well estimated by linear wave theory (Cox *et al.* 1996). Considering that there is little difference for turbulence transport of a spilling between the inner and outer surf zone (Ting and Kirby, 1996), linear wave theory can be used as a first order approximation for estimating the wave-induced water particle velocity and bottom bed shear stress across the shelf:

$$u_{b\max} = \frac{\pi H}{T \sinh(kd)} \tag{9}$$

$$u_{*w\max} = \sqrt{\frac{1}{2} f_w u_{b\max}} \tag{10}$$

Since the initiation of sediment is an average concept, the average wave-induced shear velocity, $u_{*wa} = \frac{1}{2} u_{*w\max}$, should be used for study the erosion of waves (Bijker, 1986).

Figure 6 is wave cross-shelf transformation and induced averaged shear velocity distribution along profile 1. Panel 2 shows that averaged shear velocities increase as waves propagate toward shore. On the pro-delta shelf, even for big waves with 4 m wave height, the averaged shear velocity is less than 5 cm/s. The shear velocity is much smaller than that of tidal currents and can not resuspend sediment directly. As waves move into

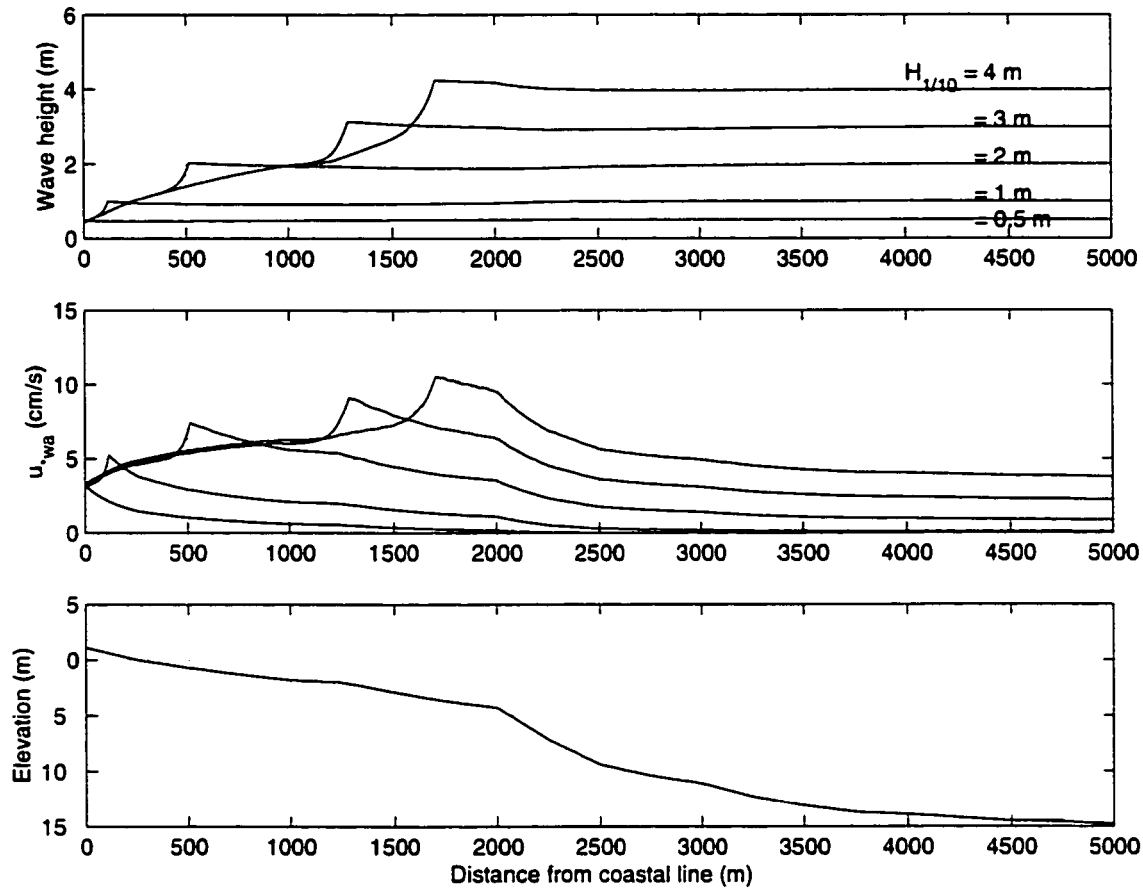

Fig. 6. Wave cross-shelf transformation and induced averaged shear velocity distribution along profile with station 1, 2 and 3. Panel 2 shows that averaged shear velocities increase as waves propagate toward shore.

the delta-front slope and subsided delta-platform, the averaged shear velocity increases rapidly, and can reach 10 cm/s at the breaking point for 4 m waves. The shear velocity is much larger than that of tidal currents and plays dominant role for sediment resuspension, as tidal currents dominate sediment transportation. So we only consider the erosional effects of waves in the surf zone while considering the effects of both waves and tidal currents elsewhere.

Cross-shelf Wave-current Induced Bed Shear Stress Distribution

The calculation of wave-current bed-shear stresses is essential for the analysis of sediment suspensions. Several models have been developed (Grant and Madsen, 1979, 1986; Smith, 1977; Bijker, 1986; Sleath, 1991). Although the Grant-Madsen model (1979) and Smith model (1977) can provide a highly resoluted current structure in the wave-current boundary layer, Bijker's method for calculating wave-current bed-shear stress has been used for reasons of simplicity.

The time-averaged value of the absolute bed-shear stress for combined wave-current flow with the presence of wave $\tau_{b,cw}$ is (Bijker, 1986):

$$\rho u_{*cw}^2 = \tau_{b,cw} = \tau_{b,c} + \tau_{b,w} = \rho u_{*c}^2 + \frac{1}{4}\rho u_{*w}^2 \qquad (11)$$

where $\tau_{b,c}$ is time-averaged current bed shear stress, $\tau_{b,w}$ is time averaged value of absolute wave shear stress; and u_{*c}, u_{*w}, and u_{*cw} are current, wave and wave-current combined shear velocity, respectively.

CROSS-SHORE EROSION RATES AND PROFILE EVOLUTION

Cross-shore Erosion Rates

The erosion rate for a cohesive bed is generally expressed empirically in terms of the excess shear stress (Mehta *et al.*, 1989; Teisson *et al.*, 1993). The equation of erosion rate proposed by Partheniades (1965) has been widely used in the modeling of cohesive sediment transport (Ariathurai and Krone, 1976; Ariathurai and Arulanandan, 1978; Nicholson and O'Connor, 1986; Mehta *et al.*, 1989):

$$\frac{dE}{dt} = \mathrm{H}(\tau_{b,cw} - \tau_c) M\left(\frac{\tau_{b,cw}}{\tau_c} - 1\right) = \mathrm{H}(u_{*cw} - u_c) M\left(\frac{u_{*cw}}{u_c} - 1\right) \qquad (12)$$

where $\mathrm{H}(x)$ is Heaviside function, E is the mass of eroded cohesive sediments per unit area (kg/m^2), M is an erosion coefficient (kg/m^2s) that is closely related to the physical-chemical properties of cohesive sediment, for this area, and u_* and u_{*c} are the bottom shear velocity and the critical shear velocity for erosion respectively.

Assuming that the shear velocity of the tidal current decreases linearly from its measured value at 5 m isobath to 0 at coastline, we can calculate the shear velocity of the tidal current shoreward of the 5 m isobath. This value may also be calculated by using

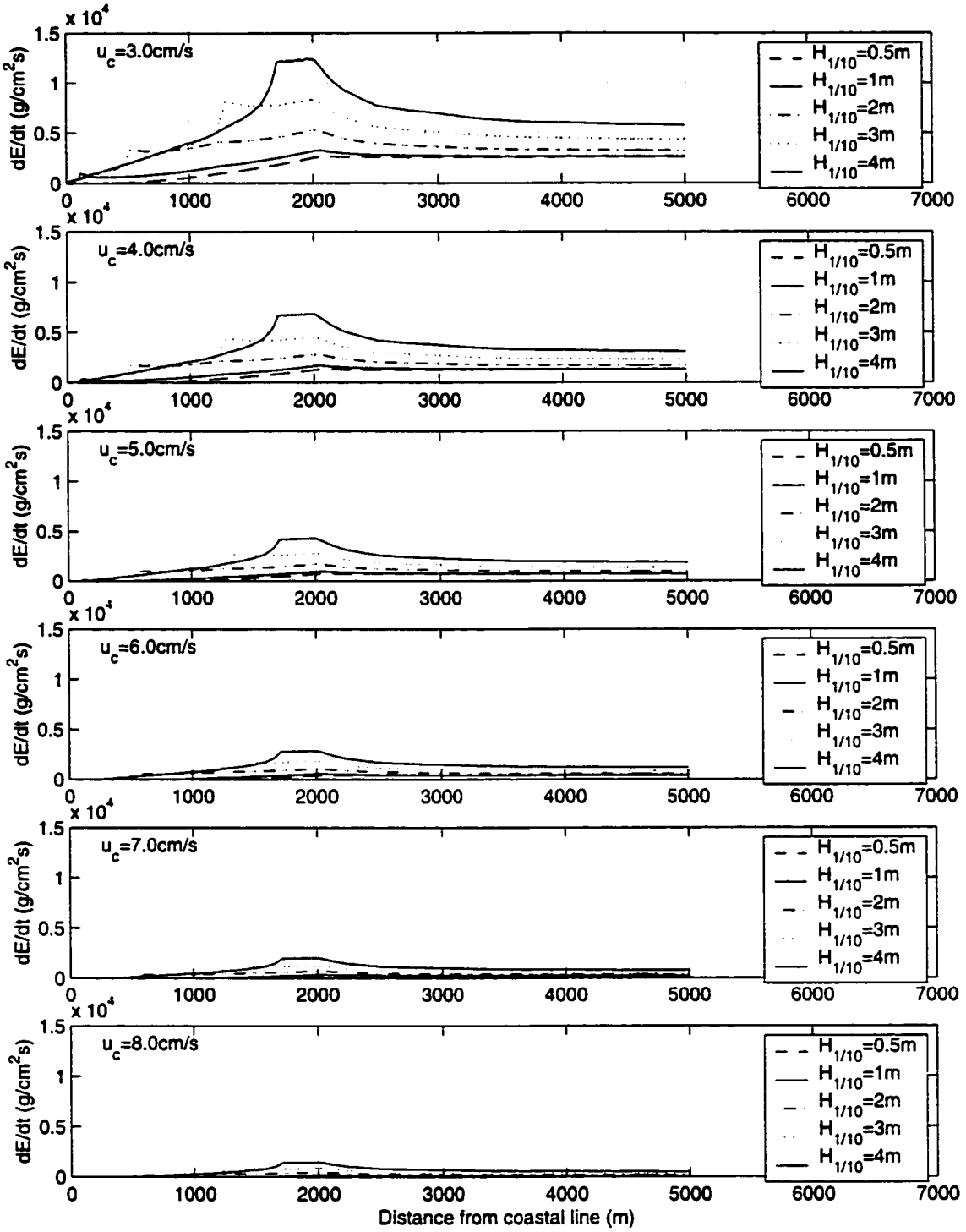

Fig. 7. Cross-shore erosion rate for different incident wave height and critical erosion shear velocity during flood maximum tidal current velocities.

interpolation and extrapolation seaward of the 5 m isobath. Cross-shore erosion rates are calculated and presented in figure 7 for different incident wave heights and critical erosion shear velocities during flood maximum tidal current velocities.

Figure 7 illustrates that as the incident wave height increases, the erosion rate increases, while the erosion rate decreases significantly as the resistance of the sediment to erosion, u_{*_c} increases. The parameter u_{*_c} plays an important role in controlling the erosion of mud. On a muddy coast, u_{*_c} is a time-dependent variable. It is closely related to the physical-chemical properties of a cohesive bed that vary as coastal erosion proceeds. Armoring of the sea bed surface and exposing of the more resistant older material dating from the early stage of the delta progradation are the two fundamental geological processes that are mainly responsible for the variation of u_{*_c} during long-term of a muddy coast erosion. As coast erosion proceeds, cohesive sediments are reworked by waves and currents into the water column and then are dispersed away from nearshore zone by tidal currents. Nevertheless, coarse particles such as sands and biological debris will redeposit locally owing to their high settling velocities so that a coarse sediment layer is gradually formed over the mud bed. An overlying coarse sediment layer of 10-15 cm thick has been found in the intertidal zone of north of this study area (Zhang et al., 1998). The coarse layer becomes more resistant to erosion with time because it thickens as coastal erosion proceeds. Thus the erosion can not reach down into the cohesive bed unless the whole coarse layer overlying it is being reworked. Only stronger waves can

rework the whole sand layer and scour down into the cohesive bed below it. An intermittent thin sand and gravel layer overlying a cohesive bottom has also been found on the glacial till coasts of the Great Lakes (Kamphuis, 1987). Through the flume experiments, Kamphuis (1990) concluded that if the surface granular material can be eroded, the cohesive sediments below it will also be eroded. If the granular material is stable, the cohesive sediments will not be eroded.

Bulk density of cohesive sediment is one of the most important parameters controlling the critical shear stress of erosion (Migniot, 1968; Mehta *et al.*, 1989). The higher the bulk density of cohesive bed, the larger the critical bottom shear stress for erosion, so the lower the erosion rate. For a coast composed of cohesive sediment, the bulk density increases vertically downward from the bottom following the log law and then reaches a constant value (Zhang et al., 1999; Schunemann and Kuhl, 1993). As the erosion proceeds, the increased bulk density of progressively exposed old deposits will result in the decrease of the erosion rate with time.

Cross-shore Profile Evolution

On an abandoned delta, erosional processes govern the evolution of coast. At the abandoned Huanghe Delta, the sea bed is composed mainly of silt and clay with a mean grain size of 7-8 ϕ. The bottom cohesive sediments are resuspended by waves and currents, especially in or landward of the breaker, and are mainly dispersed away by the

tidal currents in a suspension mode. Like the till coasts in the Great Lakes (Kamphuis, 1987), the eroded sediments are rarely redeposited in their original places, and the evolution of the muddy profile is dominated by an irreversible erosion (Yu *et al.*, 1987). Therefore, in our model, the local redeposition of eroded sediments is disregarded and the coastal profile is considered to be fully determined by the cross-shore distribution of erosion rates. The erosion rate E is characterized by a random variation because the bed shear stress is a random variable associated with a stochastic wave regime. The state of a muddy profile over a certain time scale is actually determined by a randomly varying wave series, rather than by a single wave class. So the erosion rate and profile evolution can be described as:

$$E = \int_0^t \int_0^\infty \mathrm{H}(u_{*cw} - u_c) M \left(\left(\frac{u_{*cw}}{u_c} \right)^2 - 1 \right) dH dt \tag{13}$$

$$z_b = z_{b,0} - E / \gamma \tag{14}$$

where z_{b0} is original sea-floor elevation, z_b is sea-floor elevation at time t, and γ is dry density.

Figure 8 is the simulation of cross-shore profile evolution. Curve 0 is the initial bathymetry of profile 1 (based on map of 1993, see figure 3), curves 1 through 6 express 6 different states during the course of evolution corresponding to different critical erosion shear velocities of 3.0, 4.0, 5.0, 6.0, 7.0, and 8.0 cm/s, respectively. This simulation assumes that after a unit of time, one state gives away to another. In figure 8, we assume

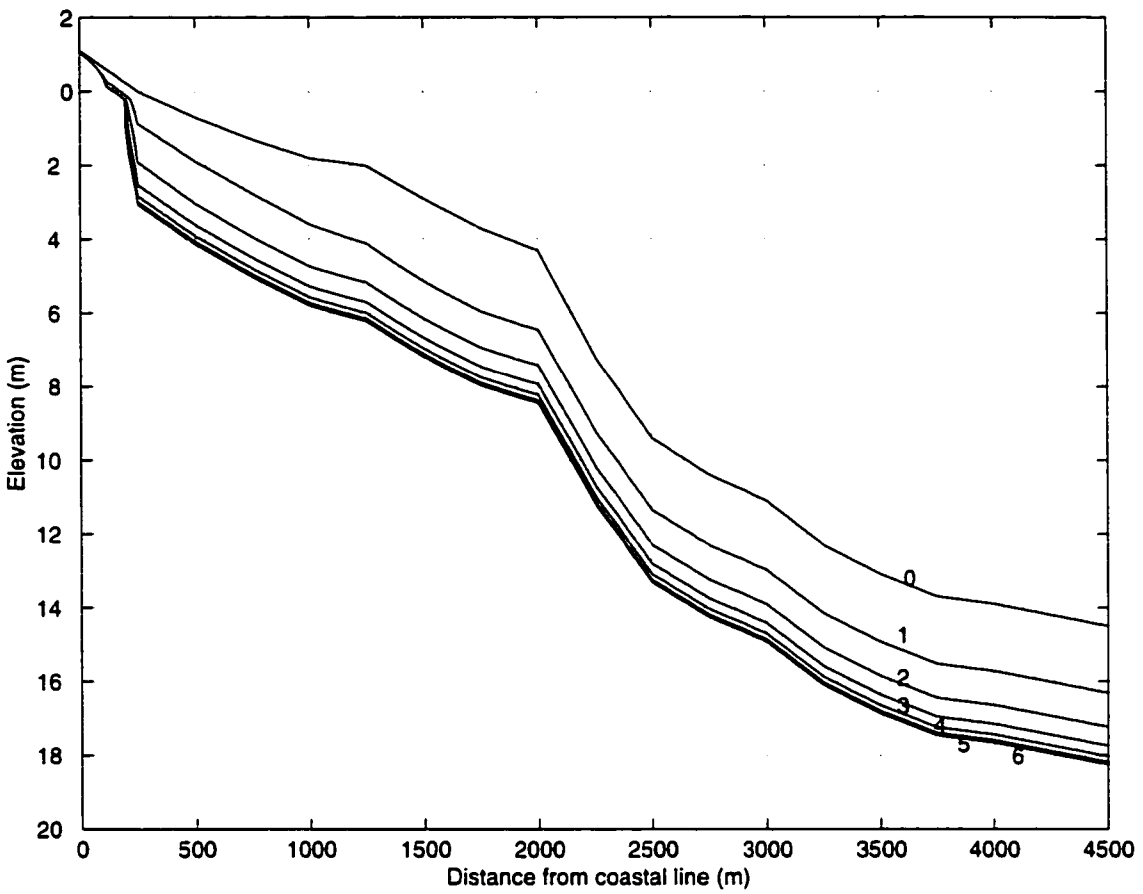

Fig. 8. Simulation of cross-shore profile evolution. Curve 0 is the initial bathymetry, curves 1 through 6 express 6 different states during the course of evolution corresponding to different critical erosion shear velocities of 3.0, 4.0, 5.0, 6.0, 7.0, and 8.0 cm/s, respectively.

the time unit is 1 year. For example, if the profile starts at status 1, after one year, it changes to status 2. Figure 8 illustrates that the evolution consists of (1) some erosion above mean sea level, (2) shoreward translation of the delta-front slope, and (3) narrowing of subsided delta-front platform. But there are different erosion patterns in different geomorphic zones. On the pro-delta shelf, as the armoring and exposing of the bottom proceeds, the critical erosion shear velocity increases. Study shows that it is about 6.0 cm/s (Fan et al., 1997). The pro-delta shelf is at status 4 with a low erosion rate, although strong tidal currents and big storms still can resuspend sediment. Studies also showed that the critical erosion shear velocities on delta front-slope and subsided delta platform are 3.5 and 3.0 cm/s (Hohe et al., 1995), respectively, so the delta front-slope is between status 1 and 2, while subsided delta platform is in status 1.

SUMMARY AND CONCLUSIONS

After one and half century evolution of the old Yellow River delta, three different morphological classes have emerged; pro-delta shelf (10 m to 15 m isobath with slope of < 1/1000); delta-front slope (5 m to 10 m isobath with slope about 1/100) and the subsided delta platform (< 5 m isobath with slope < 1/500). Tidal currents are the dominant force for the erosion of pro-delta shelf. For the delta front slope, tidal currents and waves together contribute to sea bed erosion, although the tidal current is the dominant force during calm weather. For the delta-top platform, breaking waves are the

dominant force for erosion and profile evolution. The pro-delta shelf tends to be stable. In the region of subaqueous slope, as the trend of isobath has gradually rotated into parallelism with the longitudinal axis direction of tidal current. The profile of subaqueous slope has been adjusted gradually, and erosion on the slope caused by tidal current is declining. On the prodelta shelf, the establishment of coastal defense structures has confined wave-induced erosion on seabed within the limited area that lies between the stable coastline and the delta-front slope.

While the rate of morphodynamic change of the subsided delta is waning, adjustments, as indicated by continued deepening, are still incomplete. As a consequence, the present intense along-coast flux of silt-sized material can be expected to continue into the foreseeable future, This factor will effect local harbor construction in the future, and its control must enter into engineering plans for harbor construction.

CHAPTER III

STORM DRIVEN SEDIMENT SEDIMENTATION ON THE NORTHERN CALIFORNIA SHELF: ROLE OF HIGH AND LOW CONCENTRATION REGIMES

INTRODUCTION

How are the event strata of storm and river dominated continental shelves to be interpreted? The question can be broken into two: how do storms and floods carry sediment across the continental shelf to its place of deposition, and how are these dynamics reflected in the resulting succession of event beds? Storm wave and river flooding are major processes driving sedimentation on modern, river-dominated continental shelves, and result in a central or outer shelf mud-belt beyond a nearshore zone of wave-winnowed sands. This pattern has been observed in many shelves all over the world (see page 3 and 4 for references). But the mechanisms of cross-shelf dispersal and deposition, that is, how does sediment rain out from the inshore flood plume and get to the central and outer shelf, are not well understood, nor is the nature of the resulting event stratigraphy.

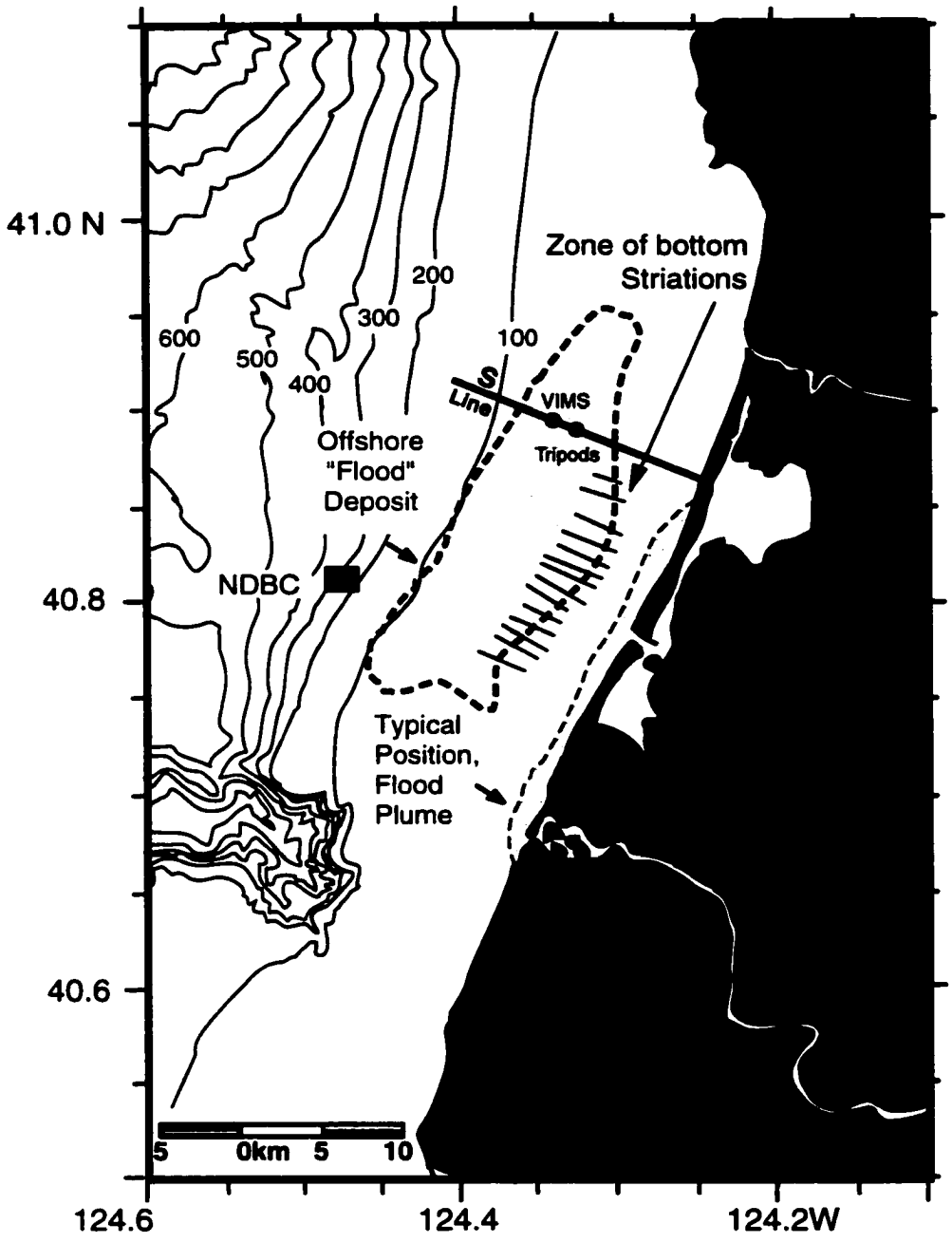

Fig. 9. Location of study area and stations. The model simulation is based on data collected from the S transect. Dashed contours are flood layer thickness (cm). The zone of striated bottom reflections is reported by Goff et al., 1999. Solid contours are water Depth. Generalized location of the flood plume is based on Geyer et al, 2000.

We address these questions by examining the dynamics of the Eel River sector of the Northern California shelf (Fig. 9). The Eel shelf extends for about 70 km from Cape Mendocino northward to Trinidad Head. Its inner portion is floored by a sand sheet which gives way to clayey silt and silty clay on the central and outer shelf (Borgeld, 1985). Grain size decreases from 250 μm to 15 μm at 60 m and offshore, then coarsens slightly at the shelf edge to 23 μm (Borgeld, 1985). Sediment deposited on the margin is provided primarily by the Mad and Eel Rivers. The Eel River accounts for about 90% of the total annual suspended-sediment load and the majority of the sediment is transported in short-duration discharge events during the winter storm season (Brown and Ritter, 1971). Peak velocities in the water column during these periods are responses to winter storm winds and are dominantly northward along the shelf (Largier et al. 1993). Borgeld (1985) examined box cores, and reported flood deposits within the Holocene mud facies and in the transition zone on the Eel Shelf near the Eel River mouth. The deposits were characterized as brownish in color, consisting of very fine sand and coarse silt, and containing wood fragments. The age at the bottom of the presumed flood layer, calculated from Pb-210 activity profiles, corresponds to the largest flood recorded for the Eel River basin, a flood that occurred in December, 1964 (Borgeld 1985).

In 1995 and 1997, two large floods were observed in Eel River. These floods deposited flood sediments on the central shelf north of the Eel River (Wheatcroft et al., 1997). But during these periods the surface flood plume did not carry sediment seaward

of the 40 m isobath (Geyer et al., 2000). Instead, between 20% to 50% of the Eel River suspended load settled out of observed plumes on the inner shelf while the remainder escaped the study area by moving northward (Geyer et al., 2001). Either these observations are atypical, or there is another mechanism transporting the sediment from the inner shelf to the central shelf.

In this chapter we assemble observations of fluid motion and sediment transport from the Eel River sector of the Northern California shelf are presented. They have been conducted by STRATAFORM colleagues during two storms in the winter of 1996. On the basis of these observations, a conceptual model of sediment transport has been constructed that could reasonably lead to such observations. The physics of sediment transport is sufficiently well understood that key aspects of the model can be tested by means of numerical experiments. To this end, two two-dimensional, across-shelf sediment transport algorithms have been developed. The first algorithm uses assemble observations of fluid motion and sediment transport to simulate sediment resuspension, deposition and the evolution of storm bed sequences. The second one simulates the density driven mud flow to study its role for flood deposition. The simulations are then compared with box cores that penetrate the 1996 horizon, collected by colleagues in the STRATFORM project. Insights gained from examination of sea floor dynamics during the 1996 storms are applied to an interpretation of a 3-year event bed succession.

OBSERVATION OF FLUID MOTIONS AND SEDIMENT TRANSPORT

Data sets used in this analysis of sediment transport and deposition of the Eel shelf include both hydrodynamical data and box core data. In this section, the nature of

these data sets is briefly described, and functional relationships are presented by which the data are reduced, fluid motions and sediment concentrations during two winter storms are described, and a hypothesis relating the observed dynamics to the observed event stratigraphy is presented.

The Hydrodynamical Data

From December 1995 to March 1996, instrumented tripods were deployed at S-50 (124° 13.826' W, 40° 53.005' N), S-60 (124° 15.19' W, 40° 53.27' N) and S-70 (124° 17.03' W, 40° 57.78' N), located at about 50m, 60 m and 70 m isobath, respectively (Cacchione et al., 1999; Wright et al., 1999; Fig. 9). This study has used 1) time series of 2.5MHz acoustic backscatter from S-50, 2) current velocity data from 10, 41, 71, and 101 cm above the bottom at S-60, 3) suspended sediment concentration data from 5, 42, 71, 104 and 131cm above the bottom at S-60, 4) the hourly-averaged significant wave height and wave period from buoy (124° 30' W, 40° 48 'N, moored in 310 m water depth) and 5) hourly Eel River discharge data measured by U.S. Geological Survey stream-gauging station at Scotia.

Wave Parameters

Wave data were reduced in the following manner. As waves travel into shallow water from deep water, the significant wave height H is estimated by a wave-transformation equation proposed by Hughes and Miller (1987), which considers the bottom friction:

$$H = H_d\left(\frac{L}{L_d}\right) \tag{15}$$

where H_d is the significant wave height in deep water, L and L_d are wave length in shallow water and deep water, respectively.

Applying linear wave theory, the wave length L and the peak value of orbital-velocity u_b at the edge of the wave boundary layer can be expressed as:

$$u_b = \frac{\pi H_s}{T \sinh(2\pi h/L)} \tag{16}$$

$$L = \left(gT^2/2\pi\right)\tanh(2\pi h/L) \tag{17}$$

where h is water depth, T is wave period, and g is acceleration of gravity.

Wave-Current Bed-shear Stresses

The calculation of wave-current bed-shear stresses is essential for the analysis of sediment suspensions that are presented on subsequent pages. Several models have been developed (Grant and Madsen, 1979, 1986; Smith, 1977; Bijker, 1986; Sleath, 1991). Although Grant-Madsen model (1979) and Smith model (1977) can give high resolution current structure in the wave-current boundary layer, Bijker's model for calculating wave-current bed-shear stress has been used for reasons of simplicity.

The time-averaged value of absolute bed-shear stress for combined wave-current flow with the presence of wave $\tau_{b,cw}$ is (Bijker, 1986):

$$\rho u_{*cw}^2 = \tau_{b,cw} = \tau_{b,c} + \tau_{b,w} = \rho u_{*c}^2 + \frac{1}{4}\rho u_{*w}^2 \tag{18}$$

Where $\tau_{b,c}$ is time-averaged current bed shear stress, $\tau_{b,w}$ is time averaged value of absolute wave shear stress; u_{*c}, u_{*w}, and u_{*cw} are current, wave and wave-current combined shear velocity, respectively. The parameter u_{*w} is determined by using the friction factor formulation suggested by Swart (1974). The parameter u_{*c} is calculated by

calculated by solving the following equations using an iterative procedure with a given mean current velocity U_{ref} at $z = z_{ref}$, (Sleath, 1991).

$$U_z = \frac{u_{*c}}{\kappa} \ln \frac{z}{z_a} \tag{19}$$

$$z_a = z_0 \left(1 + 0.19 \frac{u_b}{u_{*c}} \sqrt{\frac{u_b}{30 z_0 \omega}} \right) \tag{20}$$

where U_z is current velocity, κ is von karman's constant, z_a is the apparent roughness, z_0 is the hydraulic roughness.

Narrative: Fluid Motions and Sediment Concentrations During the 1996 Storms

Figure 10 presents a time series of bottom wave-current shear velocity u_{*cw}, sediment concentrations at 42 cm and 15 cm above bottom at S-60, and Eel River discharge from Jan. 6, 1996 to Feb. 20, 1996. There are two storms during this period. The bottom sediment concentrations are higher during these storm periods, which shows that local suspension is a important contributor of sediment to the suspended load. Calculations of correlation coefficients among these variables indicate that surface wave-current shear velocity and bottom sediment concentration are well correlated, with correlation coefficients near 0.48 and 0.56. Generally, a large bottom shear velocity can result in high bottom sediment concentrations. But the largest bottom shear velocities do not correspond to the largest bottom sediment concentrations. The average bottom shear velocity of storm 1 and storm 2 are both 2.62 cm/s, while the average bottom sediment concentrations of storm 2 is 2~3 times larger than that of storm 1 although the duration of storm 1 is longer than storm 2 (Table 5). So there must be an additional mechanism contribute to the suspended sediment concentration. The data also show that the Eel River

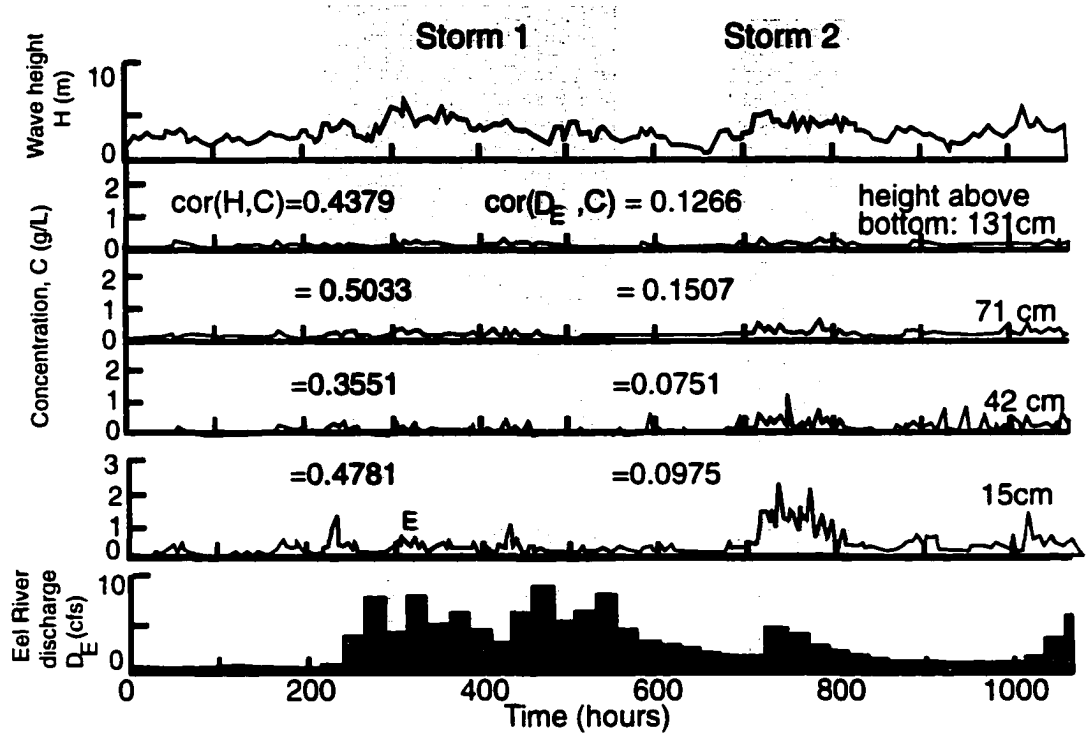

Fig. 10. Correlation between combined wave-current shear velocity, bottom sediment concentration at S-60 (C), and Eel River Discharge at station S60, for the period 1/6/1996 - 2/20/1996, Note that high near bottom concentrations on the central shelf do not result from the flood of Jan 16 to 27, but occur during a weaker wave event 10 days later.

Table 6. Statistics parameters for storm 1 and storm 2 of 1996.

	Storm 1	Storm 2
Dates of storm	1/19 ~ 1/25	2/5 ~ 2/11
Time (hrs)	150	135
Average wave-current shear velocity (cm/s)	2.62	2.62
Average sediment concentration 42cm above bottom (g/l)	0.1586	0.3088
Average sediment concentration 15cm above bottom (g/l)	0.2908	0.8378

Table 7. Correlation between Eel River discharge and sediment concentration at 15cm above bottom

Time lag (hrs)	540	510	480	450	420	390	210	0
Correlation coefficient	0.08	0.30	0.43	0.40	0.40	0.31	0.12	0.10

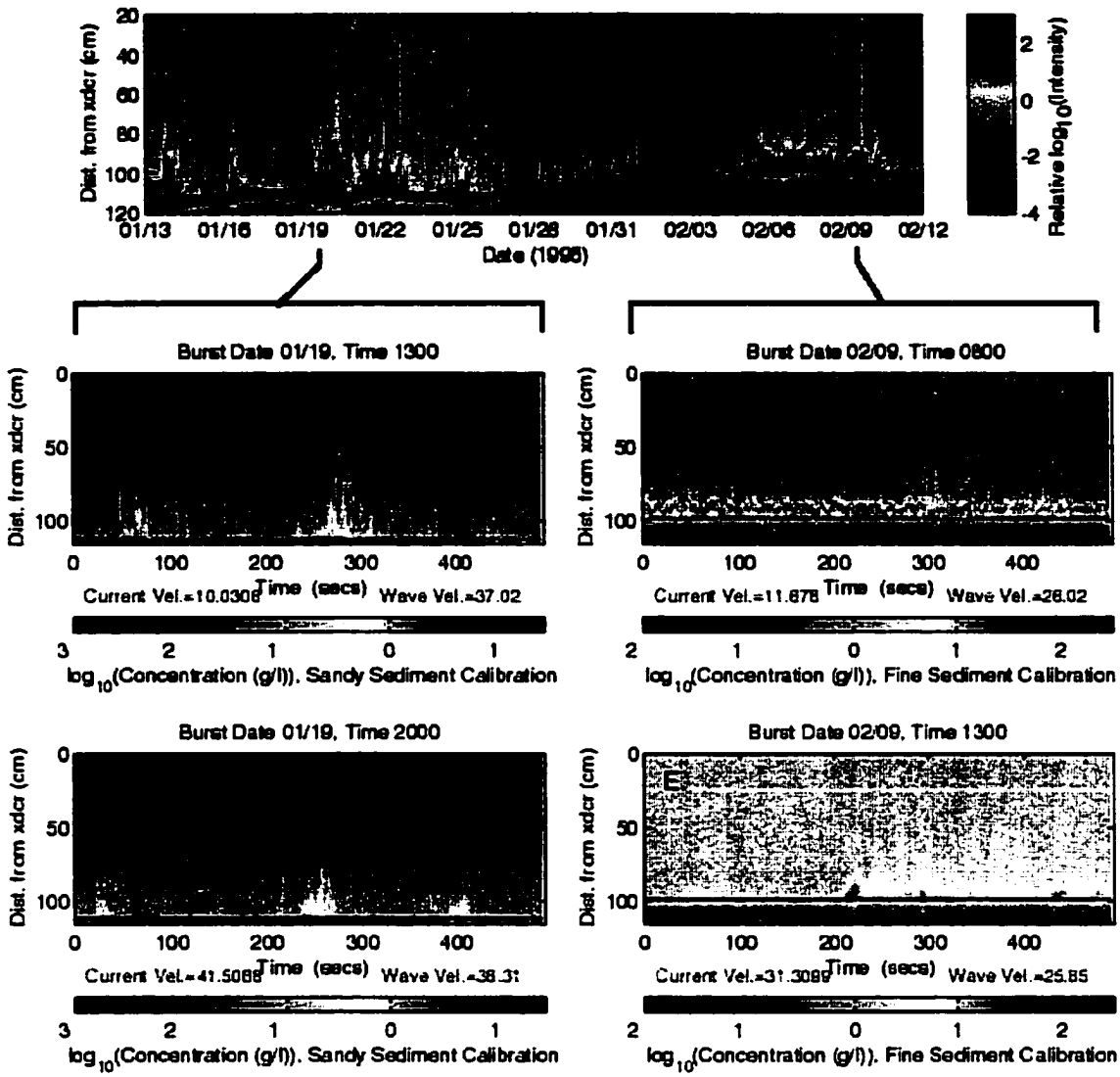

Fig. 11. Time series of 2.5 MHz acoustic backscatter fom the 50 m isobath. A: Record for the period 1/13/96 to 2/12/96. B, D; Intervals during storm 1 with low and high current velocity. Peak wave surge resuspends relatively coarse bottom sediment, which settles out between pulses. C, E: intervals during storm 2. Panel C occurs during low wave and current velocities. Near bottom sediment concentration is high and continuous, and has well defined lutocline indicating advected fine sediment. In Panel E, the lutocline is broken by more intense wave and tidal motions, and sediment rises higher in the water column.

discharges and bottom sediment concentrations are poorly correlated. However, with a 10 to 20 days lag, the correlation coefficient increases to over 0.4 (Table 6).

The time series of near-bottom sediment concentration recorded at 50 m isobath during the same two storms reveal a similar history of fluid motion and sediment suspension (Fig. 11). The data was recorded by a 2.5 MHz Acoustic Backscattering System (ABS) attached to the Geoprobe tripod on the 50 m isobath (Cacchione et al., 1999). During the period 1/13/96 to 2/12/96, (Fig. 11A), the two storms described above are clearly visible as periods during which the near-bottom nepheloid layer intermittently thickens from a few centimeters to >25 cm. However, expanded subsets for this time series, taken during periods of low mean current velocity (Fig. 11B, 11C) and high mean current velocity (Fig. 11D, 11E), show that the character of the two resuspension events was rather different, despite the fact that the wave orbital velocities were similar. In the first event (Fig. 3B, 3D), resuspension occurs at 6-8 sec intervals, corresponding to each half cycle of the 12-16 sec waves, with intensifications at 150 –200 sec intervals. The sediment falls out of suspension relatively rapidly (approximately 30 sec to fall 30 cm for the burst at 250 seconds in Fig. 3D), suggesting that wave resuspension of relatively coarse particles (fine sand and silt) is being modulated by the group wave envelope. While only two data bursts of 480 seconds are shown, this behavior, indicative of the suspension of fine sand, is seen throughout the first storm event (1/19/96 to 1/26/96).

The second event starts on 2/9/26. During period of low mean current velocity (Fig. 3C), there is a high concentration layer with a sharply defined upper boundary, that does not settle out after the passage of individual waves; behavior appropriate for clay and silt-sized particles. However, a half tidal cycle later, when the mean velocity becomes sufficiently intense (Fig. 3E), the layer is breached, and sound-scattering particles rise into the water column. This high-concentration layer is visible at several periods of low mean current during the second storm event, but is not visible during the first.

These relationships stem from the fact that during the storm 1, the Eel River discharge peaked after the wave height had begun to wane below values sufficient to retain the sediment in suspension. Because most of the sediment in the plume could not escape 40 m isobath, the flood sediment apparently underwent short-term storage on the inner shelf, until re-suspended and transported offshore by wind-driven currents associated with storm 2. It is also possible that offshore transport was gravity driven, taking the form of high concentration suspensions (fluid mud) generated in the wave boundary layer which maintained by wave energy of storm 2 (Traykovski et al., 2000). This later storm, through associated with a smaller flood discharge, generated higher near-bottom sediment concentrations than storm 1 on the 60 m isobath (Fig. 10, Fig. 11).

The Event Stratigraphic Record at S60

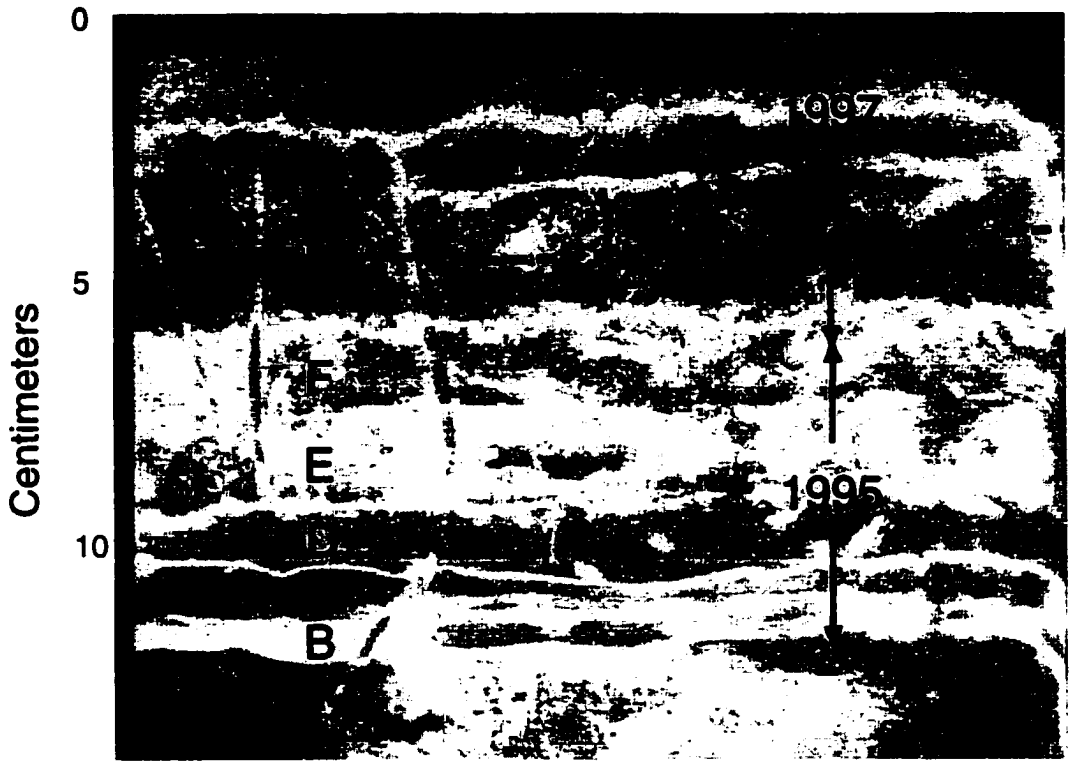

Fig. 12. Representative x-radiograph (M9707-S60-X20) from the S-line of Eel shelf. Clay-rich mud beds deposited by high concentration events alternate with sand-rich beds deposited by low concentration regimes. Letters refer to beds discussed in text. Arrows indicate portions of beds in which sub-layering occurs.

The stratigraphic consequences of events such as those described above are revealed by Fig. 12, an X-radiograph of three years of deposition (1995-1997) at station S60 on the Eel shelf. This X-radiograph is typical of several dozen obtained from this station. In the X-radiograph, beds D, E, and F comprise a distinctive 10-cm zone. Its pale color in the X-radiograph indicates that it is a low density (water-rich) and fine-grained zone. This sequence was first observed in February 1995, and is attributed to a flood in January 1995 (Drake, 1999; Bentley and Nittrouer, in press). Bed sequence G, H, and I, a darker color zone on the X-radiograph, is a high density (water-poor) and relatively coarse-grained. Bed G was first observed between February and May, 1995, and is attributed by Drake (1999) to episodic current winnowing of the surface, with continuing addition of coarse material, apparently by advection from the inner shelf, and with downward mixing of the advected material by a recovering fauna. This bed sequence continued to evolve through the early 1996 storm period described above, until it was capped by a thin mud bed at the top of bed G during the winter of 1996-1997.

Note that Drake's interpretation of the evolution of the FG sequence, and the development of the bed G cap by winnowing, advection, and bioturbation may also apply to the DE sequence. The beds that appear orange in the X-radiograph (are coarse), like bed E, have thin sub-layers attributable to current winnowing. Sand-silt-clay ratios of bottom samples from the S line suggest that such winnowing is part of a more general pattern of textural evolution. Bed E was presumably deposited from low-concentration

regimes in the quiescent interval separating two periods of intense flood discharge in January 1995 (Wheatcroft et al. 1997).

Hypothesis: Flow Regimes Reflected in Event Beds

Based on the above analysis, sediment suspensions during storm periods may be divided into low concentration suspensions and high concentration suspensions. The time series presented in Figures 10 and 11 lead to the hypothesis that high concentration suspensions, occur on the central and outer shelf during periods of storm amplification of waves and currents that are preceded by floods, and can therefore call upon on the inner shelf as a source of resuspendable fine sediment. We further hypothesize that low concentrations occur when periods of intensified wave height are not preceded by floods. In this model, high concentration regimes deposit mud-rich "flood beds," while low concentration regimes deposit sandy "storm beds."

TWO-DIMENSIONAL CROSS-SHELF SEDIMENT TRANSPORT AND BED STRATIGRAPHY MODEL

In order to test this hypothesis concerning the formation of "flood" beds on the Eel shelf, a two-dimensional, multi-grain size, cross-shelf, sediment transport and bed evolution model has been developed. The model is driven by wave data from NOAA

buoy 46022 and current data from VIMS tripod for the period 1/6/96 to 2/20/96.

Sediment Transport Model

Let C_m denote the mass sediment concentration of mth size class, $w_{s,m}$ the settling velocity of suspended particles of this size class, U_x the across-shelf component of subtidal current velocity, D_h and D_v the horizontal and vertical eddy mass diffusivities, respectively. The transport equation for the concentration C_m is (Zhang et al., 1999):

$$\frac{\partial C_m}{\partial t}+\frac{\partial U_x C_m}{\partial x}-w_{s,m}\frac{\partial C_m}{\partial z}-\frac{\partial}{\partial x}\left(D_h\frac{\partial C_m}{\partial x}\right)-\frac{\partial}{\partial z}\left(D_v\frac{\partial C_m}{\partial z}\right)=0 \qquad (21)$$

Based on the analysis of bottom sediment on the Eel shelf, the inner shelf is covered by fine sand, and the central and outer shelf are covered by silt and mud (Borgeld, 1985; Borgeld, et al., 1999). So this model has two options for sediment input at the bottom boundary. For a non-cohesive bed, the boundary sediment concentration condition of mth size class $C_{0,m}$ at z_0 is based on that of Smith and McLean (1977):

$$C_m(z_0)=C_{0,m}=\frac{f_{0,m}C_b\gamma_0 S_m}{1+\gamma_0 S_m} \text{ and } S_m=\frac{\tau_{b,cw}}{\tau_{c,m}}-1 \qquad (22)$$

Here C_b is the bed sediment concentration, γ_0 is an empirically determined sediment-entrainment parameter, $f_{0,m}$ is the fraction of the mth grain-size class in the bed, S_m is the excess shear stress. The variable $\tau_{c,m}$ is the critical stress required for initiating sediment entrainment, based on a formulation by Delft Hydraulics (1989) which considers the

influence of cohesive material. Reported values for γ_0 are site specific and vary over two orders of the magnitude (Nittrouer and Wright, 1994), and the parameter is often reserved as a calibration parameter.

For a cohesive sediment bed, experiments have led to the boundary condition:

$$-w_{s,m}C_m - D_v\frac{\partial C_m}{\partial z} = -D_m + E_m \qquad z = z_0 \qquad (23)$$

The left-hand side represents the total flux rate of grain-size class mth in the vertical direction. On the right-hand side, D_m stands for the rate of deposition that occurs when the magnitude of the bottom shear stress $\tau_{b,cw}$ is below the critical depositional shear stress τ_d, while E_m stands for the rate of erosion that occurs when $\tau_{b,cw}$ is above the threshold τ_c. These variables are usually given in the following form (Patheniades, 1965; Krone, 1962):

$$D_m = \mathrm{H}(\tau_d - \tau_{b,cw})w_{s,m}C_{0,m}\left(1 - \frac{\tau_{b,cw}}{\tau_d}\right) \qquad (24)$$

$$E_m = \mathrm{H}(\tau_{b,cw} - \tau_c)f_{0,m}M\left(\frac{\tau_{b,cw}}{\tau_c} - 1\right) \qquad (25)$$

where $\mathrm{H}(x)$ denotes the Heaviside step function of x, $w_{d,m}$ is the velocity of deposition of mth grain-size class, and M is an erosion coefficient, which usually preserved as a calibration parameter. In the absence of both field and laboratory experiments on the Eel shelf mud, The values $\tau_d = 0.6 dyne/cm^2$ for the San Francisco Bay mud (Krone, 1962);

$\tau_c = 0.9 dyne/cm^2$ and $\tau_c = 2 dyne/cm^2$ for newly deposited mud and existing mud, respectively (Schunemann and Kuhl 1993), are used in our simulations.

Outside the boundary layer, we assume

$$C_m = 0 \qquad z \to \infty \tag{26}$$

The coastal boundary provides a seaward sediment flux from the nearshore zone. Because of the poor knowledge of the nearshore sediment transport in this area, a zero-flux profile is selected. The shelf break boundary is set at a depth of 100 m with a radiation boundary condition (Camerlengo and O'Brien, 1980).

Once the sediment concentration field is known, across-shelf sediment flux can be computed. The change of sea-floor height and components can be calculated by the mass-continuity equation:

$$\frac{\partial z_{b.m}}{\partial t} = -\frac{1}{C_b}\left(\frac{\partial C_{T.m}}{\partial t} + \frac{\partial U_x C_{T.m}}{\partial x}\right) \tag{27}$$

where z_b and $C_{T.m}$ are sea-floor elevation and depth-integrated sediment concentration for mth grain-size class, respectively.

Current Parameters

Studies based on data from buoy 46022 and VIMS tripods show that there is little correlation between surface wave and bottom current. The low-frequency subtidal current near the bottom is dominantly seaward with an average of about 2 cm/s (Zhang et al.,

1999). The independence of waves and currents was also observed during Northern California Coastal Circulation Study (NCCCS) experiment and Sediment Transport Events on Shelves and Slopes (STRESS) project (Largier et al., 1993; Sherwood et al. 1994). The across-shelf component of the low-frequency subtidal current, which is responsible for the cross-shelf flux, is poorly related to the wave height on the Eel shelf. The across-shelf variation of the mean current velocities is small, particularly at water depth shallower than 100 m (Sherwood et al., 1994; Zhang et al., 1999). A time-invariant, seaward subtidal velocity of 2 cm/s is selected for the calculation of the sediment flux in our model (Zhang et al., 1999), and current velocities at 1.01 m above bottom from VIMS tripod S-60 is used for the calculation of shear stresses.

Settling Velocity w_s and Deposition Velocity $w_{d,m}$ for mth Grain-size Class

Because of the flocculation of cohesive fine sediment, suspended cohesive sediments in the marine environment commonly appear as aggregates. Size and settling velocity of suspended aggregates on the Eel shelf were measured in situ by Sternberg et al. (1999). The measurement showed that suspended load is a well sorted, and has a unimodal mass distribution with a mode occurring in the size range of 500~700 μm and a median size of 600 μm. The settling velocity associated with the median aggregate size (3.8 mm/s) is used as settling velocity of fine silt and clay (Sternberg et al., 1999) in the

following simulations. The settling velocity of sand is calculated by Stokes' law.

Eddy Mass Diffusivity

Using the Prandtl mixing-length theory with the mixing length $l = kz\left(1 - z/h\right)$, and considering the effects of density stratification (Fischer et al., 1979), the following eddy mass diffusivity takes the following form:

$$D_v = D_h = \gamma l^2 \left|\frac{\partial U}{\partial z}\right| \Big/ \left(1 + 10R_i/3\right) \tag{28}$$

where $R_i = -\frac{g}{\rho}\frac{\partial \rho}{\partial z} \Big/ \left|\frac{\partial U}{\partial z}\right|^2$ is Richardson number, γ(~0.74) is a constant for mass diffusion, ρ is the in situ density.

Numerical Solution Design

When simulating storm 1, the bottom sediment grain sizes from Borgeld (1985,1999) are used. The sediment are divided into five classes: coarse sand (0~2ϕ), fine sand (2~4ϕ), and coarse silt (4~6ϕ), fine silt (6~8ϕ), and mud (>8ϕ). When simulating storm 2, newly deposited sediments that have the same components as S60 are put on the seabed of the inner shelf. A finite difference method is used to solve equation 1 with a vertical space step 1 cm, a horizontal space step of 50 m, and time step of 3 minutes.

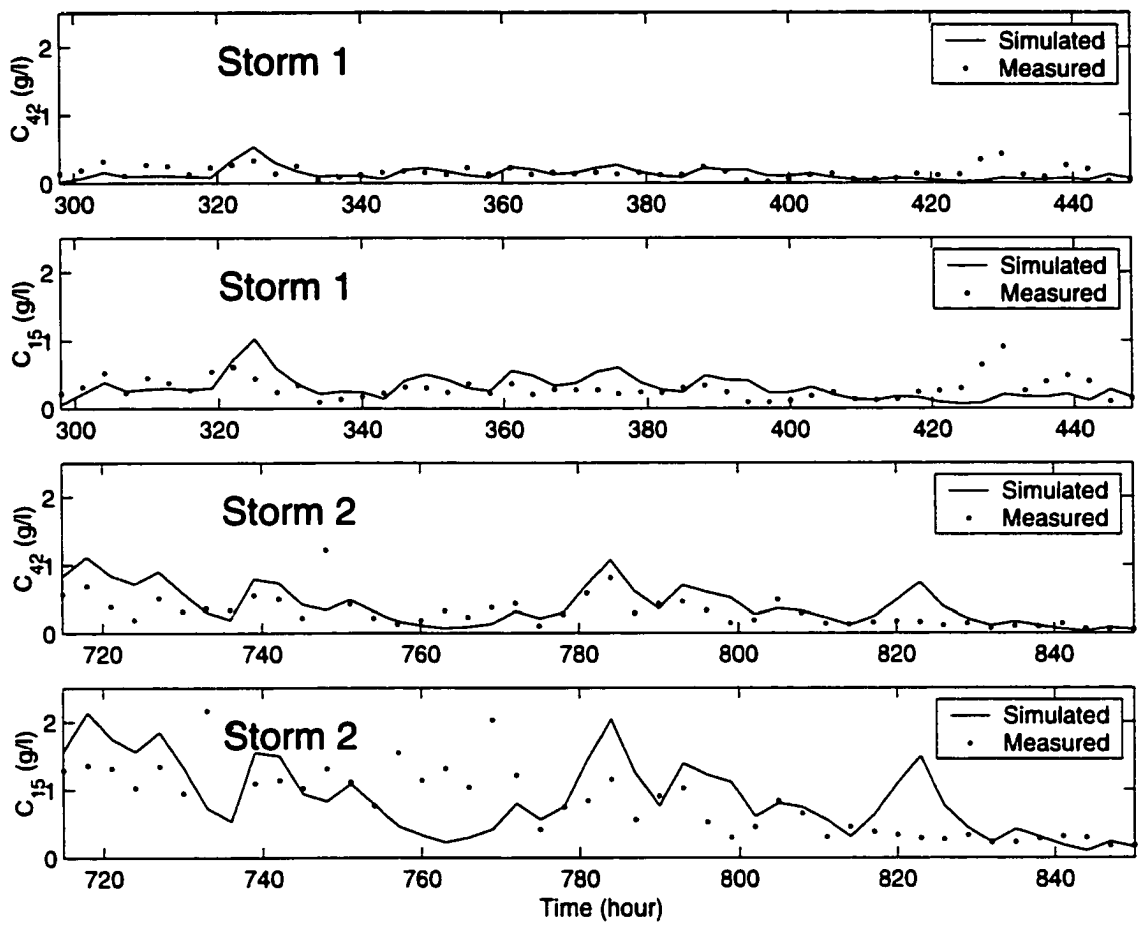

Fig. 13. Simulated and measured time series of sediment concentration 15 cm and 42 cm above the bottom at S-60.

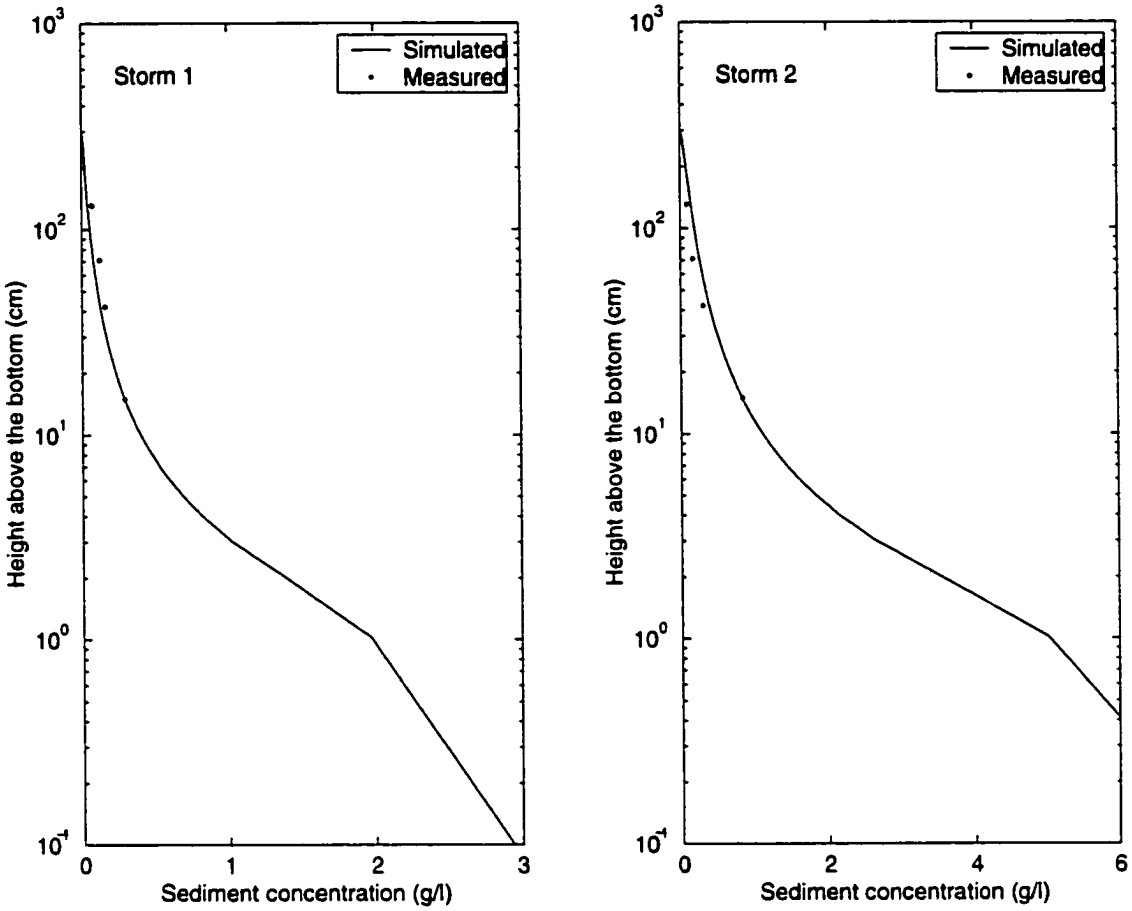

Fig. 14. Simulated and measured time-averaged sediment concentration profiles at S-60 during storm 1 and storm 2.

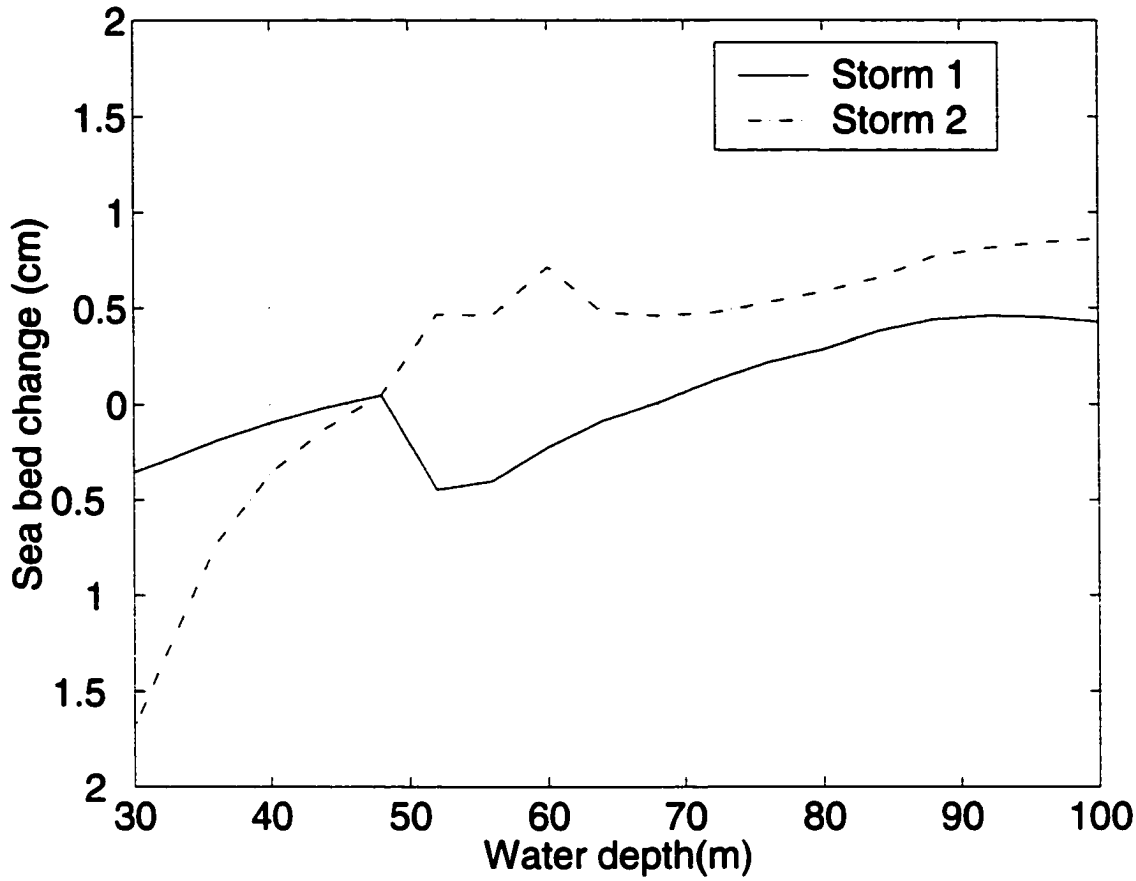

Fig. 15. Simulated cross-shelf (S-section, Fig. 9) sea bed evolution during storm 1 and storm 2.

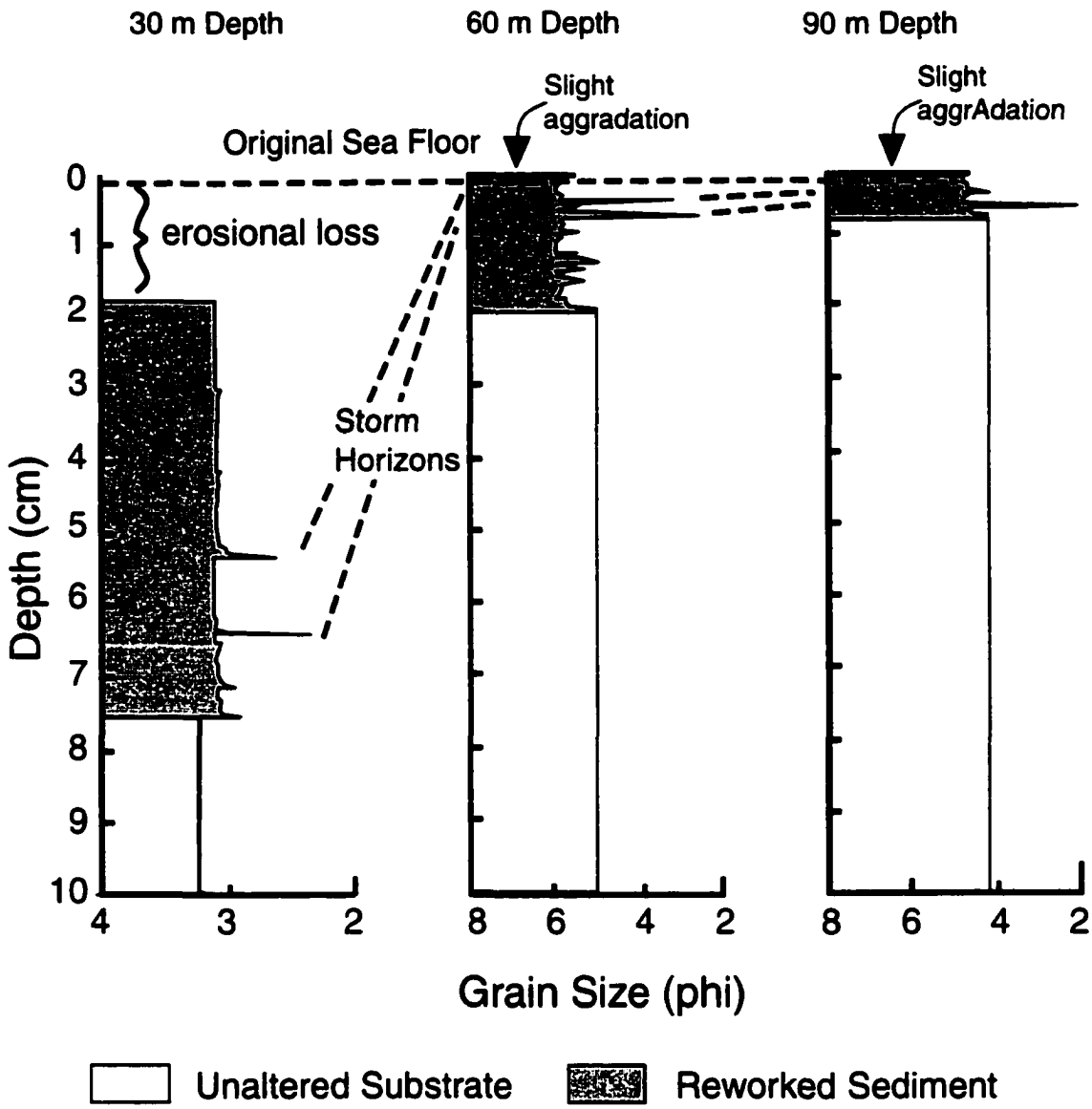

Fig. 16. Simulated cross-section of grain size distribution at 3 stations at the S line. Note the two coarse layers that mark the two storm events at each station. There has been 1.8 cm of net erosion at the inner shelf station, and slight net aggradation at the central and outer shelf stations.

Computational Results

Figure 13 presents the time series of sediment concentrations 42 cm and 15 cm above the bottom during storm 1 and storm 2 at S-60, while Figure 14 compares the resulting time-averaged sediment concentrations. The comparison between the measured data and simulated data shows good agreement. The sediment concentration during storm 2 is much higher than that in storm 1.

Figure 15 presents seabed changes during storm 1 and storm 2 assuming that all sediment settled to the bottom when the storms stopped. During the storm 1 (low concentration regime), the inner shelf and shoreward part of the central shelf experienced erosion because of the absence of a sediment source. The seaward part of central shelf and outer shelf experienced accumulation because sediment eroded from inshore was transported there. The erosion peak between 50 and 60 m water depth is the location of the discontinuity of critical erosional shear stress between fine, cohesionless sand and mud. During storm 2 (high concentration regime), the inner shelf experiences greater erosion than in storm 1 because the bottom is now assumed to be a poorly consolidated, easily eroded mud (see numerical solution design). The newly deposited sediment on the inner shelf is resuspended and transported seaward and deposited on the central and outer shelf. The highest accumulation rate is around the 60 m isobath, which is consistent with the observation of Wheatcroft et al. (1997).

Fig. 16 is a simulation of the event stratigraphy produced in the upper 10 cm of the sea floor during the period from January 6, 1996 to February 20, 1996. The two spikes apparent on the right hand margin of each columnar section are the basal lags of coarser sand formed during storms 1 and 2. Note that some deposition occurred prior to the time of maximum erosion during storm 1. The peak storm 1 event then cut into this early deposit, generated a lag, and redeposited the suspended sediment as the storm 1 bed. Storm 2 then eroded the storm 1 deposit, created a second lag, and deposited the storm 2 bed over that. This simulation also shows that during the winter storm season, fine sediment was progressively lost from the seabed at the inner shelf and deposited on central and outer shelf and slope or bypassed seaward. Note that January and February storm beds in the simulation of Fig. 16 are difficult to recognize in the box core of Fig. 12. A clay bed deposited by the winter storms of 1995/1996 was no longer evident in the July 1996 X-radiograph at S60, and the stratigraphy created during January and February of that year was partially destroyed by erosion during the Spring. The February 1996 horizon is represented by a dashed line in Figure 13.

TWO-DIMENSIONAL CROSS-SHELF DENSITY DRIVEN MUD FLOW

It is known that mud flow with a high concentration of cohesive clay particles behave as non-Newtonian flow (e.g., Coussot, 1994). When sediment concentration is in the range from 2 g/l to 700 g/l, rheology studies indicate that mud flow behaves approximately as a Bingham-plastic fluid (Krone, 1963; Migniot, 1968; Wan, 1982; and Wang et al., 1985). In simple shear, the stress-strain relation is nonlinear:

$$\mu\frac{\partial u}{\partial z}=\begin{cases}0 & if \quad |\tau|<\tau_y\\ \tau-\tau_y\,\mathrm{sgn}\left(\dfrac{\partial u}{\partial z}\right) & if \quad |\tau|>\tau_y\end{cases} \tag{29}$$

where τ_y is yield stress and μ the coefficient of viscosity. In muddy water, both τ_y and μ increase monotonically with clay concentration. The ranges of values commonly observed for such parameters values are $10^{-6}\,m^2/s<\mu/\rho<1.2\times10^{-3}\,m^2/s$ and $10^{-3}\,N/m^2<\tau_y<10^{2}\,N/m^2$. Such a fluid at rest is capable of resisting any shear stress less than the yield stress. When the yield stress is exceeded, the fluid structure changes and the material behaves like a Newtonian fluid driven by the excess of the shear stress beyond the yield stress. When the shear stress falls below the yield stress, the fluid structure changes again and there is no fluid flow (Davis, 1988; Huang and Garcia, 1997).

During high concentration regime periods in the winter of 1997 and 1998, high sediment concentrations were observed on the Eel Shelf (Ogston et al., 2000; Traykovski

et al., 2000). Between 31 December 1996 and 4 January 1997 (5 days), Ogston et al. (2000) observed fluid mud at the K63 tripod site with sediment concentration larger than 300 g/l. On January 14—21, 1997, Traykovski et al. (2000) found a thin (10-15 cm thick), high concentration (>10 g/l) layer. These sediment concentrations fall into the range of Bingham plastic mud flow, so the mud flow on the Eel River continental shelf can be described by using Bingham model.

A Bingham-fluid Model for Mud Flows on the Continental Shelf

Consider a single layer of fluid mud flowing down a continental shelf with an angle θ respect to the horizon. Let the x-axis coincide with the seabed and be directed downward. The surface of the fluid mud is designed as $z = h(x,t)$. The flow can be divided into a plug-flow region with velocity $u = u_p$ for $h_0 \le z \le h$ on top of a shear-flow region, in which u varies from zero at bottom to u_p at $z = h_0$. Here, u_p is the flow velocity in the plug-flow region, and h_0 is the depth of the shear-flow region. Hence u has uniform and parabolic distributions within the plug-flow region and the shear-flow region (Liu and Mei, 1989; Huang and Garcia, 1997):

$$u = \frac{1}{\mu}\left[\rho g'\left(\tan\theta - \frac{\partial h}{\partial x}\right)\right]\left(h_0 z - \frac{1}{2}z^2\right), \quad 0 \le z \le h_0 \tag{30}$$

Match u_p with (29) at $z = h_0$ we get

$$u_p = \frac{1}{2\mu}\rho g' h_0^2\left(\tan\theta - \frac{\partial h}{\partial x}\right), \quad h_0 \le z \le h \tag{31}$$

The total volume flux at any station is

$$q = \int_0^{h_0} u dz + u_p(h - h_0) = \frac{1}{6\mu}\rho g'\left(\tan\theta - \frac{\partial h}{\partial x}\right)h_0^2(3h - h_0) \tag{32}$$

On the yield surface,

$$\tau = \tau_y = \rho g'\left(\tan\theta - \frac{\partial h}{\partial x}\right)(h - h_0) \tag{33}$$

The fluid mud flows on the Eel River continental shelf are the results of the resuspension of newly deposited flooding deposit by storm waves. The turbulence generated by the surface gravity wave motions provides the source of energy, and fluid mud trapped within the wave boundary (Traykovski et al., 2000). Studies by Teeter (1992) and Traykovski et al. (2000) also showed that the thickness of the fluid mud layer is well represented by the variations in the wave boundary layer thickness during periods when a fluid mud layer is present. So fluid mud thickness can be get by calculating the wave boundary layer thickness δ_w (Wiberg and Smith, 1983; Smith, 1977):

$$h = \delta_w = \sqrt{f_w / 8a_b} \tag{34}$$

where a_b is the wave orbital semi-excursion amplitude near the seafloor, outside the wave boundary layer, and the wave friction factor (f_w) is calculated following Swart (1974):

$$f_w = \exp\left[5.213(k_n/a_b)^{0.194} - 5.977\right] \tag{35}$$

here k_n is the hydraulic roughness that is about 6 cm on the Eel River shelf (Traykovski et al., 2000).

When fluid mud formed, only when the wave bottom shear stress larger than the yield stress of fluid mud, the fluid mud can flow. Since yield shear stress is proportional to the sediment concentration (c) ($\tau_y \approx c^{\alpha}$), the maximum sediment concentration for the mud flow is:

$$c = \tau_y^{1/\alpha} = \tau_{b\max}^{1/\alpha} \tag{36}$$

where $\tau_{b\max}$ is the maximum wave bottom shear stress.

From (31) and (35), we can get sediment flux of mud flow at any station:

$$q_{sed} = cq \tag{37}$$

The change of sea-floor height can be calculated by the mass continuity equation:

$$\frac{\partial z_b}{\partial t} = -\frac{1}{\rho_{dry}} \frac{\partial q_{sed}}{\partial x} \tag{38}$$

here ρ_{dry} is dry sediment density.

Computational Results

As we know, fluid mud transport can only occur during high concentration regime that a storm follows a big river flood. The sand fraction of the flood plume presumable settles to the bottom within the 20 m isobath. Since the river plume, based on helicopter-based hydrographic surveys, is generally contained within the 40 m isobath by

downwelling favorable winds (Geyer et al., 2000), we assume that finer sediments discharged during the Eel River flood are deposited on the inner shelf landward of the 40 m isobath. As the storm wanes, subsequent to the flooding, fine sediment may accumulate near the bottom as a fluid mud flow as if wave orbital motion is still sufficiently intense, the consolidating deposit may flow as mud flow with the thickness of wave boundary layer. It is possible to estimate the alongshore input of fluid mud by assuming that the plum is instantaneously emplaced. In such a case, the alongshore distribution probability $p(y)$ of the consolidating deposit follows Gaussian distribution with mean y_{mean} at the S-line and deviation σ equal to half the distance from the S-line to the river:

$$p(y) = \frac{1}{\sqrt{2\pi}\sigma} e^{-\frac{(y-y_{mean})}{2\sigma^2}} \tag{39}$$

The Eel River sediment discharge can be calculated after Syvitski and Morehead (1999), Wheatcroft et al. (1997), and Geyer et al. (2000) as:

$$Q_{sed} = \alpha Q^{\beta+1} \tag{40}$$

here Q is river discharge in m^3/s, $\alpha = 0.14 \sim 0.347$, and $\beta = 1.139$.

Figure 17 shows the thickness of mud flow (panel 1) and vertical average velocity (panel) for wave height of 6 m and wave period of 13.1 sec., which are the typical conditions during the January 1995 flood. The 15 to 20 cm/s offshore average velocities between 50 to 60 meter isobaths are the same order as that observed by Traykovski et al. (2000) and Ogston et al. (2000).

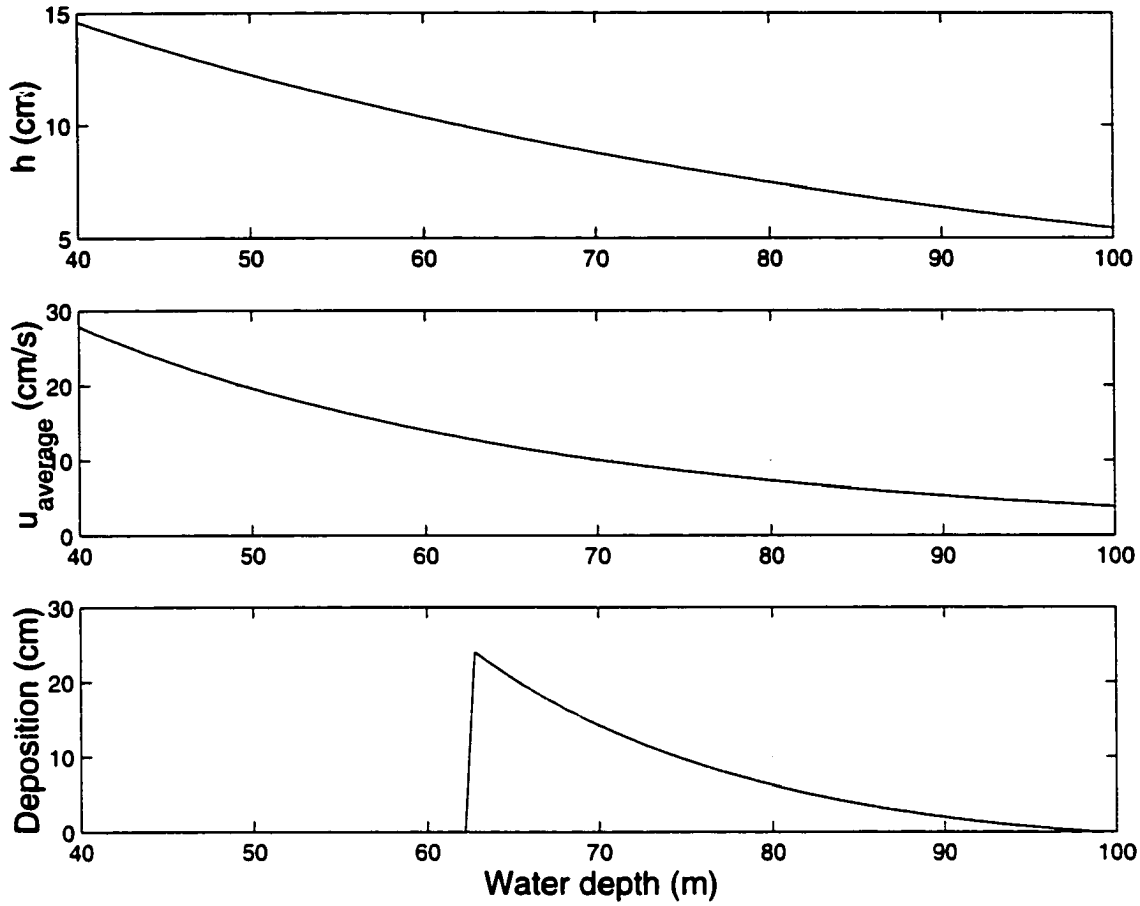

Fig. 17. Across-shelf variation of mud flow height (panel 1), vertical average flow velocity (panel 2) for typical wave height 6 m and wave period 13.1 sec, and predicted across-shelf distribution of deposition for S-transect for January 1995 floods, respectively.

Although the inner shelf boundary of the flood deposit (panel 3) is predicted to be abrupt, in reality, this transition would be more gradual because of the gravity force would tend to platten the consolidating sediment pile. The 10 to 20 cm of predicted deposition in figure 17 agrees favorably with the maximum values reported by Wheatcroft and Borgeld (2000). Numerical experiments also show that: (1) the stronger the flooding, the thicker and closer toward shore the flood deposit; (2) the stronger and longer the storms, the thinner and further offshore the flood deposit. If the storm is strong and long enough, the mud flows can reach the slope, and all the flooding fine sediment can be transported to the slope directly by this mechanism.

DISCUSSION AND CONCLUSIONS

The observations and simulations presented above confirm the initial premise that sediment transport on the Eel shelf of northern California can be best understood by distinguishing between high and low concentration regimes. In this section, we expand and modify our initial conception of these regimes, by comparing observations with simulations, and by setting these kinds of information in the context of companion studies in this volume, and of earlier published studies.

High Concentration Regimes on the Inner Shelf

As the observed by Geyer et al. (2000), during the floods of the Eel river, the fine part of the sediment discharge is ejected onto the shelf as a flood plume but within 40 m

isobath. Because river flood usually lags behind the most intense part of the storm, the storm waves tend to wane before the flood discharge peaks. As a storm wanes, sediment in the plume will settle. The sediment flocs near bottom become larger because of the larger sediment concentration (Mehta, 1991). Finally the flocs are dense enough to settle from the plume and accumulate on the bed of inner continental shelf, in a manner similar to that described by Mehta (1991). The consolidation of a mud bed from a near-bottom, high-concentration suspension may take weeks or more, in which the concentration will pass through the range described as a fluid mud (>5 g/l; Mehta, 1991). At this point, the near-bottom sediment concentration is sufficiently high that turbulence is supressed by stratification and the resulting sediment-water mixture will consist of two phases separated by an abrupt discontinuity called the lutocline (Mehta, 1991). The ABS data (Fig. 11C), the optical data and the simulations (Fig. 14) all suggest that fluid mud, characterized by a lutocline, occurred during the second storm portrayed in figure 10. Mehta's studies (Mehta, 1991) have shown that above the lutocline, a turbulent flow layer experiences dilute, low-concentration suspensions. Below it is a hyperpycnal layer, which can be divided into lutocline shear layer, mobile hyperpycnal layer (fluid mud), stationary hyperpycnal layer, and cohesive bed. A passing surface wave will generate an internal mud wave at the interface between the upper water and fluid mud that is phase-lagged with respect to the surface wave. The surface wave height decreases as its energy is translated to the internal wave, then into heat, because of the high viscosity of the mud

((Maa and Mehta, 1989). The presence of the fluid mud thus diminishes the surface wave regime and the shear stress needed to maintain its existence. The sediment above the lutocline will be transported as suspended load.

The fate of the fluid mud below the lutocline depends on the surface wave regime. In one scenario, it may be consolidated into a mud bed, then regenerated as fluid mud by a new episode of intensified surface waves. In a second scenario, surface wave intensification may occur early enough to arrest consolidation of the fluid mud, and last long enough to allow it to slide seaward in response to gravity forces. In Fig.15, the average accumulation thickness due to suspended sediment transport on the central shelf is about 0.6 cm during storm 2, which is smaller than observed accumulation of 1995 (Wheatcroft et al.,1997). The discrepancy may indicate gravity-driven advection in the wave boundary layer, as suggested by Traykovski et al. (2000), in which the storm provides the energy to maintain the flow. In a final scenario, wave orbital motion, combined with tidal or wind driven currents, may become so intense that the lutocline is broken, and its contents released into the overlying layer for transport as a dilute suspension, as appears to have occurred in Fig. 11E.

High Concentration Regimes on the Central and Outer Shelf

The observations and simulations presented in the first part of this chapter suggest that the fine sediment supplied to the inner shelf by the storm of January 19 was not

present at the 50 meter isobath until the storm of February 9 (Fig. 11). The storm of February 9, like many other such storms on the Eel shelf, resulted in marked offshore bottom flow (Cacchione et al., 1999), and will have transported suspended fine sediment to the central and outer shelf by either or both of the mechanisms described above. On the central shelf the sediment advected from the inner shelf, added to local resuspension could generate high-concentration bottom layer with maximum over 5 g/l (fluid mud) in the middle shelf as recently observed by Cacchione et al., 1999). Such muds would be redeposited on the central and outer shelf as the bottom shear stress decreases, a process dominated by flocculation effects (Krone, 1962). As the particles fall towards the bed, the increased shear causes the flocculated aggregates to break up (Krone, 1962; Partheniades et al., 1968). The large aggregates break into individual particle because of the deflocculation, the sandy and coarse silty parts settle first to form a coarser basal layer because they have larger settling velocities. In the simulation of Figure 15, the settling velocities of sand and coarse silt are used to determine the accumulation rate. As more sediment deposits towards the bed, the mud concentration builds up and form sufficiently large aggregates because of reflocculation. These newly formed aggregates settle to the bottom as a mud layer over the basal sand and coarse silt layer (Stow and Bowen, 1980; Migniot, 1968). However, purging of coarser particles from the flocs has been only partially successful. The reformed flocs have sequestered a significant portion of the

coarser load and settle quickly, The resulting bed has the peculiar, poorly sorted character noted above as characteristic of "flood" beds.

Low Concentration Regimes and the Sediment Dispersal System

Low concentration regimes have been observed during storm 1 (Fig. 10, 11B and 11D) have been simulated (Figs. 13, 14). Considerations presented above suggest that during the low concentration regime, suspended load is the main sediment transport mechanism. Because of the consolidation processes, the bottom sediment erosional resistance is greater. The resuspended sediment concentration is smaller. The main effect of each event is to continue to winnow the fine fraction out of the uppermost centimeter of sediment. Biogenic mixing between events cause fines to diffuse from the underlying high concentration bed upwards (and coarse particles downwards), so that through time, the upper 1 to 5 cm of a storm bed develops a reverse grain size gradient (Drake, 1999; Bentley and Nittrouer, in press).

The sediment dispersal system resulting from the alternation of high concentration and low concentration regimes has been simulated (Fig. 15) and can be idealized as indicated in Fig. 18. High concentration regimes involve remobilization of inner shelf silt and mud and their deposition on the central and outer shelf. Low concentration regimes result in winnowing and erosion across the shelf and bypassing of a portion of the sediment over the shelf edge. The idealized profile of Fig. 18 may be contrasted with the

plan view of the dispersal system depicted in Fig. 9. Here the zone of offshore "flood deposits" as described by Wheatcroft et al., 1997) is seen to lie just offshore from the typical position of the flood plume as described by Geyer et al. (2000). Lying between the two zones is a band of striated bottom, whose shore-normal swaths with about 100 m spacing (Goff et al., 1999) may mark a zone of seaward gravity transport.

We conclude from these considerations that flood plume deposits on the inner shelf are ephemeral beds of consolidated fluid mud. Thus, "Flood" deposits on the central and outer shelf are only secondarily flood deposits; they are, in immediate terms, high-concentration, flood-associated storm deposits, and as such their thickness varies as a function of storm intensity, as well as a function of flood discharge.

The Event Stratigraphy

The further question addressed in the introduction of this paper is, how are these dynamics reflected in the resulting succession of event beds? Event beds are not static after deposition, but may be acted on by subsequent events during early burial, until the burial process is complete (Nittrouer and Sternberg, 1981; Thorne et al., 1991). The answer to the question thus requires shift in focus from the two specific storm beds to a multi-year bed succession such as that seen in Fig. 12. As noted above, the record of depositional events of winter, 1996, so important because of the wealth of dynamical data available for this period, was partially destroyed by erosion during the following Spring. The reworking ratio for most beds in the region (ratio of minimum resuspension depth to

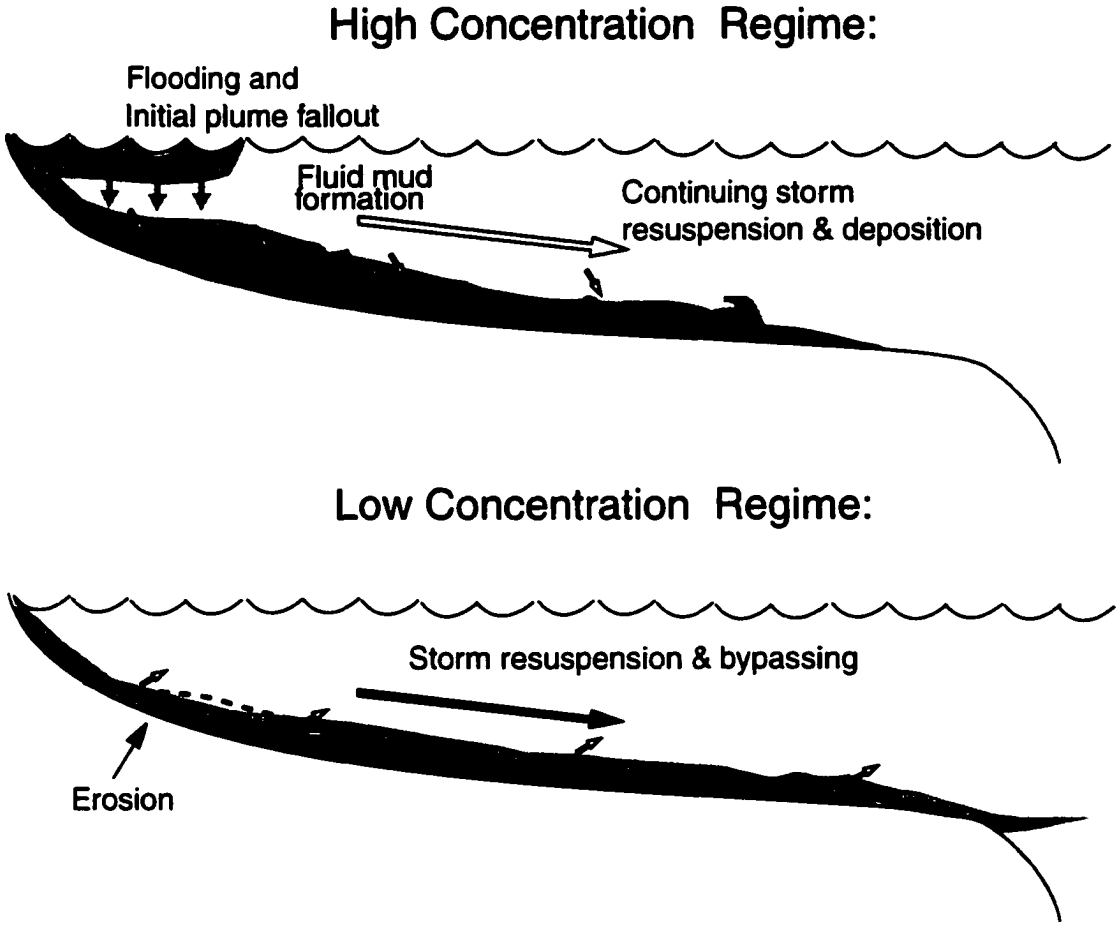

Fig. 18. Shelf regimes. High concentration regime occurs as a flood pulse passes seaward during successive storm resuspensions. During the low concentration regime fines are winnowed out of the inner and central shelf and are mainly bypassed seaward.

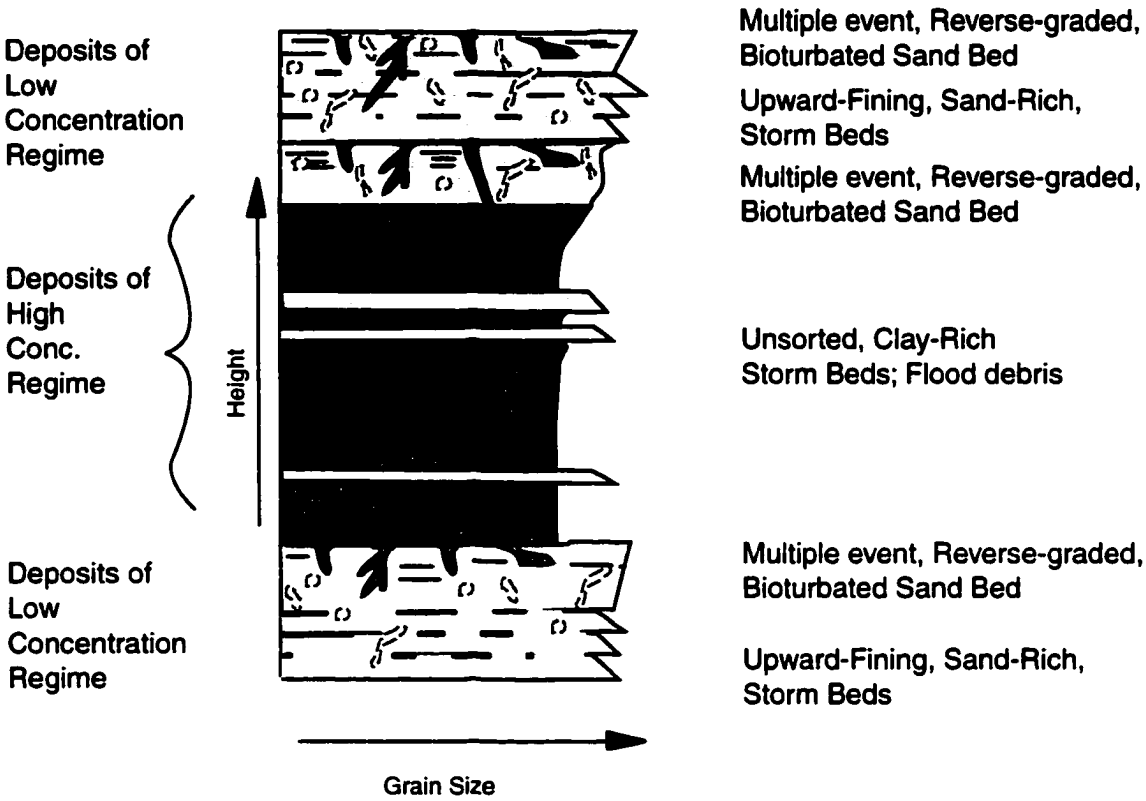

Fig. 19. Cartoon illustrating relationship between depositional regime and bed architecture on Northern California Shelf. Fine-grained sediments are intermittent deposited across the shelf, but are preserved only on the outer shelf.

accumulation per event, Thorne et al., 1991) is thought to be 0.5 or less (Zhang et al., 1997). Consequently, any bed selected for a reason other than its preservation potential has a fairly high probability of turning up damaged or missing, as have the 1996 storm beds.

A second lesson to be gained from the analysis presented in this paper is that the reworking ratio is not constant. It can be ratcheted up by very large floods, after which easily erodable inner shelf muds are available for advection to the central shelf, and may even provide their own gravity-driven transport mechanism, thus increasing the accumulation per event. Presumably as a consequence, we see the swollen "Flood bed" succession of beds C, D, E, with its reworked cap, F (Fig. 12). This succession is prominent not just because a very large amount of sediment was provided to the shelf at that time, but because the character of the sediment supplied changed the dynamics and shifted the regime toward accumulation.

The stratigraphic response to alternations of high and low concentration regimes as observed (Fig. 10 and 11) and as simulated (Fig. 15, 16 and 17) is generalized in Fig. 19. Storm resuspensions immediately after floods result in high concentration regimes that deposit relatively thick, unsorted, clay-rich beds containing woody debris. Later post-flood storm resuspensions do not attain as high concentrations. They deposit thinner, sand-rich, upward-fining beds with sharp bases, overlying the bioturbated tops of earlier event beds. In the months following a major flood event, storm intensity and

frequency tends to decrease. The main effect of each event is to winnow the fine fraction out of the uppermost centimeter of sediment. The depth of physical reworking decreases relative to the depth of biological reworking. Biogenic mixing in the lengthening intervals between events causes fines to diffuse upwards, so that through time, the upper 1-5 cm of the bed develops a reverse grain size gradient (Drake, 1999; Bentley and Nittrouer, in press). In this manner, thin storm bed sequences are reworked into reverse-graded, multi-event capping layers on the thick muddy deposits of high concentration regimes.

Conclusions

It has been shown that during winter floods, coast-hugging surface flood plumes transport water and suspended sediment northward by a combination of strong along-shelf wind-forced, currents, together with the along-coast momentum imparted by the asymmetrical geometry of the mouth (Geyer et al., 2000). Analogy with studies of similar shallow-water environments (Mehta, 1991) suggests that the formation of large flocs in a flood plume during the waning of the current leads to dense, slowly consolidating near-bottom suspensions on the inner shelf. This ephemeral mud deposit is the immediate sediment source during the subsequent transport events. If subjected to early wave activity, the suspension may slide seaward under the impetus of gravity, before further consolidation occurs. At any point in its consolidation history, bottom shear stress levels

may be sufficient to break the lutocline and resuspend the flood deposits. Inner shelf flood beds are then rapidly removed and transported seaward. Bottom grain size on the inner shelf becomes the same as or a little coarser than before the flooding, and is restored to its original noncohesive character because of bypassing of cohesive sediment from the inner shelf. The thickness of mud deposits on the middle and the outer shelf increases. In this manner, high-energy winter re-sedimentation events, occurring within days or weeks of the flood, rework mud-rich material, and attain high concentrations, in which high rates of flocculation occur, leading to poorly sorted "flood" beds. Resuspension events occurring later in the spring and summer lack the abundant supply of easily resuspended fine sediment from the inner shelf. As a consequence, they deposit thinner, sand-rich, upward-fining beds. During periods when storms are less intense and less frequent, the depth of physical reworking decreases relative to the depth of biological reworking, and thin storm bed sequences are reworked into reverse-graded, multi-event beds.

It is generally recognized that continental shelves near rivers are muddy shelves (see introduction), and that the near-field sectors of such shelves carry " expanded sections" with sand-mud alternations (Aigner, 1985; Nelson, 1985, Snedden et al., 1991). The alternations are conventionally described as genetic sand-mud couplets, and are explained as successions of storm-deposited units. Our data, and those of our colleagues presented in this paper, show the reality to be somewhat more complex; the signature of a

second agent of deposition, river flooding, is overprinted onto the storm record, and is readily extracted.

CHAPTER IV

TRANSGRESSIVE STRATIGRAPHY ON THE NORTHERN CALIFORNIA MARGINE: A PRELIMINARY TEST OF HYPOTHESIS BY THE FACIES MODEL

INTRODUCTION

The Northern California shelf (Fig. 20) is narrow (10-20 km wide); deep (shelf; break at 100 to150 m); and relatively steep (slope of 0.25° at the 60 m isobath; Borgeld, 1985). North of the Mendecino triple junction, the continental margin is undergoing active subduction. On the Eel River sector (Fig. 20), the subject of the recent STRATAFORM study (Nittrouer, 1999), there is little tectonic expression on the shelf surface. However, folds and faulted folds are actively deforming at shallow depth (Clarke, 1992). Differential land movements associated with tectonism are occurring at rates equivalent to the present rate of eustatic sea level rise (~1 mm/yr), so that of eustatic sea level rise is locally reversed.

The Eel sector is undergoing active sedimentation. Some sediment is produced by coastal erosion, but the primary sources are the Mad and Eel rivers (Brown and Ritter, 1992). Sediment is rapidly dispersed, by a rigorous hydraulic climate. It emerges from

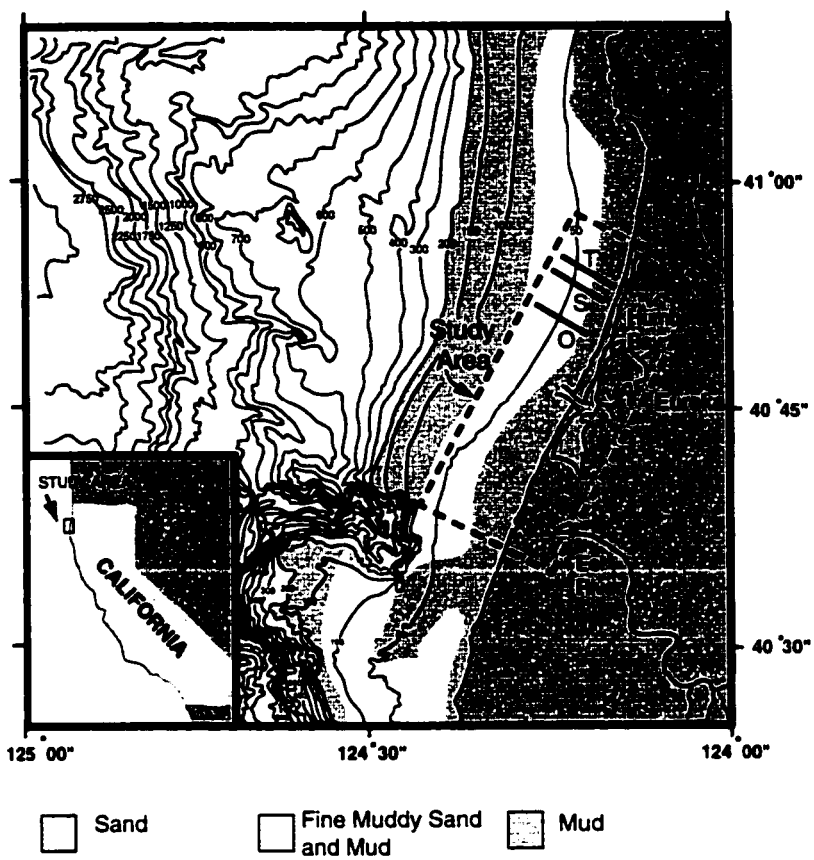

Fig. 20. The Study area with surficial grain size distribution from Borgeld, (1985) and locations of sampling transects mentioned in the text.

the river mouths in brackish, turbid plumes, and is transported to the northward, under the impetus of storm waves and currents (Geyer et al., 2000).

CONCEPTUAL MODEL FOR TRANSGRESSIVE STRATIGRAPHY

Concepts of Transgressive Shelf Facies

Recent studies of transgressive shelves allow the assemble of a generalized conceptual model for event stratigraphy in the study area. Studies of shallow marine transgressive deposits (Aigner and Reineck, 1982, Snedden and Nummedal, 1991, Nelson, 1985) suggest that in such settings there is a differential distribution of grain sizes, in which particles become finer from a landward to a seaward direction. Such seaward-fining gradients have been attributed *to progressive sorting* (Russell, 1939). The process is one of intermittent transport, in which the probability of resuspension and continued transport, at each station of the transport path, is greatest for the finest particles and least for the coarsest particles. Coarser particles thus tend to be sequestered at upstream stations, while finer particles are preferentially deposited downstream.

The same intermittency of transport leads to the division of the deposit into a succession of event beds (geologically instantaneous beds; Seilacher, 1982), and controls a second important process; *stratal condensation*. During each resuspension event, the preceding bed is partially cannibalized to form a new deposit; or entirely destroyed if it is

thin (Crowley, 1984). The degree of condensation of the resulting sedimentary column though this cannibalizing process is a function of the relationship between the annual depth of resuspension (depth of resuspension associated with the one year return period storm, a'), and the deposition per event, $\mathring{a}$. The ratio between the two parameters is the reworking ratio, $r = a'/\mathring{a}$ (Thorne et al., 1991), which describes the *preservation potential* of the bed (Zhang et al., 1997).

These processes of progressive sorting and stratal condensation have a profound influence on the character of the resulting deposit (transgressive facies assemblage; Swift et al., in review). In a transgressive setting, in which sea level is rising faster than sediment can be delivered to fill the resulting space, the shoreface undergoes erosional shoreface retreat (Swift et al., 1991). Seaward of the eroding shoreface, progressive sorting and stratal condensation lead to three characteristic sedimentary facies (Nelson, 1985; Aigner and Reineck, 1982; Snedden and Nummedal, 1991). On the inner shelf, an Amalgamated Sand Facies accumulates. Muds have no preservation potential in this facies and the basal portions of long return-period sand beds rest directly on each other. The Amalgamated Sand facies passes seaward into an Interbedded Sand and Mud Facies. In this facies the muddy tops of event beds are preserved. Sand-mud couplets, the record of single events, are intercalated with multiple-event mud beds, deposited too far seaward to receive sand. The Interbedded Sand and Mud Facies passes seaward into a Laminated to Bioturbated Mud Facies. The binomial nomenclature adopted in this chapter (see also

Zhang et al., 1997) is intended to emphasize that facies are characterized by stratal geometries as well as by grain size gradients.

Concepts of Transgressive Sequence Stratigraphy

In sequence stratigraphic terms, these several facies together comprise the Transgressive Systems Tract (Posamentier, 1989). Sequence stratigraphy views the facies-generating process of erosional shoreface retreat, cited above, as part of a more general process by which rising sea level incises a transgressive unconformity across the eroding subaerial landscape and its sediment-filled estuaries (ravinement surface; Stamp, 1922, in Swift, 1968). Seaward of the eroding shoreface, storm and flood events generate the successions of sheet-like beds described above. These beds are known to exhibit a characteristic geometry (Mitchum et al., 1977). As they accumulate, they onlap against the ravinement surface, and backstep across it. "Onlap" refers to the angular relationship of the bed terminations with the underlying surface. Where they abut against the ravinement surface, they are more nearly horizontal than this surface. The beds are also backstepping. They are envisaged as thinning both landward and seaward, and "backstepping" in the sense that the thickest portion of each subsequent bed is shifted landward relative to that of its predecessor. The thick central portion is apparent because the bed becomes thinner as it extends into the shallow, energetic, nearshore zone. The same bed will also become thinner towards the outer shelf. The problem here is not subsequent erosion, but instead

the diminishing convergence of sediment transport, as the water column deepens and bottom wave motion diminishes. As highstand approaches, a zone of sediment starvation, marked by firmgrounds, chemical precipitates and erosion, forms on the outer shelf and shifts landwards. Thus, transgressive shelf beds abut against ("toplap" against) a maximum flooding surface, as well as downlap against a ravinement surface. Since each event bed is deposited during the waning portion of the flow, it tends to fine upward. Because the shoreline is shifting steadily landward during the transgressive period, the section as a whole fines upward.

Observations of Transgressive Stratigraphy

Scales of observation of the Eel shelf include box cores (20-40 cm penetration), and piston cores and cores collected by other long core devices (Kasten corer, "slow" corer). Relatively few of these long cores have been taken. They range between one and 3 meters in length. Observations at larger spatial scales have been undertaken by means of seismic imaging (Acoustic Sediment Classification System; 5 to10 m penetration; and "Chirp" Sonar; 30 to100 m penetration)

Box cores from the Eel Shelf clearly reveal a seaward-fining grain-size gradient (for example, profiles of grain size fractions from the "O" line, Fig. 2). Core X-radiographs show that these grain-size gradients are accompanied by an orderly progression of stratal types (for example, X-radiographs from the "S" line; Fig. 3).

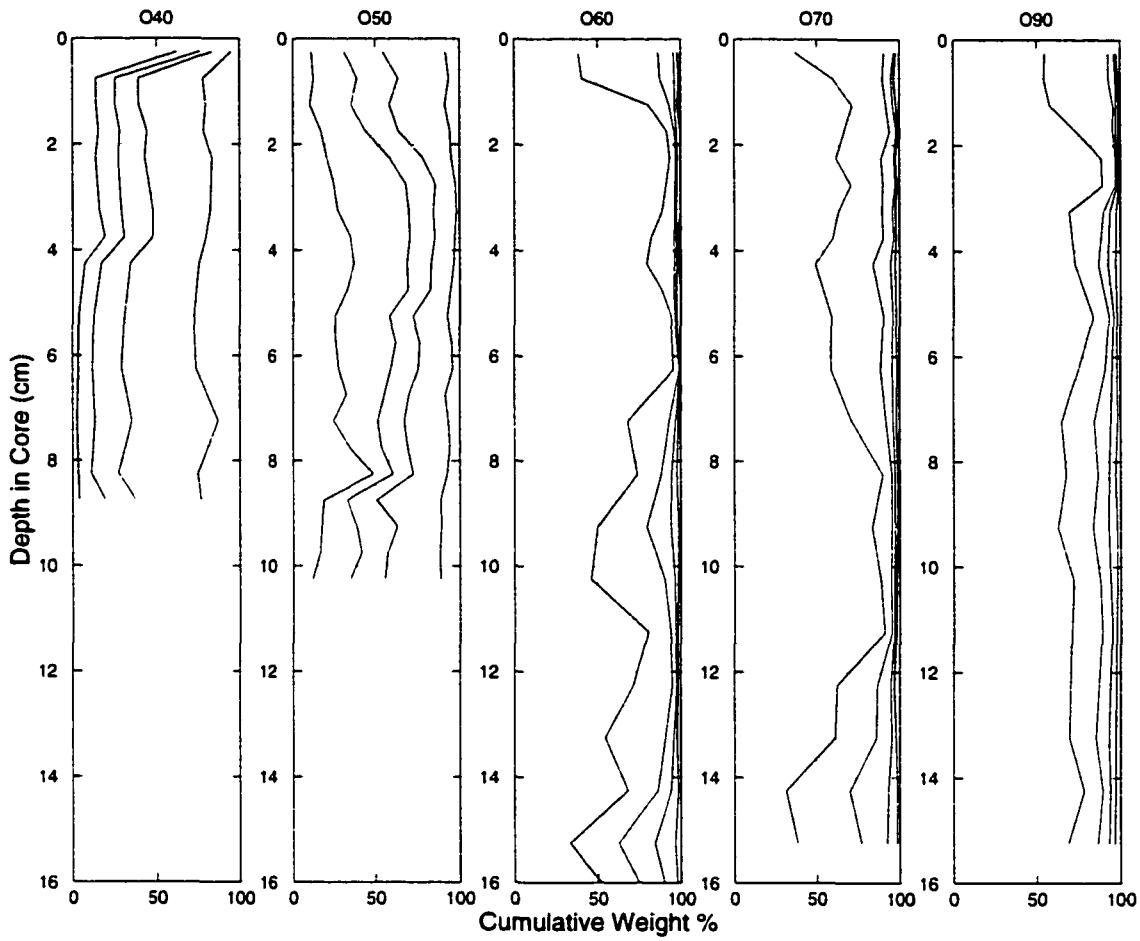

Fig. 21. Relative amounts of clay, silt, very fine sand ,fine sand and medium sand, in box cores from the O line. Boundaries are 32 μm, 64 μm, 125 μm, and 250 μm. From Drake (personal communication).

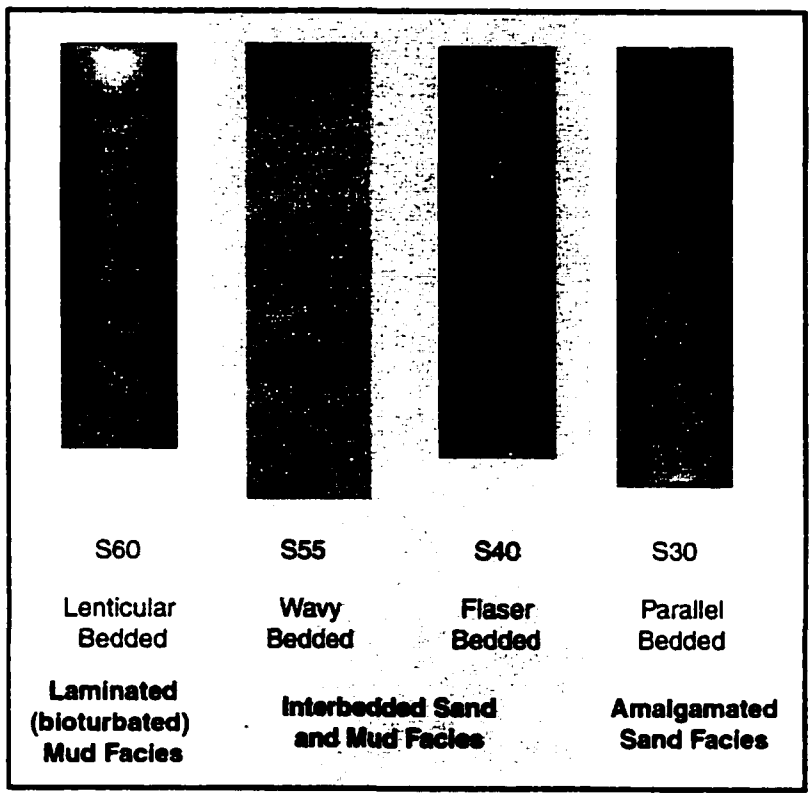

Fig. 22. Subsamples of box cores collected on the S line during the July 1997 Melville cruise.

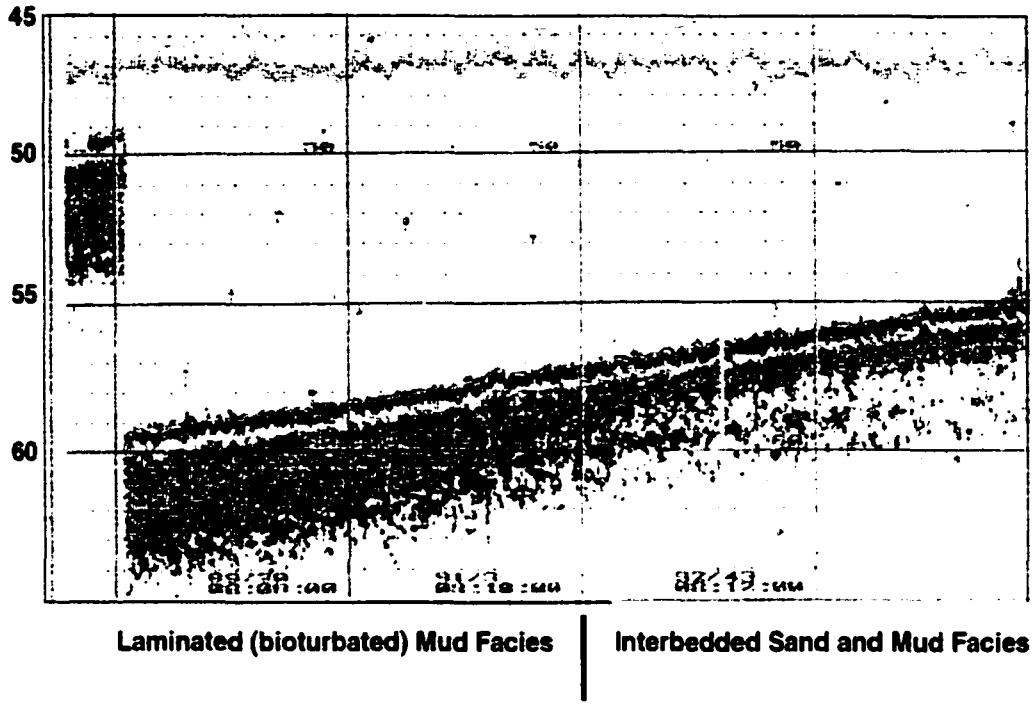

Fig. 23. Sub-bottom profile collected near the S line with an Acoustic Sediment Classification System. From Briggs and Logan, 1996.

Landward of the 40 m isobath, fine sand with parallel bedding prevails, although the sand-on-sand contacts are difficult to discern in the cores. Between 40 and 50 m water depth, scattered lenses of finer material appear in the fine sand. In some cases this pattern appears to be a "flaser" pattern (Reineck and Singh, 1980) in which isolated mud drapes lie in the troughs of waves ripples. In other examples, the steeply dipping orientation of the lenses suggests that they are mud-filled burrows. Between 50 and 60 m, mud beds are more nearly continuous, but are ripple-perturbed ("wavy bedded" pattern, Reineck and Singh, 1980). Yet further seaward, localized sand lens occur in a laminated mud matrix. (Lenticularly bedded sand and mud, (Reineck and Singh, 1980).

A regular seaward change in stratal characteristics can also be observed in seismic images. Records collected with an Acoustic Sediment Classification System reveal an abrupt increase in penetration of the sea floor, from about 2 m to 5 m seaward of the 55 m isobath, apparently a response to the increase in the frequency of mud interbeds (Briggs and Logan, 1996; Fig. 23). The zone between 55 m and 60 m water depth is characterized by a stratified pattern, which becomes uniformly transparent seaward of the 60 m isobath. Chirp sonar records reveal an acoustically transparent layer of presumed upper Holocene age about 10 m thick (Driscoll, pers. com.; Fig. 24). Below this layer, the older Holocene is more obviously stratified, and these lower reflectors bear an onlapping relationship with the underlying strata of presumed Pleistocene age. The upper

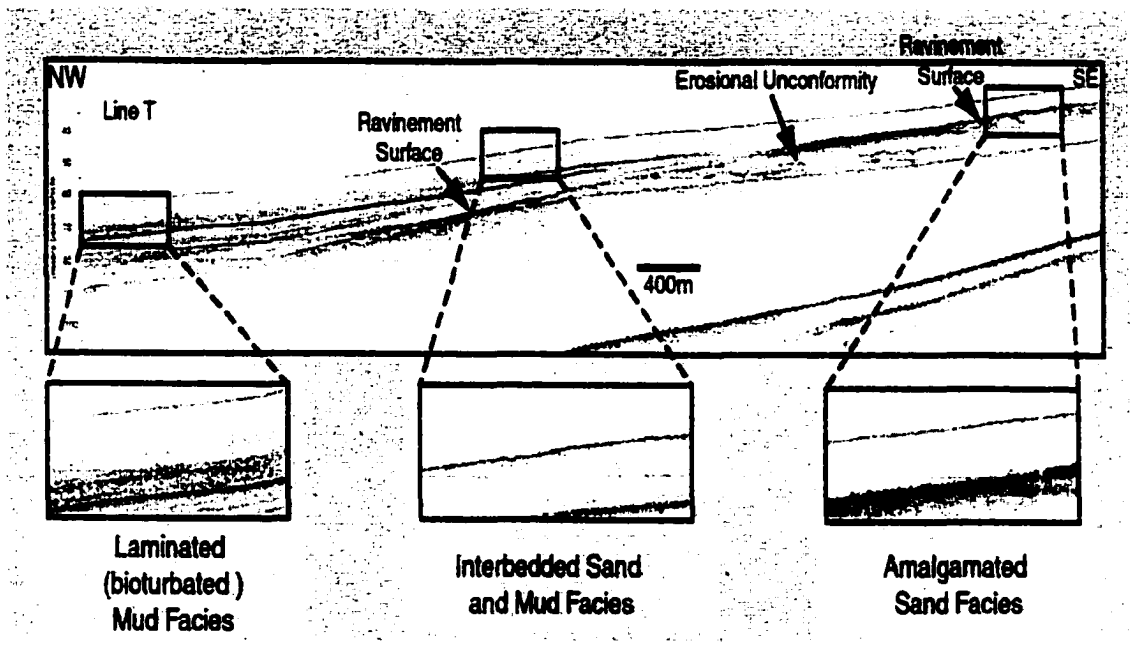

Fig. 24. Chirp sonar profile of the T-line. See text for explanation. Data collected by N. Driscoll, Scripps Institute of Oceanography.

transparent layer exhibits a (faintly) banded zone between the 45 and 60 m isobaths, similar to that seen with the Acoustic Sediment Classification System.

Hypotheses to be Tested

Some aspects of this conceptual model can be tested more readily by further observations; others by computation (numerical modeling). Still other aspects are not readily constrained by either the observations so far collected on the Eel shelf, or by the models in their present stage of evolution. In this paper we focus on the three-dimensional lithologic gradients of the transgressive systems tract on the eel shelf. Phrasing this concern as an hypothesis, we propose that on the Eel shelf, the Holocene transgressive systems tract consists of back-stepping, seaward-fining event beds, whose timelines (bedding planes) dip more gently than do their gradational facies boundaries.

SIMULATIONS OF TRANSGRESSIVE STRATIGRAPHY

Building Bedding Algorithms

Storm-driven sediment transport regimes on the Northern California shelf can be classified as low-concentration regimes and high concentration regimes (Fan et al, in revision). *Low concentration regimes* occur during storm periods when there has been no recent flood deposition on the inner shelf. At such times, sediment deposited by earlier

floods or derived from coastal erosion is suspended by wave orbital motions and is redistributed by wind-driven and tidal currents. *High concentration regimes* occur during storm periods that follow a major flood, when flocs settling from turbid flood plumes, collect in dense, near-bottom layers, that may slide seaward under the impetus of gravity. In this section, we present algorithms that compute the characteristics of beds deposited by low and high concentration regimes, (EVENT 1, EVENT 2), and briefly describe their use in a probabilistic model that assembles bed successions from wave height and river discharge frequency distributions (FACIES).

Dynamics of Cross-shelf Sediment Transport

Mid-latitude low-pressure systems transit eastward across the Northern California margin with a periodicity of 7-14 days during the winter (Largier, et al,, 1993). Many of these are accompanied by winds sufficiently intense to generate wind and wave-generated currents and resuspend significant amounts of sediment on the Eel shelf. In addition, cumulative rainfall during the storm passage may be sufficient to flood the Eel and Mad rivers. The flood waters emerge from the rivers as turbid, coast-hugging low-salinity plumes extend northward from river mouths (Geyer et al., 2000). The turbidity consists of particle aggregates (flocs) containing some fine sand and much silt and clay. As the flocs settle onto the shoreface, concentrations near the seabed may build up to 15 g/l or more, sufficient to create a fluid mud (Traykovski et al., 2000). If the orbital

motions of storm waves are still intense, further consolidation does not occur. Instead the fluid mud may slide seaward under the impetus of gravity at velocities of 5 to 10 cm/sec until it reaches the central shelf. Here, as wave orbital motion decreases and the slope becomes more gentle, deposition occurs (Traykovski et al., 2000). A consolidating inner-shelf mud bed may still be capable of seaward gravity transport for weeks after the initial event, if appropriate wave conditions occur. Beds deposited by this high-concentration, gravity-transport regime are poorly sorted, mud-rich, and contain pebble or sand-sized wood fragments. If, however, intense waves do not occur until after consolidation has been completed, then much or all of the bed will undergo wave resuspension and be transported offshore at relatively low concentrations. The low-concentration resuspension process is much more efficient in unmixing flood-deposited mud than is the high concentration gravity transport process. During low-concentration resuspension, much of the finer material escapes the system altogether, going toward or over the shelf edge and leaving a residue enriched in sand on the sea floor. Consequently, low-concentration events lead to thinner, sandier beds than do the fluid mud flows.

Modeling Storm Beds Deposited from Low Concentration Regimes

A two-dimensional cross-shelf sediment transport model has been developed to storm bed formation by low concentration regimes (EVENT I). The model is described

in detail elsewhere (Zhang et al., 1999; Chapter III of this thesis), and its structure will be only summarized here.

Let C_m denote the mass sediment concentration of mth size class, $w_{s,m}$ the settling velocity of suspended particles of this size class, U_x the across-shelf component of subtidal current velocity, D_h and D_v the horizontal and vertical eddy mass diffusivities, respectively. The transport equation for the concentration C_m is (Zhang et al., 1999):

$$\frac{\partial C_m}{\partial t}+\frac{\partial U_x C_m}{\partial x}-w_{s,m}\frac{\partial C_m}{\partial z}-\frac{\partial}{\partial x}\left(D_h\frac{\partial C_m}{\partial x}\right)-\frac{\partial}{\partial z}\left(D_v\frac{\partial C_m}{\partial z}\right)=0 \qquad (41)$$

The inner Eel shelf is covered by fine sand, and the central and outer shelf are covered by silt and mud (Borgeld, 1985; Borgeld, et al., 1999). So this model has two options for sediment input at the bottom boundary. For a non-cohesive bed, the boundary sediment concentration condition of mth size class $C_{0,m}$ at z_0 is based on that of Smith and McLean (1977):

$$C_m(z_0)=C_{0,m}=\frac{f_{0,m}C_b\gamma_0 S_m}{1+\gamma_0 S_m} \text{ and } S_m=\frac{\tau_{b,cw}}{\tau_{c,m}}-1 \qquad (42)$$

Here C_b is the bed sediment concentration, γ_0 is an empirically determined sediment-entrainment parameter, $f_{0,m}$ is the fraction of the mth grain-size class in the bed, S_m is the excess shear stress. The variable $\tau_{c,m}$ is the critical stress required for initiating sediment

entrainment, based on a formulation by Delft Hydraulics (1989) which considers the influence of cohesive material. Reported values for γ_0 are site-specific and vary over two orders of the magnitude (Nittrouer and Wright, 1994), and the parameter is often reserved as a calibration parameter.

For a cohesive sediment bed, experiments have led to the boundary condition:

$$-w_{s,m}C_m - D_v\frac{\partial C_m}{\partial z} = -D_m + E_m \qquad z = z_0 \qquad (43)$$

The left-hand side represents the total flux rate of grain-size class mth in the vertical direction. On the right-hand side, D_m stands for the rate of deposition that occurs when the magnitude of the bottom shear stress $\tau_{b.cw}$ is below the critical depositional shear stress τ_d, while E_m stands for the rate of erosion that occurs when $\tau_{b.cw}$ is above the threshold τ_c. These variables are usually given in the following form (Patheniades, 1965; Krone, 1962):

$$D_m = \mathrm{H}(\tau_d - \tau_{b.cw})w_{s,m}C_{0.m}\left(1 - \frac{\tau_{b.cw}}{\tau_d}\right) \qquad (44)$$

$$E_m = \mathrm{H}(\tau_{b.cw} - \tau_c)f_{0.m}M\left(\frac{\tau_{b.cw}}{\tau_c} - 1\right) \qquad (45)$$

where $\mathrm{H}(x)$ denotes the Heaviside step function of x, $w_{d,m}$ is the velocity of deposition of mth grain-size class, and M is an erosion coefficient, which usually preserved as a calibration parameter. In the absence of both field and laboratory experiments on the Eel shelf mud, The values $\tau_d = 0.6 dyne/cm^2$ for the San Francisco Bay mud (Krone, 1962);

$\tau_c = 0.9 dyne/cm^2$ and $\tau_c = 2 dyne/cm^2$ for newly deposited mud and existing mud, respectively (Schunemann and Kuhl 1993), are used in our simulations.

Outside the boundary layer, we assume

$$C_m = 0 \qquad z \to \infty \tag{46}$$

The coastal boundary provides a seaward sediment flux from the nearshore zone. Because of the poor knowledge of the nearshore sediment transport in this area, a zero-flux profile is selected. The shelf break boundary is set at a depth of 100 m with a radiation boundary condition (Camerlengo and O'Brien, 1980).

Once the sediment concentration field is known, across-shelf sediment flux can be computed. The change of sea-floor height and components can be calculated by the mass-continuity equation:

$$\frac{\partial z_{b,m}}{\partial t} = -\frac{1}{C_b}\left(\frac{\partial C_{T,m}}{\partial t} + \frac{\partial U_x C_{T,m}}{\partial x}\right) \tag{47}$$

where z_b and $C_{T,m}$ are sea-floor elevation and depth-integrated sediment concentration for mth grain-size class, respectively.

The wave height variation during a storm is generalized as a parabolic process with its peak at the middle of the storm duration, and used as driving force. A two-layer, eddy diffusivity model of the wave-current combined benthic boundary layer, developed by Grant and Madsen (1979) and Glenn and Grant (1987) is used. The outputs of the model are storm bed thickness and grain size.

Modeling Storm Beds by Gravity Processes

If a major flood creates a consolidating mud bed on the inner shelf during or prior to an episode of high waves, then resuspension of the mud may create a fluid mud (Traykovski et al, 2000). It is known that fluid mud behaves approximately as Bingham plastic. When fluid mud flows downslope due to gravity, the fluid mud velocity in the bottom shear layer u, the above plugging layer u_p, and the yield shear stress τ_0 are (Liu and Mei, 1989):

$$u = \frac{1}{\mu}\left[\rho g'\left(\tan\theta - \frac{\partial h}{\partial x}\right)\right]\left(h_0 z - \frac{1}{2}z^2\right) \qquad 0 \le z \le h_0 \qquad (48)$$

$$u_p = \frac{h_0}{2\mu}\left[\rho g'\left(\tan\theta - \frac{\partial h}{\partial x}\right)\right] \qquad h_0 \le z \le h \qquad (49)$$

$$\tau_0 = \rho g'\left(\tan\theta - \frac{\partial h}{\partial x}\right)(h - h_0) \qquad (50)$$

where μ is the coefficient of viscosity, ρ is fluid mud density, $g' = g\Delta\rho/\rho$ is the gravity acceleration, $\tan\theta$ is sea bed slope, h is the thickness of fluid mud layer, and h_0 is the interface of shear flow and plugging flow. So the fluid flux is:

$$q = \frac{h_0^2}{6\mu}\left[\rho g'\left(\tan\theta - \frac{\partial h}{\partial x}\right)\right](3h - h_0) \qquad (51)$$

Studies by Teeter (1992) and Traykovski et al. (2000) show that the thickness of the fluid mud layer can be approximated as the wave boundary layer. Since the yield shear stress of the fluid mud is proportional to sediment concentration, and since the fluid mud can flow only when bottom wave shear stress is larger than fluid mud yield shear stress, we can use the bottom wave shear stress as yield shear stress to calculate the maximum sediment that can be held in the fluid mud layer. The output of this model is the bed thickness. The grain size of the bed is considered as constant.

Synthetic Event Stratigraphy

Since the atmosphere and the ocean are coupled chaotic systems, storm and flood beds accumulate as effectively random successions. Consequently, the time series of storm bed generation at sea floor must be treated as a stochastic process. The succession of the storm beds actually preserved is just one of many possible realizations of the formative process, each as potentially 'valid' as any other (Zhang et al., 1997). We have therefore built a synthetic hydraulic history of about 400 years duration in order to study event stratigraphy and facies change on the northern California margin. Gumbel distributions (extreme event distributions) of river discharge and wave height have been compiled from Eel river discharge data supplied by the United States Geological Survey (Eel River, Scotia California Station) and wave data from NOAA's NDBC buoy 46022. A Monte Carlo algorithm is used to generate a sequence of floods and storms from this

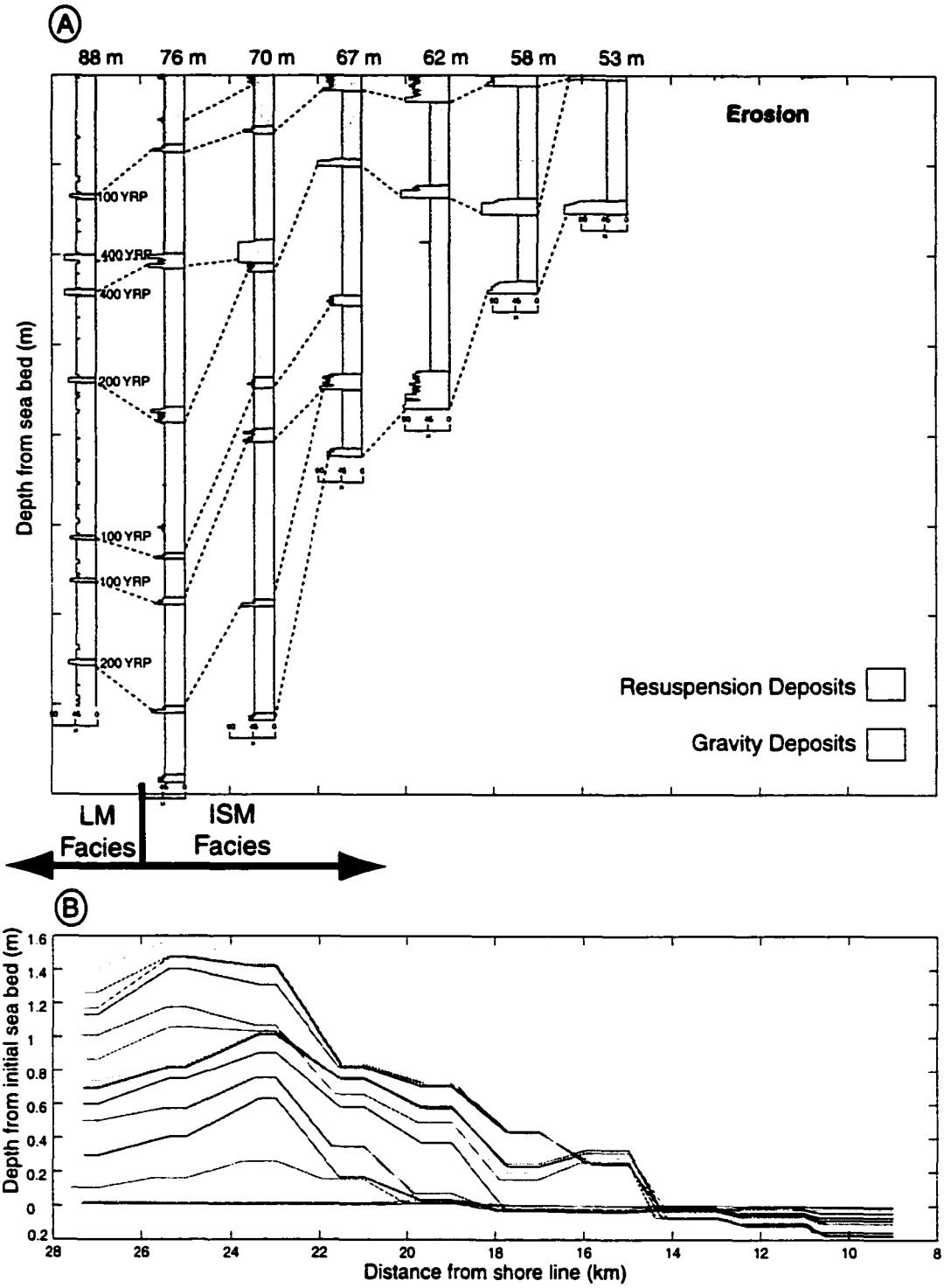

Fig. 25. Synthetic event stratigrpaphy simulated by FACIES with return periods in years (YRP) noted. The boundary between the Interbedded Sand and Mud Facies and the Laminated Mud Facies is indicated. A: virtual cores. B: 20-year time lines.

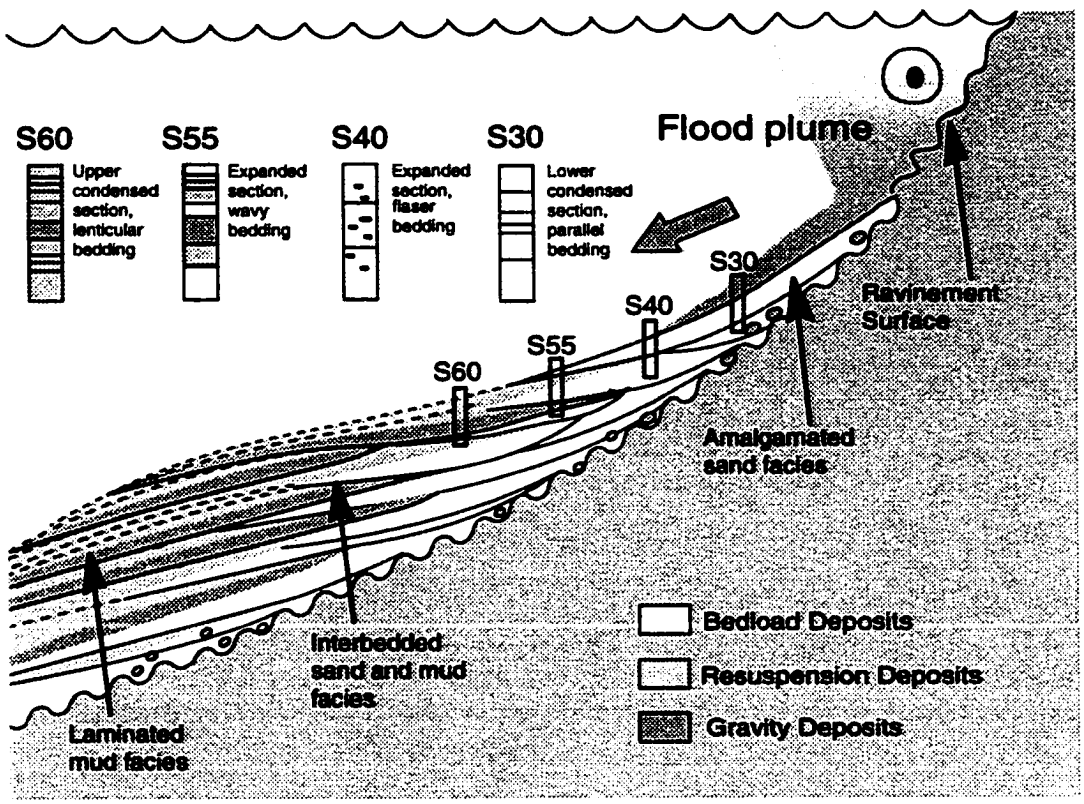

Fig. 26. Conceptual model of the transgressive systems tract, Eel Shelf, based on observations and simulations.

data. If there is no flood just before a storm, EVENT I with suspension processes is used to calculate storm bed thickness, while if there is a flood during or just before the storm, EVENT II with gravity processes is used. The initial muddy deposit on the inner shelf is calculated by assuming that the sediment deposition rate follows a Gaussian distribution whose mode shifts along-shore with the scale of the flood.

In the simulation of Fig. 25a, approximately 400 floods and 800 storms have occurred. An examination of 20-year time lines (Fig, 25 b) show that shelf floor is erosional out to the 40 m isobath. At 53 m, a 100-year return period flood, combined with a 2-year return-period storm has generated a 'flood' bed (product of a fluid mud flow) approximately 30 cm thick. Mean diameter of the sediment is 45 μm. This major bed can be traced all the way to the 88 m isobath. The bed is capped by a 2 cm 'storm' bed, produced by resuspension, with no fluid mud addition. Storm beds produced by such low-concentration regimes (resuspension only) are notably sandier, with mean diameter around 90 μm, and thinner; this one thickens to 8 cm at the 62 m isobath, but becomes thin again, seaward of that. Note that stratal continuity is poor between the 40 and 76 m water depth. Long return-period events cut down through short return-period events and collapse their time lines into bundles. Mean bed thickness reaches a maximum at the 76 m station. Between 76 m and 80 m, the stratigraphic section becomes much more complete, and time lines separate. Many of the 'storm' beds that form protruding ledges between 'flood' beds in the synthetic column for 76 m become notches between 'flood'

beds on the 88 m column. These beds are anomalously sandy at 76 m, but sand does not travel as far seaward as mud during low concentration resuspension events, and the same beds appear as mud anomalies at 88 m. The contrast in lithologic properties and stratal geometry between 76 m and 88 m indicates that the boundary between the interbedded Sand and Mud Facies lies between the two stations.

DISCUSSION AND CONCLUSIONS

The simulation of event strata (Fig. 25) may be compared with Fig. 26, a composite sketch that attempts to synthesize the conceptual model with observations and the simulation. The simulated beds are onlapping a surface, which on its inner margin is undergoing active erosion (ravinement surface). Note that the simulation does not account for sea level change. The absence of this variable is presumably not of major concern since the eustatic rise over 400 years would be on the order of 40 centimeters. The simulation can be viewed as having taken place at the beginning of highstand, when sea level rise has become negligible. The shoreface is still undergoing erosional retreat, at this time, but river mouths have completed the geomorphic transition from estuaries to deltas and are yielding copious amounts of fine sediment.

The biggest discrepancy between the simulation and observation is lack of a well-developed Amalgamated Sand Facies. In the simplified model, the only method of

sediment introduction is the initiation of a fluid mud episode, or through erosion of the inner shelf floor. The shoreface, with its high-energy surf dynamics is not accounted for. If these dynamics were included, the relatively coarse sediment provided in copious quantities by shoreface erosion would drive the boundary between sedimentation and erosion back in to the foot of the shoreface. That being said, it should be noted that the Amalgamated Sand Facies is often thin or absent on interfluves and is typically thick only in the capping deposits of transgressed estuaries ("trailing sands").

The test of hypothesis described in the introduction to this paper may be considered to have a positive outcome. The simulation reproduces a facies boundary seen in core and seismic observations (Figs. 21-24), between the Interbedded Sand and Mud Facies and the Laminated Mud Facies. In Figure 6, the facies transition is completed between the virtual core at 76 m and the virtual core at 88 m, and must dip more steeply seaward than any time line.

UPSCALING FROM FACIES TO SEQUENCE

Event strata are the fundamental units from which facies and, ultimately, depositional systems and depositional systems tracts are built (Thorne, et al, 1991). A

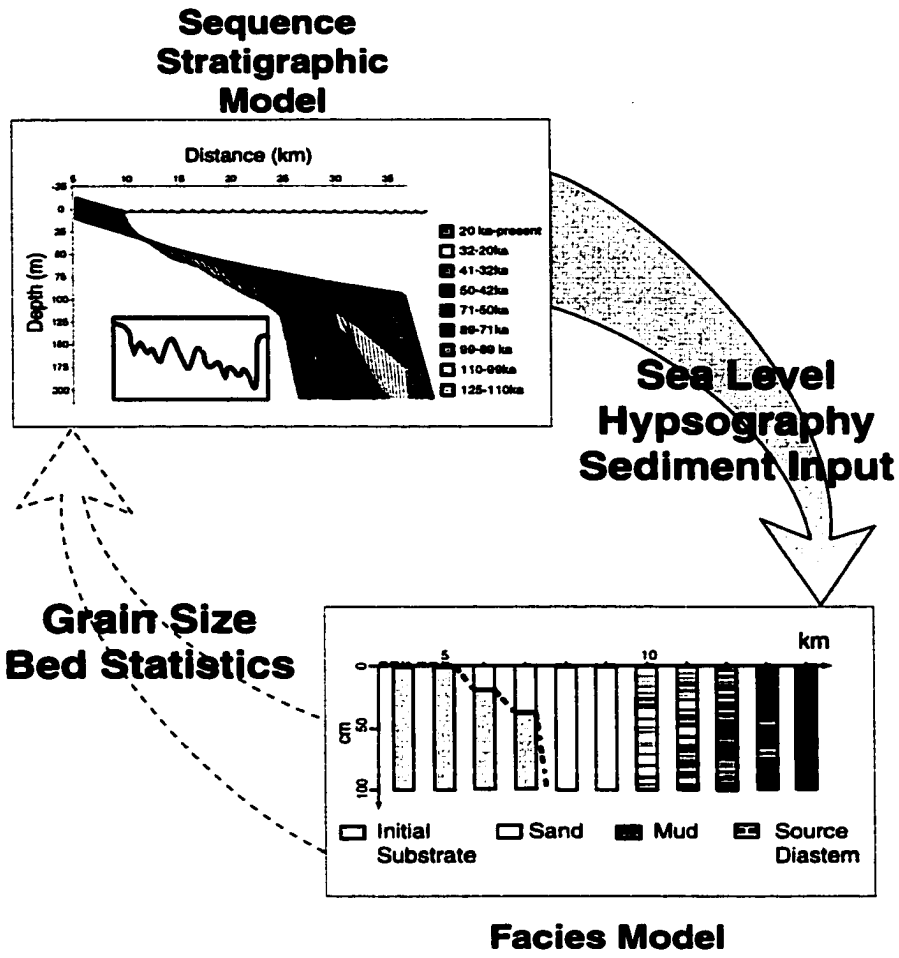

Fig. 27. Scheme for connecting FACIES and SEQUENCE models. See text for explanation. FACIES image from Zhang et al., 1997; SEQUENCE image from Carey et al., 1999.

comprehensive model of continental shelf sedimentary processes must, therefore, link these scales. A major success of STRATAFORM modeling efforts has been the numerical integration of the event and facies scales (Zhang, et al., 1997, 1999; Fan, et al., in revision). Work now proceeds on the integration of the stratigraphic scale.

SEQUENCE, developed in cooperation with colleagues at Lamont-Doherty Earth Observatory (Sreckler et al., 1999, Carey, et al., 1999) and URS Corp (Niedoroda et al., 1995) is a forward numerical model that simulates stratigraphic sequences. After creating an initial profile, the model uses defined sea level and sediment input curves, along with parameters defining tectonic subsidence, isostastic response to sediment and water loading, compaction, and erosion in the system, to calculate the resulting profile, an example of which can be seen in Figure 27. The time interval over which such calculations take place may be defined by the user.

This flexibility allows us to numerically link the scales of modeling. For each time step, as SEQUENCE calculates the new profile, it passes to FACIES the user defined sea level and sediment input, along with the preliminary hypsography. Given this information, in addition to its own unique input parameters, FACIES calculates grain size and bed statistics at each location for use by the large-scale model. Through iteration of this feedback loop, SEQUENCE determines a final profile for each time step. The calculated stratal parameters describe the constituent facies built by the model making it possible to map the extent of the resulting depositional systems (Swift, et al., 1991). This map may be displayed over the resulting time lines and sediment properties, as calculated through this process, can also be displayed in SEQUENCE down synthetic wells

(Steckler, 1999). As shown by the dotted arrow in Figure 27, this integration has not yet been fully implemented.

REFERENCES

Aigner, T. and Reineck, H.E., 1982. Proximality trends in modern storm sands from the Helegoland Bight (North Sea) and their implications for basin analysis. Senckenbergiana marit. 14, 183-215.

Alexander, C.R., Simoneau, A.M., 1999. Spatial variability in sedimentary processes on the Eel continental slope. Mar. Geol. 154, 243-254.

Allen, J.R.L., 1982. Sediment structures: their character and physical basis. Elsevier, Amsterdam, 664pp.

Ariathurai, R. and Arulanandan, K., 1978. Erosion rate of cohesive soils. J. Hydr. Div. ASCE 104, 279-283.

Ariathurai, R. and Krone, R.B., 1976. Finite element model for cohesive sediment transport. J. Hydrol. Div. ASCE 102, 323-338.

Bagirov, E., and Lerche, I., 1999. Probability and sensitivity analysis of two dimensional basin modeling results. In Harbaugh, J.W., Watney, W.L., Rankey, E.C., Slingerland, R. and Goldstein, R.H. (Eds), Numerical Experiments in Stratigraphy: Recent Advances in Stratigraphic and Sedimentologic Computer Simulations. Soc. of Econ. Paleontol.Mineral. Spec. Publ., pp. 35-68.

Basco, D.R., 1985. A qualitative description of wave breaking. J. Waterw. Port. Coast. Ocean Eng. ASCE 111, 171-188.

Battjes, J.A., 1974. Surf similarity. In: Proc. 14th Coast. Eng. Conf., ASCE, pp. 448-480.

Battjes, J.A. and Janssen, J.P.F.M., 1978. Energy loss and set-up due to breaking of random wave. In: Proc. 16th Coast. Eng. Conf., ASCE, pp. 569-587.

Battjes, J.A. and Sakai, T., 1981. Velocity field in a steady breaker. J. Fluid Mech. 111, 121-137.

Bedford, K.W. and Lee, J., 1994. Near-bottom sediment response to combined wave-current conditions, Mobile Bay, Gulf of Mexico. J. Geophys. Res. 99, 16161-16177.

Berlamont, J., Ockenden, M., Toorman, E. and Winterwerp, J., 1993. The characterization of cohesive sediment properties. Coast. Eng. 21, 105-128.

Bijker, E.W., 1986. Coastal Engineering, Vol. II. Lecture notes. Delft Univ. Technology, Delft, The Netherlands.

Birch G. F., 1977. Surficial sediments on the continental margin off the west coast of South Africa. Mar. Geol. 23, 305-337.

Bishop, C., Skafel, M. and Nairn, R., 1992. Cohesive profile erosion by waves. In: Proc. 23rd Coast. Eng. Conf., ASCE, pp. 2976-2989.

Bodin, J. H., Steckler, M. S., and Watts, A. B., 1981. Observations of flexure and the rheology of the oceanic lithosphere. J. Geophys. Res. 83, 4975-4987.

Borah, D.K., Alonso, C.V. and Prasad, S.N., 1982. Routing graded sediments in streams: formulation. J. Hydraul. Eng. 108, 1486-1503.

Borgeld, J. C., 1985. Holocene stratigraphy and sedimentation on the Northern California continental shelf. Ph.D. Dissertation, Univ. of Washington, 178 pp.

Borgeld, J.C., Hughes Clarke, J.E., Goff, J.A., Mayer, L.A. and Curtis, J.A., 1999. Acoustic backscatter of the 1995 flood deposit on the Eel River shelf. Mar. Geol. 154, 197-210.

Bouchard, R. J., and Borgeld, J. C., 1988. Graded sands from the Eel River Continental Shelf, Northern California: storm generated deposits. Arcata, CA, Humolt State University, Telonicher Marine Laboratory technical report TML-17, 36pp.

Briggs and Logan, 1996. Eel river study. Cruise reports for W960A, Leg 2. Naval Research Laboratory, Stennis Space Center, Bay Saint Louis, MS., 86 pp.

Brown, W. M., and Ritter, J. 1971. Sediment transport and turbidity in the Eel river basin, California. U.S. Geological Survey Water Supply Paper 1986, 70pp.

Brϕker Hedegaard, I., Roelvink, J.A., Southgate, H.N., Pechon, P., Nicholson, J., Hamm, L., 1992. Intercomparison of coastal profile models. In: Proc. 23rd Coast. Eng. Conf., ASCE, pp. 2108-2121.

Burban, P.Y., Xu, Y.J., McNell, J. and Lick, W., 1990. Settling speeds of flocs in fresh water and seawater. J. Geophys. Res. 95, 18213-18220.

Cacchione, D.A. and Drake, D.E., 1982. Measurements of storm-generated bottom stresses on the continental shelf. J. Geophys. Res. 87, 1952-1960.

Cacchione, D.A., Grand, W.D., Drake, D.E. and Glenn, S.M., 1987. Storm-dominated bottom boundary layer dynamics on the California continental shelf: measurements and predictions. J. Geophys. Res. 92, 1817-1827.

Cacchione D. A. et al. 1994. Bottom stress estimates and sand transport on northern California inner continental shelf. Continental Shelf Research. 14(10,11), 1271-1290.

Cacchione, D.A., P.L. Wiberg, P.L., Lynch, J., Irish, L., and Traykovski, P.A., 1999. Estimates of suspended sediment flux and bedform activity on the inner portion of the Eel continental shelf. Mar. Geol. 154, 83-97.

Camerlengo, A.L. and O'Brien, J.J., 1980. Open boundary conditions in rotating fluids. J. Comp. Phys. 35, 12-35.

Carey, J.S., Swift, D.J.P., Steckler, M., Reed, C.W., and Niedoroda, A.W., 1999. High resolution sequence stratigraphy modeling: effects of sedimentation processes in numerical experiments in stratigraphy. Soc. Econ. Paleontol. Mineral. Spec. Publ., 151-164.

Chorley, R.J., Schumm, S.A. and Sugden, D.E., 1984. Geomorphology. Methuen, 605pp.

Clarke, S. J. Jr., 1992. Geology of the Eel River Basin and adjacent region: Inplications for late Cenozoiuc Tectonics of the Southern Cascadia Subduction Zone and the Mendecino Triple Junction. Am. Assoc. Petroleum Geologistrs Bull. 76, 199-224.

Coleman, J.M., 1988. Dynamic changes and processes in the Mississippi River delta. Geol. Soc. Amer. Bull. 100, 999-1015.

Cox, D.T., Kobayashi, N. and Okayasu, A., 1996. Bottom shear stress in the surf zone. J. Geophys. Res. 101, 14337-14348.

Crowley, K.D., 1984. Filtering of depositional events and the completeness of sedimentary sequences. J. Sed. Petrol. 54, 127-136.

Curray, J.R., 1960. Sediments and history of the Holocene transgression, continental shelf, northwest Gulf of Mexico. In: Shepard, F.P., Phleger, F.B. and Van Andel, T.H. (Eds.), Recent Sediments, northwest Gulf of Mexico, Amer. Assoc. Petrol. Geol., pp. 221-226.

Curray, J.R., 1964. Transgressions and regressions. In: Miller, R.L. (Ed.), Papers in Marine Geology. Shepard commemorative volume, MacMillan, New York, pp. 175-203.

Curray, J.R., 1969. Shore zone sand bodies: barriers, cheniers, and beach ridges. In: Stanley, D.J. (Ed.), The New Concepts of Continental Margin Sedimentation. AGI, Washington, D.C., JCII-1-18.

Dally, W.R., Dean, R.G., Dalrymple R.A., 1985. Wave height variation across beach of arbitrary profile. J. Geophys. Res. 90, 11,917-11,927.

Davidson-Arnott, R.G.D., 1986. Rates of erosion of till in the nearshore zone. Earth Surf. Proc. Landforms 11, 53-58.

Davidson-Arnott, R.G.D. and Ollerhead, J., 1995. Nearshore erosion on a cohesive shoreline. Mar. Geol. 122, 349-365.

Davies, P. J., 1979. Marine geology of the continental shelf off southeast Australia. Bull. Bur. Miner. Resour. Geol. Geophys. Aust. 195.

Dean, R.G., 1991. Equilibrium beach profiles: Characteristics and applications. J. Coast. Res. 7, 53-84.

Deigaard, R., Fredsoe, J. and Hedegaard, I.B., 1986. Suspended sediment in the surf zone. J. Waterw. Port, Coast. Ocean Eng. 112, 115-128.

Delft Hydraulics, 1989. Nogat offshlore pipeline, Report on erodability tests, report H1050, Delft Institute of hydraulics, Delft, the Netherlands. 32 pp.

DeVries, J.W., 1992. Field measurements of the erosion of cohesive sediments. J. Coast. Res. 8, 312-318.

Dietz, R.S., 1963. Wave base, marine profile of equilibrium, and wave built terraces: a critical appraisal. Geol. Soc. Amer. Bull. 74, 971-990.

Drake D. E., 1998. Temporal and spatial variability of the sediment grain size distribution on the STRATAFORM shelf: the flood layer of 1995.

Duke, W.L., Arnott, R.W. and Cheel, R.J., 1991. Shelf sandstones and hummocky cross stratification: new insights on a stormy debate. Geology 19, 625-628.

Dyer, K.R. and Soulsby, R.L., 1988. Sand transport on the continental shelf. Annual Rev. Fluid Mech. 20, 295-324.

Eidsvik, K.J., 1993. Parameterization of wave effects upon large-scale bottom boundary layer flow. Cont. Shelf Res. 13, 903-918.

Emery, K.O., 1952. Continental shelf sediments off southern California. Geol. Soc. Amer. Bull. 63, 1105-1108.

Fan, S., Yu, Z., Jin L., 1997. Dynamical mechanism and modeling of recession and accretion of mud flat. Part I wave and current (in Chinese). Acta Oceanologica Sinica 19(3), 67-76.

Fan, S., Yu, Z., Jin L., 1997. Dynamical mechanism and modeling of recession and accretion of mud flat. Part II sediment transport and mud flat processes model (in Chinese). Acta Oceanologica Sinica 19(3), 77-85.

Fenneman, N.M., 1902. Development of the profile of equilibrium of the subaqueous shore terrace. J. Geol. 10, 1-32.

Fisher, W.L., and McGowen, J.H., 1967. Depositional systems in the Wilcox Group of Texas and their relationship to the occurrence of oil and gas. Gulf Coast Assoc. Geol. Soc. Trans. 17, 105-125.

Fredericks, J.J., Trowbridge J.H., Williams III, A.J., Lentz, S.J., Butman, B. and Gross, T.F., 1993. Fluid mechanical measurements within the bottom boundary layer over the northern California continental shelf during STRESS. Technical Report, WHOI-93-32, Woods Hole Oceanography Institution, 116pp.

Fredsoe, J. and Deigaard, R., 1992. Mechanics of Coastal Sediment Transport. World Scientific, 369pp.

Gaughan, M.K., Komar, P.D., 1975. The theory of wave propagation in water of gradually varying depth and the prediction of breaker type and height. J. Geophys. Res. 80, 2991-2996.

Geyer, W.R., Hill, T.M., and Traykovski, P., 2000. The structure of the Eel River plume during floods. Cont. Shelf Res. 20, 2067-2094.

Gibbs, R.J.,1985. Settling velocity, diameter and density for flocs of illite, kaolinite and montmorillonite. J Sedimentary Petrology 55, 65-68.

Glenn, S.M., and Grant, W.D., 1987. A suspended sediment stratification correction for combined wave and current flows. J. Geophys. Res. 92, 8244-8264.

Goda, Y., 1990. Distribution of sea state parameters and data fitting. In: Herbich, J.B., (Ed.), Handbook of coastal and ocean engineering, Vol.1. Gulf Publishing Company, Houston, pp. 371-408.

Gong, C., Ge, M., 1994. Wave study for the planning of Zhongshan Harbor, Jiangsu Province(in Chinese). Internal Rep., Hehai University.

Grant, W.D. and Madsen, O.S., 1979. Combined wave and current interaction with a rough bottom. J. Geophys. Res. 84, 1797-1808.

Grant, W.D. and Madsen, O.S., 1986. The continental-shelf bottom boundary layer. Ann. Rev. Fluid Mech. 18, 265-305.

Green, M.O., Vincent, C.E., McCave, I.N., Dickson, R.R., Rees, J.M. and Pearson, N.D., 1995. Storm sediment transport: observations from the British North Sea shelf. Cont. Shelf Res. 15, 889-912.

Gross, T.F., Isley, A.E. and Sherwood, C.R., 1992. Estimation of stress and bed roughness during storms on the Northern California shelf. Cont. Shelf Res. 12, 389-413.

Gu, J.L., Gong, C.Z. and Lu, X.L., 1990. The threshold movement of cohesive sediment due to wave action (in Chinese). In: Gong, C.Z. (Ed.), Sediment Deposition in Lianyungang. Hehai University Press, Nanjing, pp. 116-124.

Harris, C., and P. L. Wiberg, 2001. A two-dimensional, time-dependent model of suspended sediment transport and bed reworking for continental shelves. Computers and Geosciences 27, 675-690.

Horikawa, K., Kuo, C.T., 1966. A study of wave transformation inside the surf zone. Proc. 10th int. Conf. Coastal Eng., ASCE, pp. 217-233.

Horn, D.P., 1992. A review and experimental assessment of equilibrium grain size and the ideal wave-graded profile. Mar. Geol. 108, 161-174.

Huang, J.W., and Sun, X.Q., 1985. Experiments on erosion of sediments in Lianyungang (in chinese). Rept. of Nanjing Hydralic. Research. Inst., 17pp.

Huang, X., and Garcia, M.H., 1997. A perturbation solution for Binham-plastic mudflows. J. Hydr. Engrg., ASCE 123, 986-994.

Hughes, S.A. and Miller, H.C., 1987. Transformation of significant wave height. J. Waterw. Port Coast. Ocean Eng. ASCE 113, 588-605.

Huhe, O., and Yang, M., 1996. Experimental study of the properties of cohesive sediment of the Old Yellow River Delta (in Chinese). Report by the Inst. Mech., Chineses Acad. of Sci..

Jin, L., 1978. Basic information for Lianyungang Harbor construction (in Chinese). Internal Rep., Headquarter of Lianyungang Harbor Construction.

Jin, L. and Zhang, Q.S., 1983. Estimation of elements of design waves in Lianyungang (in Chinese). In: Proc. of Conf. on Wind Waves in Lianyungang, Jiangsu.

Johnson, D.W., 1919. Shore Processes and Shoreline Development. John Wiley, New York, 584pp.

Jonsson, I.G., 1966. Wave boundary layers and friction factors. In: Proc. 10th Coast. Engr. Conf., ASCE, pp. 127-148.

Kachel N. B. and Smith J. D. 1989. Sediment transport and deposition on the ashingtong continental shelf. In: M. L. Landry and B. M. Hickey (eds.), Coastal Oceanography of Washington and Oregon. Elsevier, Amsterdam, Neth., pp 287-348.

Kamphuis, J.W., 1978. Attenuation of gravity waves by bottom friction. Coast. Eng. 2, 111-118.

Kamphuis, J.W., 1987. Recession rate of glacial till bluffs. J. Waterw. Port, Coast. Ocean Eng. ASCE 113, 60-73.

Kamphuis, J.W., 1990. Influence of sand and gravel on the erosion of cohesive sediment. J. Hydr. Res. 28, 43-53.

Kamphuis, J.W., 1995. Wave height from deep water through breaking zone. J. Waterw., Port, Coast. Ocean Engr., ASCE 120, 347-367.

Komar, P.D., and Reimers, C.E., 1978. Grain shape effects on settling rates. J. Geol. 86, 193-209.

Krone, R.B., 1962. Flume studies of the transport of sediment in estuarial shoaling processes. Final Report, Hydr. Engr. Lab. and Sanitary Engr. Res. Lab., U. of California, Berkeley, 110 pp.

Krone, K.B., 1963. A study of rhelogic properties of estuarial sediments. Ser. Rep. No. 63-8, Hydr. Engr. Lab. and Sanitary Engr. Res. Lab., U. of California, Berkeley.

Kulm, L.D., Roush, R.C., Harlett, J.D., Neudeck, R.H., Chambers, D.M. and Runge, E.J., 1975. Oregon continental shelf sedimentation: interrelationships of facies distribution and sedimentary processes. J. Geol. 83, 145-176.

Largier, J.L., Magnell, B.A., and Winant, C.D., 1993. Subtidal circulation over the Northern California shelf. J. Geophys. Res. 98, 18147-18179.

Lau, Y.L. and Krishnappan B.G., 1994. Does Reentrainment Occur during Cohesive Sediment Settling? , J. Hydraul. Engng. ASCE 120, 236-244.

Lesueur, P., Tastet, J. P. and Marambat L., 1996. Shelf mud field formation within historical times: examples from offshore the Gironde estuary, France. Cont. Shelf Res. 16,1849-1870.

Lick,W., 1982. Entertainment, deposition and transport of fine sediment in lakes. Hydrobiologia 91,31-40.

Lippmann, T.C., Brookins, A.H. and Thornton, E.B., 1996. Wave energy transformation on natural profiles. Coast. Eng. 27, 1-20.

Liu, K.F. and Mei, C.C.,1989 . Spreading of a thin sheet of fluid mud on an incline. J. Coast. Res. 5, 139-149.

Lyne, V.D., Butman, B. and Grant, W.D., 1990. Sediment movement along the U.S. east coast continental shelf, II: Modeling suspended sediment concentrations and transport rates during storms. Cont. Shelf Res. 10, 429-460.

Maa, P. Y. and Mehta, A. J., 1989. Considerations on soft mud response to waves. In: Neilson, B. J., Kuo, A. , Brubaker, J. (eds.), Estuarine circulation. Humana Press, Clifton, NJ, pp. 309 -336.

Madsen, O.S., Wright, L.D., Boon, J.D. and Chisholm, T.A., 1993. Wind stress, bed roughness and sediment suspension on the inner shelf during an extreme storm event. Cont. Shelf Res. 13, 1303-1324.

McCave, I. N. 1972. Transport and escape of fine-grained sediment from shelf areas. In: Swift D. J. P., Duane, D. B. and Pilkey, O. H. (eds.) Shelf Sediment Transport. Dowden, Hutchinson & Ross, Stroudsburg. pp. 225-248

McCave, I. N. 1984. Erosion, transport and deposition of fine-grained marine sediments. In: Stow, D. A. V. and Piper, D. J. W. (eds.) Fine grained sediments: Deep-Water processes and facies. Spec. Publs Geol. Soc. Lond. Blackwell Scientific Publications, Oxford.

McCave, I. N. 1985. Recent shelf clastic sediments. In: Brenchley P. J. and Williams B. P. J. (eds.). Sedimentology, recent developments and applied aspects. The Geological Society of London. Spec. Public. 18. pp. 49-65.

McCave, I. N. and Jones, K.P.N.,1988. Deposition of ungraded muds from high-density non-turbulent turbity currents. Nature 333, 250-252.

Mehta A. J. 1991. Understanding fluid mud in a dynamic environment. Geo-Marine Letters 11, 113-118.

Mehta, A.J., Hayter, E.J., Parker, W.R., Krone, R.B. and Teeter, A.M., 1989. Cohesive sediment transport, I: Process description. J. Hydra. Engr. 115, 1076-1093.

Mehta, A. J., and Partheniades, E.,1975. An investigation of the depositional propertied of flocculated fine sediments. J. Hydraul. Res. 13, 1037-105.

Migniot, C., 1968. A study of the physical properties of different very fine sediments and their behavior under hydrodynamic action(in French). La Houille Blanche 7, 591-620.

Mimura, N., 1993. Rates of erosion and deposition of cohesive sediments under wave action. In: Mehta, A.J. (Ed.), Nearshore and Estuarine Cohesive Sediment Transport, AGU, pp. 247-264.

Mitchum, R, M, Jr., P. R. Vail and J. B. Sangree, 1977. Seismic stratigraphy and global changes of sea level, Part 6: Stratigraphic interpretation of seismic reflection patterns in depositional sequences. In C. E. Payton, ed., Seismic Stratigraphy-applications to hydrocarbon exploration. Am. Assoc. Petroleum Geologists Mem. 26, Tulsa, OK, pp. 117-143.

Moore, D.G. and Curray, J.R., 1964. Wave base, marine profile of equilibrium and wave built terraces, discussion. Geol. Soc. Amer. Bull. 47, 1267-1274.

Nairn, R.B. and Southgate, H.N., 1993. Deterministic profile modeling of nearshore processes, Part II: Sediment transport and beach profile development. Coast. Eng. 19, 57-96.

Nelson, L. H., 1982. Modern Shallow water graded sand Layers from Storm surges, Bering Shelf: a mimic of Bouma sequences and turbidite systems. J. Sed Petrology 52, 537-545.

Nicholson, J. and O'Connor, B.A., 1986. Cohesive sediment transport model. J. Hydr. Eng. ASCE 112, 621-640.

Niedoroda, A.W., Swift, D.J.P. and Thorne, J.A., 1989. Modeling shelf storm beds: Controls of bed thickness and bedding sequence. In: R.A. Morton and D. Nummedal (Eds.), Shelf Sedimentation, Shelf Sequence and Related Hydrocarbon Accumulation, Gulf Coast Section, 7th Annu. Res. Conf. Proc., SEPM, pp. 15-39.

Niedoroda, A.W., Reed, C.W., Swift, D.J.P., Arato, A. and Hoyanagi, K., 1995. Modeling shore-normal large scale coastal evolution. Mar. Geol. 126, 180-200.

Nielsen, P., 1981. Dynamics and geometry of wave-generated ripples. J. Geophys. Res. 86, 6467-6472.

Nielsen, P., 1992. Coastal bottom boundary layers and sediment transport. World Scientific Publishing Company, Singapore, 324 pp.

Nittrouer C. A.,., 1999. STRATAFORM: Overview of its design and synthesis of its results. Marine Geology, v. 154, p. 3-12.

Nittrouer, C.A. and Sternberg, R.W., 1981. The formation of sedimentary strata in an allochthonous shelf environment: the Washington Continental Shelf. Mar. Geol. 42, 201-232.

Nittrouer, C.A. and Wright, L.D., 1994. Transport of particles across continental shelves. Rew. Geophys. 32, 85-113.

Nittrouer, C.A., and Kravitz, J.H., 1995. Integrated continental margin research to benefit earth and ocean sciences. Eos, Trans. AGU 76, 121-126.

Odd, N.V.M. and Owen, M.W., 1972. A two-layer model of mud transport in the Thames Estuary. Proc. Inst. Civ. Engs., Suppl. 9, 175-205.

Ogston A.S., Cacchione, D.A,, Sternberg, R.W., and Kineke, G.C., 2000. Observations of storm and river flood-driven sediment transport on the northern California continental shelf. Continental Shelf Research 20, 2141-2162.

Parchure, T.M. and Mehta. A.J., 1985. Erosion of soft cohesive sediment deposits, J. Hydr. Eng. ASCE 111, 1308-1326.

Partheniades, E., 1965. Erosion and deposition of cohesive soils. J. Hydra. Div. ASCE 91, 105-139.

Partheniades, E., 1986. A fundamental framework for cohesive sediment dynamics. In: Mehta, A.J. (Ed.), Estuarine Cohesive Sediment Dynamics. Springer, Berlin, pp. 219-250.

Partheniades, E., 1993. Turbulence, flocculation and cohesive sediment dynamics. In: Mehta, A.J. (Ed.), Nearshore and Estuarine Cohesive Sediment Transport. AGU, Washington, D.C., pp. 40-59.

Peregrine, D.H. and Svendsen, I.A., 1978. Spilling breaker, bores and hydraulic jumps. In: Proc. 16th Coast. Engr. Conf., ASCE, pp. 540-550.

Pilkey, O.H., Young, R.S., Riggs, S.R., Smith, A.W.S., Wu, H. and Pilkey, W.D., 1993. The concept of shoreface profile of equilibrium: A critical review. J. Coast. Res. 9, 255-278.

Pullen, J.D., and Allen, J.S., 2000. Modeling studies of the coastal circulation off Northern California: shelf response to a major Eel River flood event. Continental Shelf Research 20, 2213-2238.

Posamentier, H. W., and P.R. Vail, 1988. Eustatic controls on clastic deposition II - Sequence and systems tract models. In Wilgus, C.K, Hastings, B.S., Kendall, C., Posamentier, H.W., Ross, C.A. and Van wagoner, J.C., Sea-level Changes: An Integrated approach. Tulsa, Soc. Econ. Paleon. Mineral. Spec. Publ. 42, pp. 124-154.

Qian, N. and Dai, D.Z., 1980. The problems of river sedimentation and the present status of its research in China. In: Proc. Int. Symp. River Sed. pp. 1-39.

Reading, H. C., 1986. Sedimentary environment and facies. Blackwell Scientific Publications, Oxford, 615 pp.

Reed, C.W., Niedoroda, A.W. and Swift, D.J.P., 1999. Modeling sediment entrainment and transport processes limited by bed armoring. Mar. Geol. 154, 143-154.

Reineck, H.E., and I.B. Singh, 1980. Depositional Sedimentary environments. Springer Verlag, New York, 549 pp.

Rhodes, E.G., 1982. Depositional model for a Chenier Plain, Gulf of Carpenteria, Australia. Sedimentology 29, 201-221.

Roed, L.P. and Smedstad, O.M., 1984. Open boundary conditions for forced waves in a rotating fluid. J. Sci. Stat. Comp. 5, 414-426.

Roelvink, J.A. and Broker, I., 1993. Cross-shore profile models. Coast. Eng. 21, 163-191.

Ross, M.A. and Mehta A.J.,1989. On the mechanics of lutoclines and fluid mud. J. Coastal Research 5:511-61

Russell, R.D., 1939. Effects of transportation on sedimentary particles. In: Trask, P.D. (Ed.)., Recent Marine Sediments. Amer. Assoc. Petrol. Geol., pp. 32-47.

Sallenger, Jr., A.H. and Holman, R.A., 1985. Wave energy saturation on a natural beach of variable slope. J. Geophys. Res. 90, 11939-11944.

Schaffer, H.A., Madsen, P.A., Deigaard, R.,1993. A boussinesq model for waves breaking in shallow water. Coast. Engr. 20, 185-202.

Schoellhamer, D.H., 1988. Two-dimensional Lagrangian simulation of suspended sediment. J. Hydr. Eng. 114, 1192-1209.

Schoonees, J.S., Theron, A.K., 1995. Evaluation of 10 cross-shore sediment transport/morphological models. Coastal Eng. 25, 1-41.

Schunemann, M. and Kuhl, H., 1993. Experimental investigations of the erosional behavior of naturally formed mud from the Elbe estuary and adjacent Wadden Sea, Germany. In: Mehta, A.J. (Ed.), Nearshore and Estuarine Cohesive Sediment Transport. AGU, Washington, D.C., pp. 314-330.

Seilacher, A., 1982. General remarks about event deposits. In: Einsele, G. and Seilacher, A. (Eds.), Cyclic and Event Stratification. Springer-Verlag, pp. 161-174.

Shepard, F.G., 1932. Sediments on continental shelves. Geol. Soc. Amer. Bull. 43, 1017-1039.

Sherwood, C.R., Butman, B., Cacchione, D.A., Drake, D.E., Gross, T.F., Sternberg, R.W., Wiberg, P.L. and Williams III, A.J., 1994. Sediment-transport events on the northern California continental shelf during the 1990-1991 STRESS experiment. Cont. Shelf Res. 14, 1063-1099.

Shi, N., Larsen, L.H. and Downing, J.P., 1985. Predicting suspended sediment concentration on continental shelves. Mar. Geol. 62, 255-275.

Skafel, M.G. and Bishop, C.T., 1994. Flume experiments on the erosion of till shores by waves. Coast. Eng. 23, 329-348.

Skafel, M.G., 1995. Laboratory measurement of nearshore velocities and erosion of cohesive sediment (till) shorelines. Coast. Engr. 24, 343-349.

Sleath, J.F.A., 1991. Velocities and shear stresses in wave-current flows. J. Geophys. Res. 96, 15,237-15,244.

Smith, J.D. and McLean, S.R., 1977. Boundary layer adjustments to bottom topography and suspended sediment. In: J.C.J. Nihoul, J.C.J. (Ed.), Bottom Turbulence. Elsevier, Amsterdam, pp. 1213-1250.

Snedden, J.W., and D. Nummedal, 1991. Origin and Geometry of Storm-deposited storm beds in modern sediments of the Texas Continental Shelf. P. 231-245, In Swift, D.J.P., Oertel, G. and Tillman, T.W. (eds), Shelf Sand and Sandstone Bodies, Geometry, Facies and Sequence Stratigraphy. Int. Assoc Sed. Petrol. Spec. Publ. 14.

Sommerfield C. K. and Nittriuer C. A., (in press). Modern accumulation rates and a sediment budget for the Eel River shelf, USA: A flood-dominated depositional environment. Marine Geology.

Stamp, L.D., 1921. On cycles of sedimentation in the Eocene strata of the Angle-Franco Belgian basin. Geological Magazine v. 58, p. 108-114, 194-200.

Steckler, M.S., D.J. Reynolds, B.J. Coakley, B.A. Swift, and R. Jarrard, 1993. Modelling passive margin stratigraphy, in H.W. Posamentier, C.P.Summerhayes, B.U. Haq, and G.P. Allen, eds., Sequence Stratigraphy and Facies Associations: International Association of Sedimentologists Special Publication 18, pp. 19-42.

Steckler, M.S., D.J.P. Swift, J.P. Syvitski, J.A. Goff and A.W.Niederoda, 1996. Stratigraphic modeling of continental margins. Oceanography 9, 183-188.

Steckler, M.S., 1999. High-resolution sequence stratigraphic modeling I: the inteplay of sedeimentation, erosion, and subsidence. High resolution sequence stratigraphy modeling: effects of sedimentation processes in numerical experiments in stratigraphy. Soc. Econ. Paleontol. Mineral. Spec. Publ., pp. 139-150.

Sternberg, R.W., Ogston, A. and Johnson, R., 1996. A video system for in situ measurement of size and settling velocity of suspended particulates. J. Sea Res. 36, 127-130.

Svendsen, I.A., 1987. Analysis of surf zone turbulence. J. Geophys. Res. 92, 5115-5124.

Swart, D. H., 1974. Offshore sediment transport and equilibrium beach profiles. Delft. Hydr. Lab. Publ., No.131, 32 pp.

Swift, D.J.P., 1970. Quaternary shelves and the return to grade. Mar. Geol. 8, 5-30.

Swift, D.J. P., 1968. Coastal erosion and transgressive stratigraphy. J. Geol. 76, 444-456.

Swift, D.J.P., Ludwick, J.C. and Boehmer, W.R., 1972. Shelf sediment transport, a probability model. In: Swift, D.J.P., Duane, D.B. and Pilkey, O.H. (Eds.), Shelf Sediment Transport: Process and Pattern. Dowden Hutchinson & Ross, Stroudsburg, PA, pp. 195-223.

Swift, D.J.P., 1974. Continental shelf sedimentation. In: Burk, C.A. and Drake, C.L. (Eds.), The Geology of Continental Margins. Springer-Verlag, New York, pp. 117-135.

Swift, D.J.P., Sears, P.C., Bohlke, B. and Hunt, R., 1978. Evolution of a shoal retreat massif, North Carolina shelf: inferences from area geology. Mar. Geol. 27, 19-42.

Swift, D.J.P. and Field. M.E., 1981. Evolution of a classic sand ridge field: Maryland sector, North America inner shelf. Sedimentology 28, 461-482.

Swift, D.J.P., Han, G. and Vincent, C.E., 1986. Fluid process and sea floor response on a modern storm-dominated shelf: middle Atlantic shelf of North America, Part I: the storm current regime. In: Knight, R.L. and McLean, J.R. (Eds.), Shelf Sands and Sandstone Reservoirs. Can. Soc. Petrol. Geol. Mem. 11, pp. 99-119.

Swift, D. J. P., B. S. Parsons, A. Foyle, and G. F. Oertel, Submitted. Between Beds and Sequences: Stratigraphic Organization at Intermediate Scales in the Quaternary of the Virginia Coast, USA. Sedimentology.

Swift, D.J.P., Phillips, S. and Thorne, J.A., 1991. Sedimentation on continental margins, IV: lithofacies and depositional systems. Spec. Publ. Int. Ass. Sediment. 14, 89-152.

Syvitski, J., L. Pratson. P.L. De Boer, M. Garcia, M. Steckler., H. Lee, M. Perlmutter, G. Parker, P. Wiberg, and D. Swift, 1997. Earthworks: a large scale and complex numerical model to understand the flux and deposition of sediment over various time scales. In Pawlowsky-Glahn, Proceedings of the Third Annual Conference of the international Association of mathematical Geologists. International Center for Numerical Methods, Universitat Politechnica de Catalunya, 08034, Barcelona, Spain, pp. 12-25.

Teeter, A., 1992. Erosion of cohesive dredged material in open-water disposal sites. Dredging Research Program DRP-1-07, U.S. Army Corps of Engineers.

Teisson, C., Ockenden, M., Le Hir, P., Kranenburg, C. and Hamm, L., 1993. Cohesive sediment transport processes. Coast. Eng. 21, 129-162.

Thomas, W.A. and Prasuhn, A.L., 1977. Mathematical modeling of scour and deposition. J. Hydra. Eng. 103, 851-863.

Thorne, J.A., Grace, E., Swift, D.J.P. and Niedoroda, A.W., 1991. Sedimentation on continental margins, III: the depositional fabric - an analytical approach to stratification and facies identification. Spec. Publ. Int. Ass. Sediment. 14, 59-87.

Thornton, E.B. and Guza, R.T., 1982. Transformation of wave height distribution. J. Geophys. Res. 88, 5925-5938.

Ting, C.K.F. and Kirby, J.T., 1996. Dynamics of surf-zone turbulence in a spilling breaker. Coast. Eng. 27, 131-160.

Traykovski, P., Geyer, W.R., Irish, J.D., and Lynch, J.F., 2000. The role of wave-induced density-driven fluid mud flows for cross-shelf transport on the Eel River continental shelf. Cont. Shelf Res., 20, 2113-2140.

Trowbridge, J.H., Butman, B., and Limeburner, R., 1994. Characteristics of the near-bottom suspended sediment field over the continental shelf off northern California based on optical attenuation measurements during STRESS and SMILE. Cont. Shelf Res. 14, 1257-1272.

Tucker, M.J., 1991. Waves in Ocean Engineering. Ellis Horwood Ltd., 431pp.

Van Leussen, W., 1988. Aggregation of particles, settling velocity of mud flocs - a review. In: Dronkers, J. and van Leussen, W. (Eds.), Physical Processes in Estuaries. Springer Verlag, Berlin, pp. 347-403.

Walker, R.C. and James, N.P., 1992. Facies Models: Response to sea level change. Geol. Assoc. Can., 454pp.

Wan, Y., 1989. The evolution of old Yellow River delta (In Chinese). J. Oceanol. Limnol. 20(1), 66-74.

Wan, Z., 1982. Bed material movement in hyperconcentrated flow. Ser. Paper No. 31, Inst. of Hydrodyn. and Hydraul. Engrg., Tech. Univ. of Denmark, Lyngby, Denmark.

Wang, M, Duan, W., Tan, G., and Zhan, Y., 1985. On the structure and movement mechanism of flow with hyperconcentration of sediment. Paper presented at Int. Workshop on Flow at Hyperconcentrations of Sediment, Int. Res. And Training Ctr. On Erosion and Sedimentation (IRTCES), Beijing, China.

Wells, J.T. and Coleman, J.M., 1981. Physical processes and fine-grained sediment dynamics, coast of Surinam, South America. J. Sed. Petrol. 51, 1053-1068.

Wheatcroft, R.A., Borgeld, J.C., 2000. Oceanic flood deposits on the northern California shelf: large-scale distribution and small-scale physical properties. Cont. Shelf Res. 20, 2163-2190.

Wheatcroft, R.A., Borgeld, J.C., Born, R.S., Drake, D.E., Leithold, E.L., Nittrouer, C.A. and Sommerfield, C.K., 1996. The anatomy of an oceanic flood deposit. Oceanography 9, 158-162.

Wheatcroft, R.A., Sommerfield, C.K., Drake, D.E., Borgeld, J.C. and Nittrouer, C.A., 1997. Rapid and widespread dispersal of flood sediment on the northern California margin. Geology 25, 163-166.

Wiberg, P.L., Drake, D.E. and Cacchione, D.A., 1994. Sediment resuspension and bed armoring during high bottom stress events on the northern California inner continental shelf: Measurements and predictions. Cont. Shelf Res. 14, 1191-1219.

Wolanski E. et al. 1992. The role of turbulence in the settling of mud plocs. J. Coastal Research 8(1), 35-46.

Wright, L.D., Boon, J.D., Green, M.O. and List, J.H., 1986. Response of the mid shoreface of the southern mid-Atlantic Bight to a "northeaster". Geo-Mar. Letters. 6, 153-160.

Wright, L.D., Boon, J.D., Kim, S.C. and List, J.H., 1991. Modes of cross-shore sediment transport on the shoreface of the Middle Atlantic Bight. Mar. Geol. 96, 19-51.

Wright, L.D., Hepworth, D.A., Kim, S. C., and Gammisch, R. A., 1996. STRATFORM VIMS cruise and status report (Dec. 1995 - Mar. 1996). Virginia Institute of Marine Science, The College of William and Mary.

Wright, L.D., Xu, J.P. and Madsen, O.S., 1994. Across-shelf benthic transports on the inner shelf of the Middle Atlantic Bight during the "Halloween Storm" of 1991. Mar. Geol. 118, 61-77.

Wright, L.D., Kim, S.C. and Friedrichs, C.T., 1999. Across-shelf variations in bed roughness, bed stress and sediment suspension on the northern California shelf. Mar. Geol. 154, 99-115.

Xu, J.P. and Wright, L.D., 1995. Tests of bed roughness models using field data from the Middle Atlantic Bight. Cont. Shelf Res. 15, 1409-1434.

Young B. D. and Tang C. L. 1990. Storm-forced baroclinic near-internal currents on the grand bank. J. Phys. Ocen. 20, 1725-1741.

You, Z.J., 1994. A simple model for current velocity profiles in combined wave-current flows. Coast. Eng. 23, 289-304.

Yu, G., 1993. Preliminary study for the planning of Zhongshan Harbor, Jiangsu Province (in Chinese). Internal Rep. 9406, River and Harbors Res. Inst., Nanjing, China.

Yu, Z., Fan, S., Jin, L., 1998. The Old Yellow River underwater delta and the harbor construction (in Chinese). Acta Geographica Sinica 53,158-166.

Yu, Z., Jin, L., Chen, D. C., 1984. The erosion processes of the Old Yellow River underwater delta. Acta Oceanologica Sinica 8(2),197-206.

Yu, Z., Zhang, Y., Chen, D. and Jin, L., 1987. The hydrodynamic characteristics of nearshore waters and the discharging process on mud flats. Chin. J. Oceanol. Limnol. 5, 95-106.

Zhang, Y., Swift, D.J.P., Niedoroda, A.W., Reed, C.W. and Thorne, J.A., 1997. Simulation of sedimentary facies on the Northern California Shelf. Geology 25, 635-638.

Zhang, Y., Swift, D.J.P., Yu, Z., and Jin, L., 1998. Modeling of coastal profile evolution on the abandoned delta of the Huanghe River. Mar. Geol. 145, 133-148.

Zhang, Y., Swift, D.J.P., Fan, S., Niedoroda, A.W., Reed, C.W., 1999. Two-dimensional numerical modeling of storm deposition on the northern California shelf. Mar. Geol. 154, 155-167.

VITA

Shejun Fan

Born: Luoyang, China, October 7, 1966

EDUCATION

2001 Doctor of Philosophy in Oceanography
Department of Ocean, Earth & Atmospheric Sciences
Old Dominion University, 4600 Elkhorn Avenue, Norfolk, VA 23529

1990 Master of Science in Fluid Mechanics
Department of Naval Architecture & Ocean Engineering
Shanghai Jiao Tong University
1954 Huashan Rd., Shanghai, 200030 China

1987 Bachelor of Science in Mechanics
Department of Mechanics
Peking University, 5 Yiheyuan Rd., Beijing, 100871 China

SELECTED PUBLICATIONS

Zhang, Y. Swift, D. J. P., Fan, S., Niedoroda, A.W., and Reed, C.W., 1999. Two-dimensional modeling of storm deposition on the northern California shelf. Marine Geology, 154,155-167.

Yu Z., Fan S., and Jin L., 1998. The Old Yellow River underwater delta and the harbor construction. ACTA GEOGRAPHICA SINICA, 53, 158-166.

Fan S., Yu Z., and Jin L., 1997. Dynamical mechanism and modeling of recession and accretion of mud flat. Part I. wave and current. ACTA OCEANOLOGICA SINICA, 19(3), 67-76.

Fan S., Yu Z., and Jin L., 1997. Dynamical mechanism and modeling of recession and accretion of mud flat. Part II. sediment transport and mud flat Processes model. ACTA OCEANOLOGICA SINICA, 19(3), 77-85.

Fan S., Yu Z., and Jin L., 1997. Accretion process model of mud flat of Haizhou Bay. OCEANOLOGIA ET LIMNOLOGIA SINICA, 28(4), 411-418.

Mei, C., Fan, S., and Jin, K., 1997. Resuspension and transport of fine sediments by waves. Journal of Geophysical Research, 102(C7), 15,807-15,821.

Zou G., Fan S., 1990. Numerical calculation of wave running-up on beach. Journal of Hydrodynamics, 5(1):30-37.